Order Number 8919489

The effects of reduced dimensionality and elastic scattering on the current voltage characteristics of resonant tunneling diodes

Wolak, Edmund Leonard, Ph.D.

Stanford University, 1989

U·M·I
300 N. Zeeb Rd.
Ann Arbor, MI 48106

THE EFFECTS OF REDUCED DIMENSIONALITY AND ELASTIC SCATTERING ON THE CURRENT VOLTAGE CHARACTERISTICS OF RESONANT TUNNELING DIODES

A DISSERTATION
SUBMITTED TO THE DEPARTMENT OF APPLIED PHYSICS
AND THE COMMITTEE ON GRADUATE STUDIES
OF STANFORD UNIVERSITY
IN PARTIAL FULFILLMENT OF THE REQUIREMENTS
FOR THE DEGREE OF
DOCTOR OF PHILOSOPHY

By

Edmund Leonard Wolak

March 1989

I certify that I have read this dissertation and that in my opinion it is fully adequate, in scope and quality, as a dissertation for the degree of Doctor of Philosophy.

Professor James S. Harris Jr. (Principal Advisor)

I certify that I have read this dissertation and that in my opinion it is fully adequate, in scope and quality, as a dissertation for the degree of Doctor of Philosophy.

Professor David Bloom (Electrical Engineering)

I certify that I have read this dissertation and that in my opinion it is fully adequate, in scope and quality, as a dissertation for the degree of Doctor of Philosophy.

Professor Malcom Beasley (Applied Physics)

Approved for the University Committee on Graduate Studies:

Dean of Graduate Studies

Abstract

Two terminal devices with negative differential conductance effects (NDC) have been used for several decades in a variety of electronic applications. The existing diode technologies which give such effects have a limited number of adjustable parameters, and constraints on frequency of operation which have limited their application. The development of molecular beam epitaxy (MBE) has enabled the developement of a new class of quantum devices including the resonant tunneling diode (RTD). The RTD has shown the potential to operate from D.C. into the THz frequency range. The range of adjustable parameters available give the RTD great flexibility in design, but also increase the complexity of understanding transport through the device.

The current-voltage (I-V) characteristics of an RTD are modeled within the assumption of coherent electron wavefunctions through the structure and a seperation of variables condition. These assumptions are broken by the presence of ionized impurities within the device, yet such impurities are essential to device design. In order to determine the effect of such impurities on the I-V characteristics, a set of RTD's was fabricated with different types of impurities in the center of the device. A shift in the peak current of the device is correctly predicted by the I-V model, however, a degradation of the ratio of the peak current density to the valley current density (peak to valley ratio), is not correctly predicted by the model. A scattering assisted tunneling mechanism is proposed to account for the discrepancy.

Advanced lithographic techniques have created the capability to introduce addtional quantum confinement transverse to the direction of current flow. The effects of this additional confinement in a resonant tunneling device are studied theoretically. First the problem is solved assuming that the variables can be seperated in the direction along and

the direction transverse to the current flow. It is found that under these conditions that no addtional peaks are manifested in the current-voltage characteristics of these devices. The violation of the seperation of variables condition is introduced as a perturbation to the previous system. It is found that a perturbation due to an elastic scattering center can cause additional structure in the current-voltage characteristics of such devices.

Acknowledgments

I have many people to thank for being able to write this thesis, but first and foremost I must thank my advisor Jim Harris for creating a unique environment within which to do research. This environment not only includes leading edge materials and processing capabilities, but also a highly talented pool of individuals that I feel lucky to have worked with. I would also like to thank Professor David Bloom for being on my thesis committee, and for working to create a cooperative effort between his group and Professor Harris's group. Professor Beasley's presence on my reading committee is greatly appreciated, as is his interest in this topic which is outside his immediate sphere of responsibility.

Kevin Lear has had a huge positive impact on the resonant tunneling effort at Stanford University. His advice and assistance in device fabrication, as well as many discussions about the device physics of resonant tunneling diodes are greatly appreciated. Steve Chou has been a real leader in the field of resonant tunneling and I have gained much from my collaborations with him. His initiative to consider systems with reduced dimensionality, as well as his very effective techniques of research and presentation have had a positive impact on my work. Eric Hellman has always been there to advise, consult, proofread, and to stimulate my efforts. His knowledge of physics is greatly respected by me.

Byung Gook Park has been wonderful to work with in simulating quantum devices, and he has shown great insight into solving various quantum problems and was very helpful in integrating the Poisson equation solver (FISH1D) with my transmission coefficient code to develop the ballistic model. The can-do attitude of Phil Pitner, as well as his crystal growth efforts and design input were an important part of doing the elastic scattering experiment in my thesis. Alex Harwit helped me get started in the field and made a substantial contribution to our first publication. Ken Shepard's understanding of physical phenomena, as well as his knowledge of analytical techniques were a crucial part of solving

the problem of elastic scattering in a system with reduced dimensionality. Thierry Weil and Dominique Thomas from Thomson CSF were very helpful in discussions of the physics of resonant tunneling devices, and Dominique's measurements and discussions were very useful in the work on elastic scattering in resonant tunneling devices.

The members of David Bloom's group were very helpful in stimulating discussions on resonant tunneling devices and in the sharing of some facilities. Scott Diamond has always made an extra effort to collaborate with our group in this area; and Mark Rodwell, Lance Goddard, Rob Marsland, Ekmel Ozbay, Pauline Prather and Ursula Keller have all been helpful. Not all of my experimental efforts are reflected in this thesis, but I would like to thank Won Seong Lee and Yi-Ching Pao for growing wafers for me and offering processing advice on additional projects. The efforts of Jim Adkisson, Peng Cheng, Paul de la Houssaye, Stephanie Koch, Kurt Lehman, David Liu, Tony Ma, Darrell Schlom, Ken Williams, Gideon Yoffe and several of the people mentioned above, are greatly appreciated for their efforts in building and maintaining the facilities which make RTD fabrication and simulation possible, as well as useful discussions. Eric Larkins is appreciated for his discussions as well as his efforts at building our MBE capability at Stanford. Gail Chun-Creech, Lachen Pence, Paula Perron and Sherie Harvey have always been helpful with administrative support.

As a result of Professor Harris being liberal in sending his graduate students to various conferences, I have had the pleasure of meeting and discussing device physics with Gerry Sollner, Elliot Brown, Joel Schulman, Ken Rousseau, H.C. Liu, and Norman Klucksdahl. I am most grateful to Elliot for the time he has spent encouraging me and the knowledge that he has shared with me and other members of the Bloom and Harris groups.

Finally, I would like to thank my Mother and Father for telling me to go get a PhD.

Table of Contents

FIGURES

I. Introduction

The remarkable advances in computation and communications technologies in the last half century have been made possible by the invention and development of a vast array of solid state electronic and optical devices. By striving to achieve higher speeds of operation, and greater levels of integration, ever more powerful computing and communications tools have been created. The transistor, the laser and a host of other devices have been invented and reinvented many times in a multitude of materials systems. As materials growth and fabrication technologies continue to improve, it becomes possible to use new physical phenomena in solid state devices, in addition to optimizing the performance of existing devices.

In the area of communication, there are applications for devices with negative differential resistance (NDR). NDR occurs when an increased bias (applied voltage) across a device results in decreased current flow through the device as shown in figure 1.1. This effect is useful for a number of reasons. By applying the proper bias across the device, it can be used to convert D.C. power into high frequency oscillations. Other applications include signal processing, and using the resonant tunneling device as a load element in a logic circuit.

The existing technologies for obtaining NDR include; the Gunn diode, the IMPATT diode and the Esaki tunnel diode[1]. Unfortunately, there are physical limitations to each of these devices. The Gunn diode operates by transferring charge from the high mobility gamma valley of a semiconductor (typically GaAs) to the low mobility L valley under large electric fields. This device is very important in microwave communications, however, it is fundamentally limited to operating below 150 GHz, and actual operation frequencies are significantly lower (~80 GHz). The IMPATT diode only oscillates at a specific frequency, fixed by its drift region. It is capable of producing a large power output, however, it is

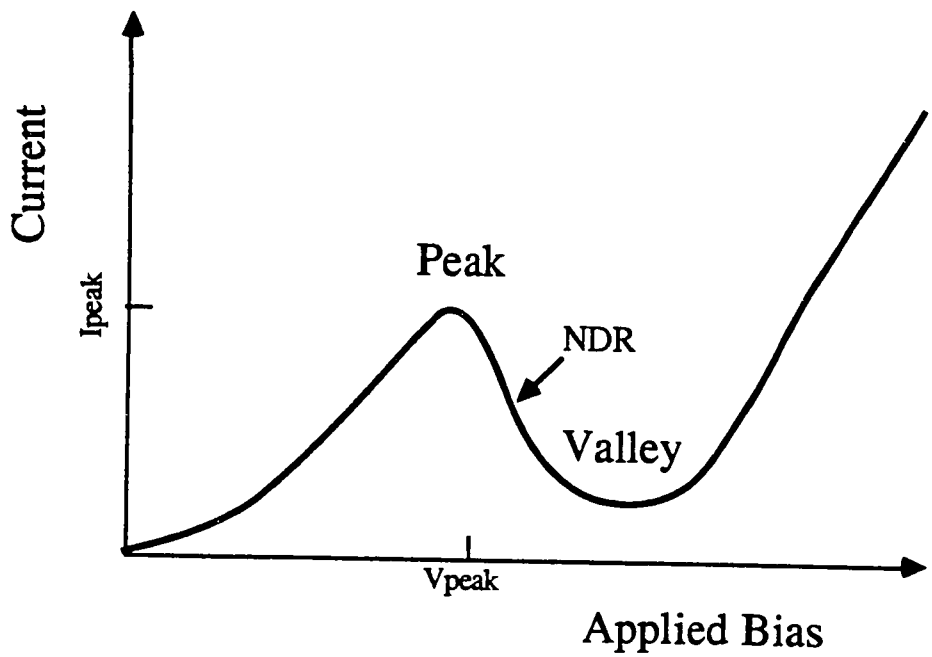

Figure 1.1 - A Schematic diagram of a current-voltage characteristic which exhibits negative differential resistance (NDR).

plagued by noise. The Esaki tunnel diode operates by tunneling from the conduction to the valence band through the band gap in a p/n junction diode. This is accomplished by degenerately doping the emitter and collector contacts with n and p-type dopants, respectively. Due to the required proximity of the adjacent contact layers and the very high doping required to achieve tunneling, the capacitance of this device is very large and thus the frequency response is seriously limited. Ultimately, new types of devices will be used to accommodate the demand for increased communication frequencies and signal processing capabilities.

Recently, a new group of high speed electronic devices has been made possible by advances in crystal growth technologies. One of these devices, the resonant tunneling diode (RTD), exhibits NDR at room temperature and has shown the potential to oscillate up to several hundred GHz[2]. The potential of RTDs lies in the fact that several of the parameters can be varied resulting in the possibility of achieving both low capacitance and high current density, and thus operation at higher frequencies than are currently possible with either Esaki or Gunn diodes. The flexibility in design parameters also provides the possibility of adjusting the resonant bias condition, the peak to valley ratio, and the peak current density in order to meet circuit design specifications.

In addition to specific investigation of RTDs, one would hope to gain a greater understanding of related device categories. Specifically, the high speed ballistic or hot electron transistor, relies on a similar double barrier structure and shares similar charge transport and quantum physics with these devices[3]. The RTD can also be used as an energy filter within other devices such as the heterojunction bipolar transistor to create new electronic applications[4]. In addition, the double barrier structure is a very simple case of a finite superlattice, superlattices being the foundation for several classes of optoelectronic devices. Perhaps the greatest potential for these devices is the possibility of using several

resonant states within the device, or several such devices in series, to provide the building blocks for multi-state logic systems.

In this thesis several aspects of the RTD will be studied in detail. In chapter 2, background information on the crystal structure, material system, crystal growth, and device operation are given. In chapter 3, the fundamental mechanism for achieving NDR is explored. By using a time independent formalism, a method of calculating the current-voltage characteristics is illustrated. The limitations of the model are discussed, and alternative approaches for the calculation are discussed.

One of the sources of breakdown of the coherent model is elastic scattering effects. A major source of elastic scattering centers is ionized impurities placed in and around the RTD. Since ionized impurities are needed to provide the carriers for the device to operate it is important to understand something about the effect of such centers on the current-voltage characteristics in order to optimize the structure. Another reason to explore this effect is that ionized impurities must be used within the base of a hot-electron transistor structure in order to achieve three terminal operation. Thus the understanding of such effects is critical to the design of such devices. A study of elastic scattering centers is described in chapter 4.

Recent advances in lithographic techniques, specifically e-beam lithography, have made it possible to define structures perpendicular to the growth direction down to quantum dimensions. In chapter 5, the effects of such confinement are explored under a set of simplifying assumptions, including the separation of variables. In actual devices, however, the separation of variables condition is easily broken. By using first order perturbation theory, it is possible to study the impact of effects, such as elastic scattering, by using the unperturbed wavefunctions as a basis.

Conclusions and suggestions for future work are made in chapter 6.

References:

1. Sze, Physics of semiconductor devices, chapters 10-12.

2. T. C. L. G. Sollner, W.D. Goodhue, P.E. Tannenwald, C.D. Parker and D.D> Peck, Appl. Phys. Lett., **43**, 588, 1983.

3. M. Heiblum, I.M. Anderson, and C. M. Knoedler; Appl. Phys. Lett 49 (4), 207, 1986.

4. Federico Capasso, Khalid Mohammed, and Alfred Y. Cho, IEEE J. Quantum Electron, **QE-22**, (1986).

2. Background

The development of Molecular Beam Epitaxy (MBE) and Metal Organic Chemical Vapor Deposition (MOCVD) have created the capability to control crystalline structure in the direction of growth down to atomic dimensions. By using materials systems which are closely lattice matched, but which have band offsets, usually in conjunction with differences in the band gap, this control of crystal structure can be used to vary the potential energy and the effective mass of electrons and holes along the direction of growth. This sort of control has not only led to the development of devices such as the Modulation Doped Field Effect Transistor (MODFET), where the effects of quantum mechanical confinement must be included in order to accurately model the operation of the device, but also devices such as the resonant tunneling diode (RTD) where quantum effects are the basis of device operation.

In this chapter, the background information needed to understand the mechanics of RTDs will be discussed. The GaAs/InGaAs/AlGaAs material system, currently the most popular system for RTDs, is discussed in the first section. The use of molecular beam epitaxy to grow quantum devices is covered in the second section. The crystal structure of a resonant tunneling diode and some general comments on fabrication are made in the third section. The basics of RTD operation are sketched out in the fourth section.

2.1 The GaAs/AlAs material system

The GaAs/AlAs system has been studied extensively and has been used to fabricate a variety of electronic devices[1,2,3,4]. These materials have several distinct advantages over silicon, the dominant semiconductor technology. The band gap of GaAs is significantly wider than that of Si, 1.42eV vs. 1.12eV for Si, which contributes to a very low intrinsic carrier concentration for GaAs. As a result, undoped GaAs material is semi-insulating

which makes it advantageous for use as a substrate for microwave circuits. Silicon, on the other hand, needs to be grown on other substrate materials, typically saphire, for use in high-frequency circuits. In addition, GaAs has high mobility at low fields which gives it advantages for use in Field Effect Transistors (FETs) and other high speed electronic devices.

Another advantage of GaAs is the fact that the material has a direct bandgap (both conduction and valence band minima are at the gamma point), which allows radiative recombination of electron hole pairs to be the predominant relaxation mechanism for high quality materials. As a result, GaAs and the related III-V compounds are used in a variety of optoelectronic applications including lasers[5], light emitting diodes[6], modulators[7] and detectors[8]. A continuous spectrum of $Ga_xAl_{1-x}As$ alloys, ranging from pure GaAs to pure AlAs can be fabricated by a number of methods. The conduction band minimum remains at the gamma point for x ranging from 0 to 0.45, the magnitude of the direct bandgap is given by $1.42 + 1.25x$ [9]. Between 0.45 and 1.0 the conduction band minimum is at the X point where it remains for high Al content alloys through pure AlAs. Once the conduction band minimum switches over to the X point, the material is no longer direct gap and the strength of radiative recombination is greatly reduced. The energy gap between the valence band maximum and the X point of the conduction band is $1.9 + 0.125x + 0.143x^2$ as illustrated in figure 2.1.

The primary dopants used in GaAs/AlGaAs are Si for n-type doping and Be for p-type doping[10]. It is possible for GaAs to incorporate $5x10^{18}/cm^3$ of Si as n-type dopants before saturation is reached, though this number varies depending on substrate temperature and the As to Ga flux ratio. For high As flux ratios and low substrate growth temperatures (around 550 C), it is possible to increase the saturated Si doping level. If the saturated doping level is surpassed, it is possible for the additional Si atoms to displace As atoms and

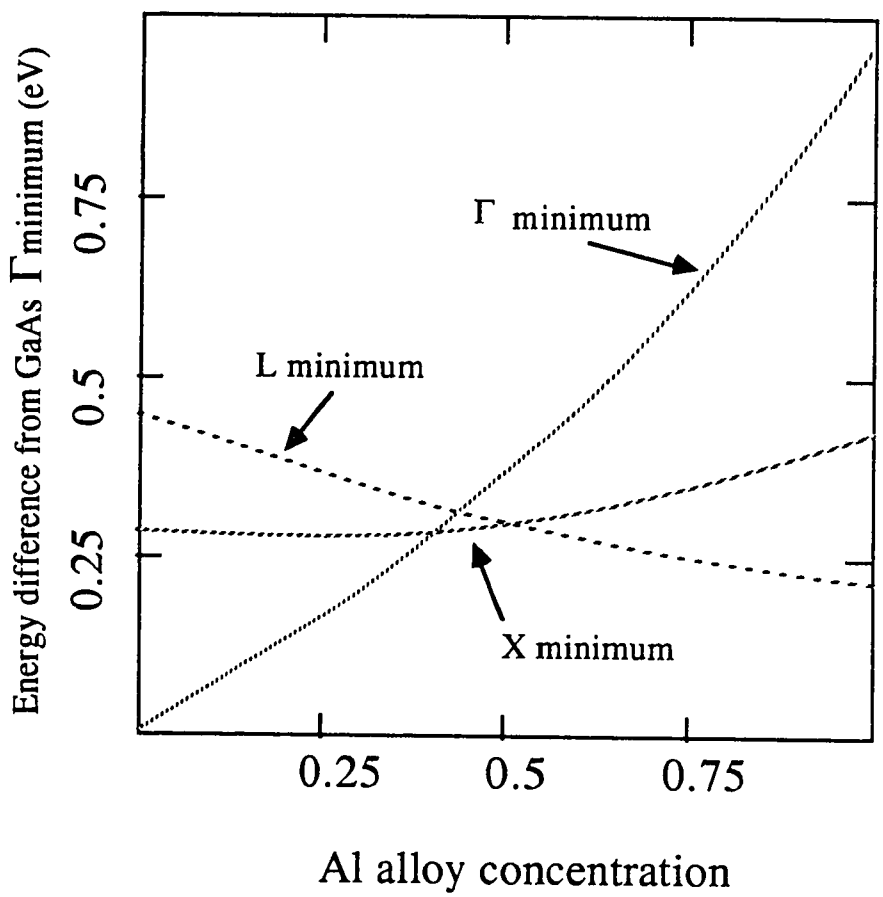

Figure 2.1 - The energies of the conduction band minima associated with three symmetry points are plotted as a function of the Al alloy concentration in a GaAs/AlAs alloy (after ref. 9). For low Al content alloys, the bandgap is direct, for Al concentrations of over 40% the bandgap becomes indirect.

act as acceptors, thus partially compensating the material. Also, it is possible for excess Si atoms to "ride the growth surface" or "surf" during the crystal growth process, adding impurities where they are not desired. The saturated doping level for Be is much higher than for Si in GaAs, and values of up to $1x10^{20}/cm^3$ have been reported[10].

The $Ga_xAl_{1-x}As$ system is lattice matched to within 0.3%;[9] the alloys, as well as pure GaAs and AlAs, have the same zincblende crystal structure; two alternating lattices of FCC crystals with type III and type V materials. Due to the nearly identical crystal structures of these materials, it is possible to fabricate a wide variety of crystal heterostructures, i.e. a crystal which includes an interface(s) between two (or more) types of materials. The differences in bandgaps result in conduction and valence band offsets at the heterojunction. Approximately 60% of this offset is estimated to occur in the conduction band, the balance in the valence band[11].

Indium alloyed with GaAs, grown on a substrate which is lattice matched to GaAs is used when a narrower bandgap material is desired. $In_yGa_{1-y}As$ is not lattice matched to GaAs and thus $In_yGa_{1-y}As$ layers induce strain depending on their thickness and composition[12]. The relationship between the bandgaps of strained $In_yGa_{1-y}As$ alloys which are commensurate with the GaAs lattice is poorly understood, in part because strain may modify the bandgap, depending on the thickness of the $In_yGa_{1-y}As$ material. Presently, the bandgap of the $In_yGa_{1-y}As$ is estimated by using a linear interpolation between GaAs and InAs (with a bandgap of 0.35 eV) based on the In content.

By using different materials, the bandgap, and thus the electron potential can be modified as a function of position in the material. By sandwiching a narrow bandgap material between two wider bandgap material layers, a potential well is formed. A wide bandgap material sandwiched between two narrow bandgap material layers forms a

potential barrier. Quantum devices are fabricated by using crystal growth techniques which create hetero-interfaces that are planer to within atomic dimensions and can control well and barrier layer thickness down to dimensions where quantum mechanical effects become important. The list of successful quantum devices includes; quantum well lasers[5], quantum well photodetectors[6], resonant tunneling devices[13] and modulation doped field effect transistors (MODFET's)[14]. Several other types of devices rely on the ability to control the electron potential as a function of position, though quantum confinement is not crucial to their operation. These include the heterojunction bipolar transistor[15] and the heterostructure laser[16].

Despite these advantages over silicon, GaAs is unlikely to ever enjoy the predominant role now enjoyed by Si in the semiconductor business. The chief advantage of Si is that the native oxide both passivates the surface and greatly simplifies the fabrication process. The Si fabrication process has been adapted to mass production techniques for decades. In addition, Si is much easier to handle and process than GaAs due to the relative fragility of GaAs wafers. Silicon is also much less expensive than GaAs because Ga is relatively rare. The unique advantages of GaAs, however, guarantee a niche for it in the semiconductor industry.

2.2 Molecular Beam Epitaxy of GaAs/AlAs

MBE is essentially a very well controlled evaporation process which takes place in an ultra-high vacuum chamber[1,2,10]. Typically, each component element which is to be incorporated into the crystal has a separate high-precision computer-controlled evaporator. The flux is controlled by the temperature of the evaporator crucible. With the correct flux ratios and substrate temperature it is possible to grow a very high quality crystal on the substrate. Crystalline composition is changed by opening and closing shutters located

between the evaporator and the substrate as shown in figure 2.2. Both alloy composition and impurity concentration can be effectively controlled in this fashion, however, some impurities may tend to diffuse during the growth process. The epitaxial structures are grown on a single crystal substrate, typically consisting of a material lattice matched to the desired epitaxial structure.

The substrate is heated to a temperature which optimizes the growth dynamics by using either direct or radiative substrate heating. GaAs tends to grow best at temperatures between 550 and 650 C. The best $Al_xGa_{1-x}As$ is typically grown between 680 and 800 C, the best $In_yGa_{1-y}As$ between 480 and 520 C. The temperature of crystal growth is determined by the exact structure desired, and the substrate temperature may be changed during the growth process to achieve the optimal growth conditions of each type of crystal.

The Ga/As flux ratio has an important influence on the material quality. Typically, a flux gauge ratio 10-20, of As over Ga is used. Too high an As flux ratio leads to a large defect density, to low leads to Ga balling up on the surface. Typically, the ratio of As over Ga goes up for growing $Al_xGa_{1-x}As$ due to the increased total group III flux.

Due to the strong relationship between the crystalline and interface quality of the epitaxial structures and the performance of RTDs, steps taken during the crystal growth process are crucial to RTD design. Uniformity of crystal growth over the wafer is assisted by rotating the substrate under the incident flux. Calibration can be done to atomic dimensions using reflection high energy electron diffraction (RHEED) pattern. An intensity peak occurs when a smooth interface is presented to the electron beam whereas intermediate points in the growth process have many small islands and thus have a rough surface which scatters the RHEED beam. By interrupting the growth process, coalescence of these islands and smoothing of the interface occurs. Such interruptions are often used to defeat the effects of interface non-uniformity.

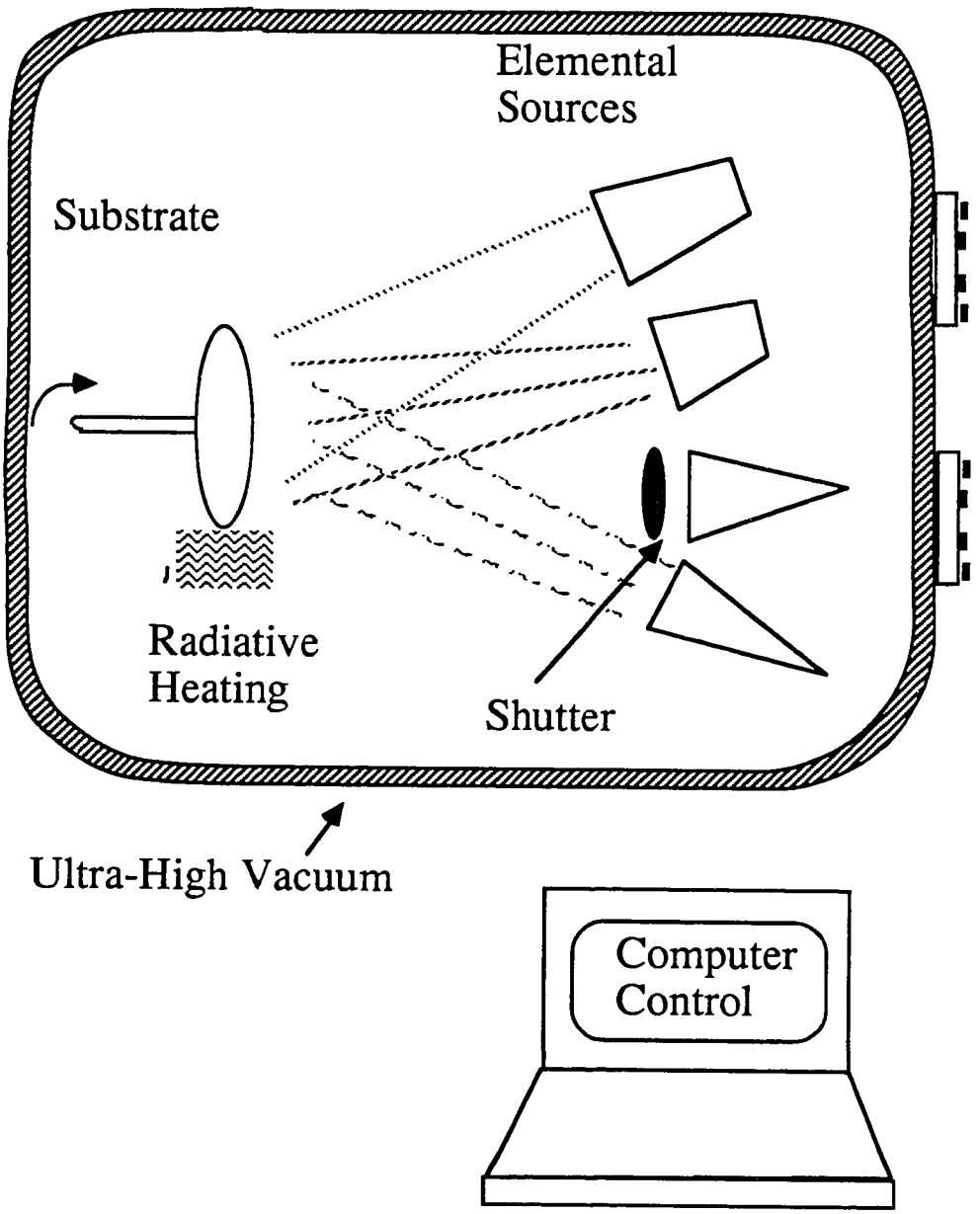

Figure 2.2 Schematic diagram of some of the many elements in device quality MBE growth.

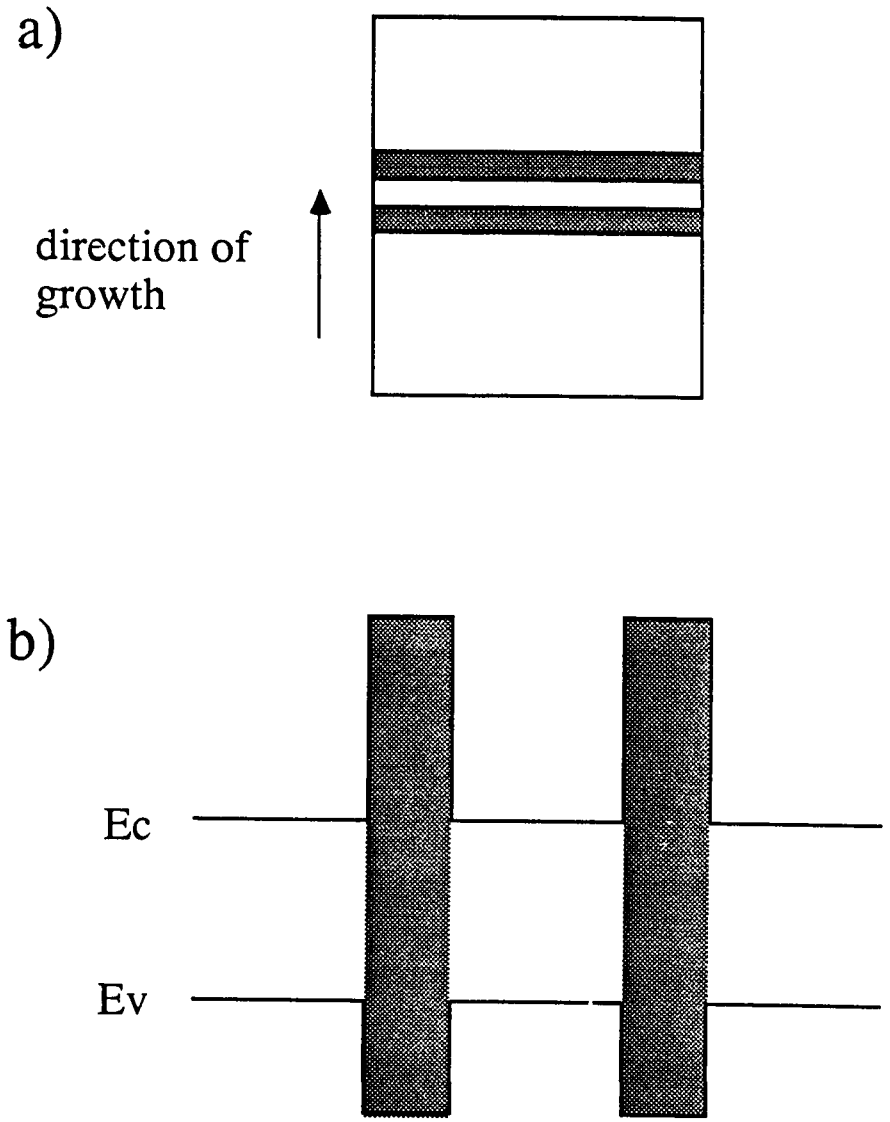

Figure 2.3 - The crystal structure of an RTD is illustrated schematically in a, with an illustration of conduction band minimum and valence band maximum along the growth direction shown in b).

2.3 The Structure of a Resonant Tunneling Diode

RTDs are fabricated by growing crystals with two thin (11-100Å) barriers separated by a well which is narrow enough to allow observable quantum interference effects between the barriers (generally 30-400Å)[13,17,18]. The barriers are made by growing material which has a wider bandgap than the surrounding layers or well. The discontinuities of electron potential along the direction of growth act as a potential barrier system for the electron as shown in figure 2.4. The emitter and collector of the device are doped in order to provide the tunneling carriers and to reduce series resistance. The barriers and well are not doped so that elastic scattering doesn't destroy the wave coherence of the electrons through the device. A more extensive discussion of doping in resonant tunneling diodes is given in chapter 4 of this thesis.

The actual fabrication of RTDs is straightforward, once the epitaxial structure has been fabricated. Device fabrication consists of defining a suitable area, and applying ohmic contacts to the emitter and collector regions. The resistance of the contact and interconnect metal must be less than the intrinsic NDR of the RTD in order for NDR to be observable[19]. The most common methods of device isolation include physically etching mesa type structures[13], or using ion implantation to create damage to the crystal structure[20] and rendering it insulating as shown in figure 2.3. Once isolation is achieved, it is necessary to make an ohmic contact to the emitter and collector sides of the diode. This may be done by using either alloyed or non-alloyed ohmic contacts. The use of non-alloyed ohmic contacts is becoming popular for the top side of the crystal, so that alloying will not introduce defects and alloy spikes through the RTD well and barriers from the ohmic contact material. If an alloyed ohmic contact is used on the top side, a thick (>0.4 micron) buffer layer is grown over the RTD to avoid such "spiking" behavior. Because it is hard to grow good GaAs over a non-alloyed contact structure, the bottom contact is typically alloyed, but it can be distant from the isolated part of the RTD.

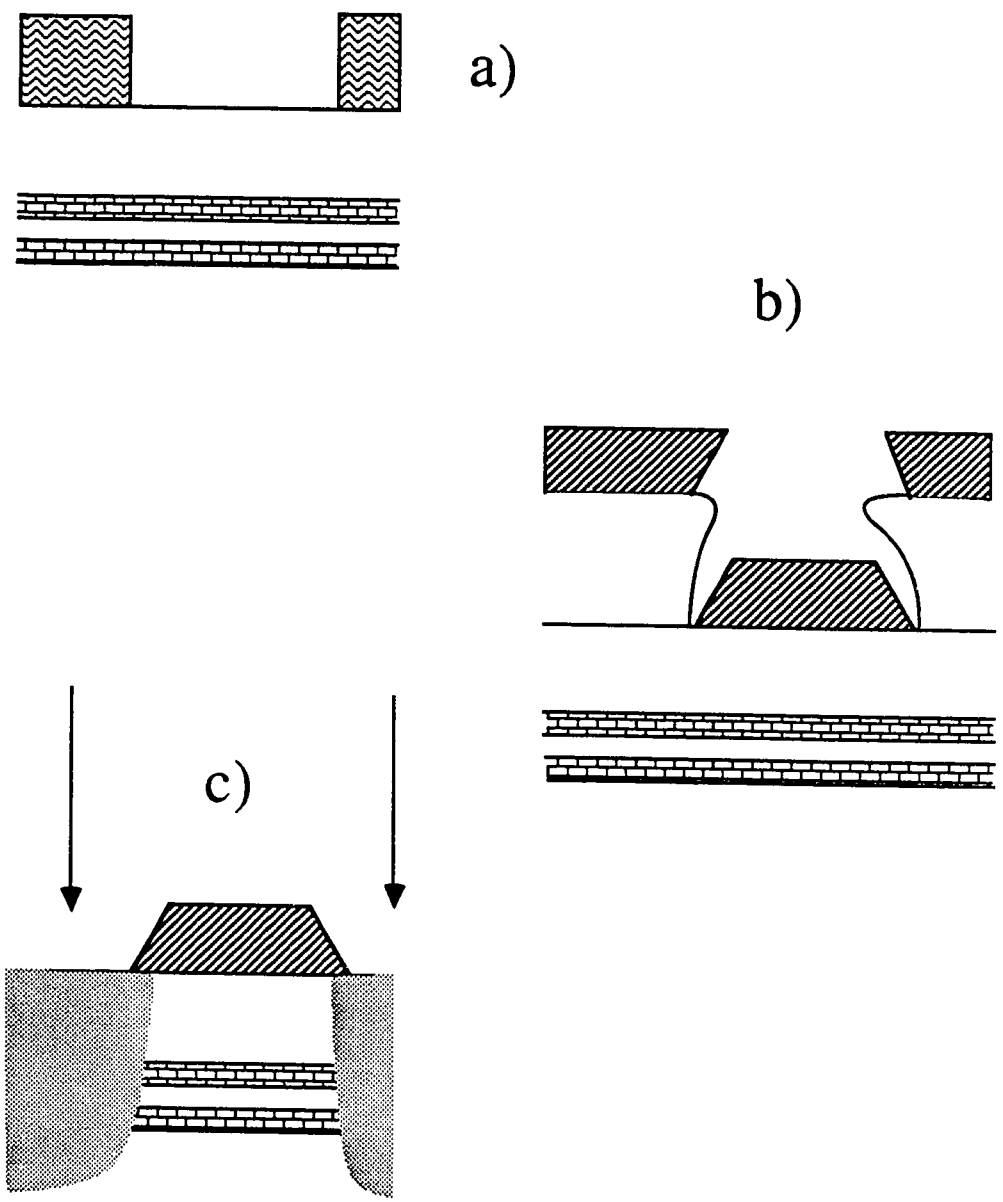

Figure 2.4 a-c Ion implantation process. Photoresist is lithographically patterned in step (a) to allow for evaporation of ohmic contact metal in step (b). If a non-alloyed ohmic contact is used, the metal itself can act as a mask for ion implantation isolation of the RTD (c).

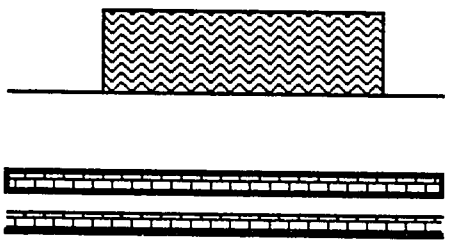

d)

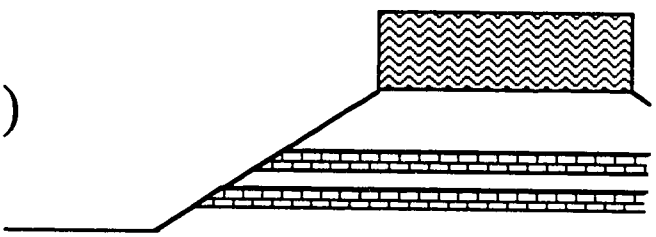

e)

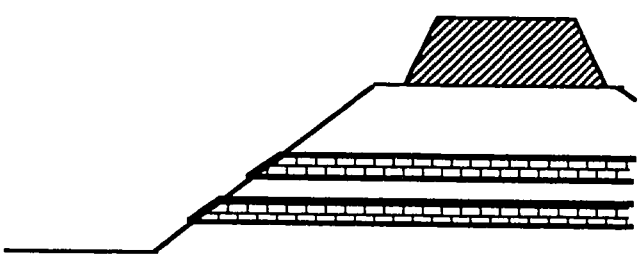

f)

Figure 2.4 d-f Mesa etch process. Photoresist is patterned to the size of the desired device in (d). The resist is used as an etch mask so that the material which is not to be a part of the device is cleared away (e). Contact metal can then be deposited on top of the mesa using lithographic techniques (f).

Several materials have been used to fabricate RTDs. Historically, the most common material system has been GaAs for the well and surrounding emitter and collector layers, and $Al_xGa_{1-x}As$ or AlAs for the barriers, as shown in figure 2.4. This is due to the maturity of MBE which has developed, and the fact that the first good RTD results were obtained in this material system[13]. The $In_{0.48}Ga_{0.52}As$ / $In_{0.47}Al_{0.53}As$ material system (lattice matched to InP) may increase both the performance and applicability of these devices as such materials become more commonplace[21]. The best peak to valley ratios in RTDs have come from this later material system, due to the larger difference between the relative energies of the Γ and X-valley minima[22]. The possibility of using non-alloyed ohmic contact technology may eventually make practical three terminal quantum interference devices possible in materials lattice matched to InP. The Si-Ge material system has also been used to make RTDs. This introduces the very attractive possibility of integrating Si-Ge RTDs with Si based microcircuits[23].

2.4 RTD operation

The RTD relies on quantum mechanical interference and resonance effects in order to manifest NDR on a macroscopic level. The effect is analogous to a rather leaky Fabry-Perot interferometer with a broad band of incident frequencies. At zero bias, the tunneling of electrons (or holes) from one side to the other must be the same in both directions and thus no net current flows as shown in figure 2.5. As the bias level is increased, current will start to flow from the side which has it's majority carriers at a higher potential; this side is called the emitter and the other side the collector. At first, the incident electrons tunnel through the barriers with a probability similar to that of the product of tunneling through each of the barriers individually. As the bias is increased, a resonance condition can occur where the reflected electron wavefunction from the first barrier is

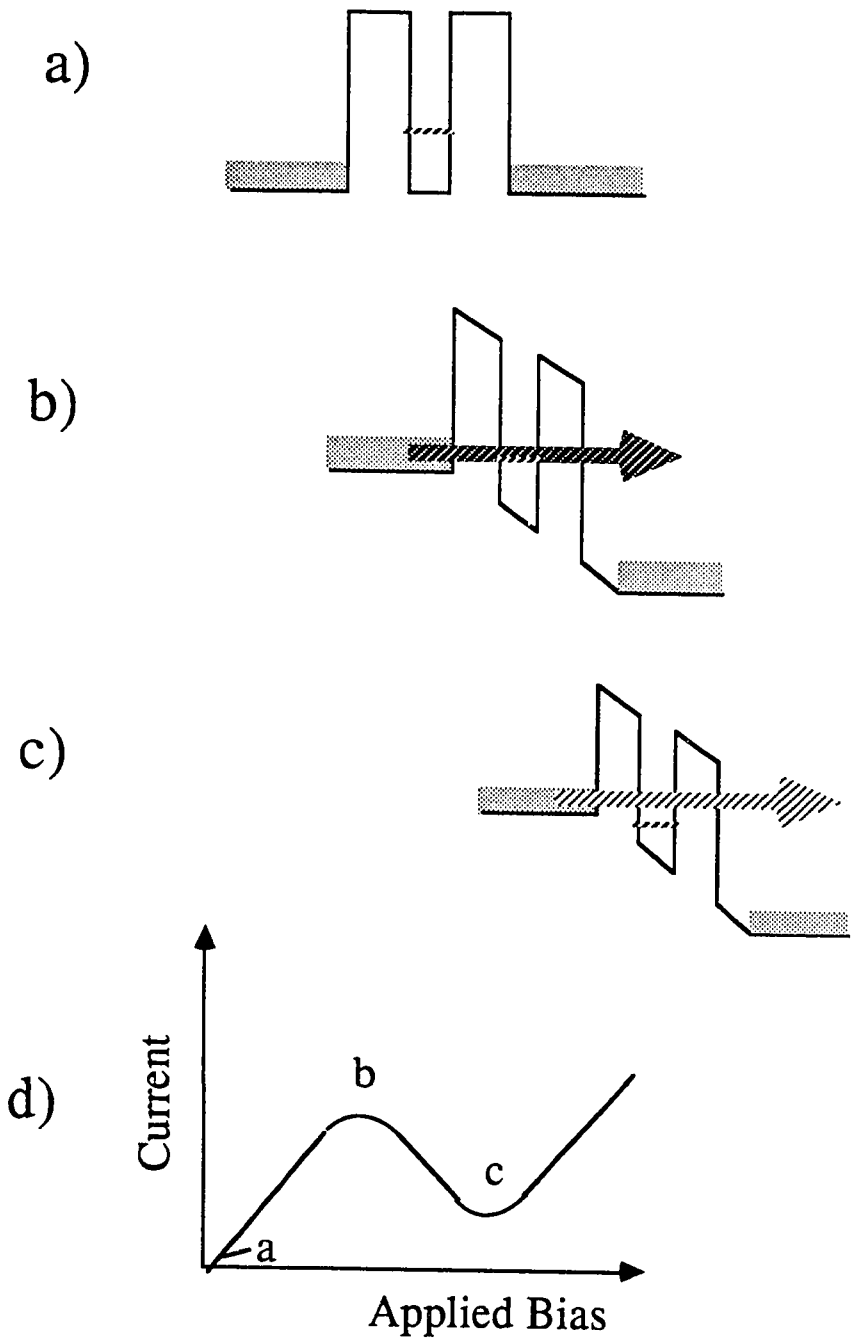

Figure 2.5 - A resonant tunneling diode band structure is illustrated for a) zero bias, b) at resonance and c) past resonance. A schematic of the current-voltage characteristics are shown for these points in d).

partially cancelled by the reflected electron wavefunction from the second barrier. When the bias across the device is such that a relative number of the carriers is in this resonance condition, a peak current will be observed. Further increase in the applied bias will terminate the resonance condition resulting in reduced carrier flow, this is referred to as negative differential conductance. The low current region at higher bias than the resonant peak is called the "valley" of the current-voltage (I-V) characteristics. Two important figures of merit for RTDs are the peak current density and the peak to valley ratio, which is the ratio of the maximum peak current to the minimum valley current.

Since it is possible to have multiple resonant states in a quantum well, it is possible to observe several resonances in the current-voltage characteristics of a RTD. One application of multiple regions of NDR is high speed frequency multiplication and division. This could be very useful for high frequency communications. A more exotic, and potentially more promising application of multiple resonant states is as a building block of multi-state logic systems.

References

1. M. G. Panish and A. Y. Cho, Spectrum 17 (4), 18 (1980).

2. K. Ploog, Molecular Beam Epitaxy of III-V compounds, in "Crystals-Growth, Properties, and Applications", Springer-Verlag, Heidelberg, (1979).

3. S. M. Sze, Physics of Semiconductor Devices, 2nd Edition, Wiley Interscience, New York (1981).

4. Michael Shur, "GaAs Devices and Circuits", Plenum Press, New York (1987).

5. M. I. Nathan, W. P. Dumke, G. Burns, F. H. Dills, and G. Lasher, Appl. Phys. Lett. 1, 62 (1962).

6. B. G. Streetman, Solid State Electronic Devices, 2nd ed., Prenice-Hall, Inc., Englewood Cliffs, N.J., 1980.

7. T.H. Wood, C. A. Burrus, D.A.B. Miller, D.S. Chemla, T. C. Damen, A. C. Gossard, and W. Wiegmann, Appl. Phys. Lett. 44, 16 (1983).

8. T.H. Wood, C.A. Burrus, Ah.H. Gnauck, J.M. Wiesenfeld, D.A.G. Miller, D.S. Chemla, and T.C. Damen, Appl. Phys. Lett. 47, 190 (1985).

9. Sadao Adachi, J. Appl. Phys. 58 (3), R1 (1985).

10. Michal Shur, "GaAs Devices and Circuits", p 119, Plenum Press, New York (1987).

11. Federico Capasso and Giorgio Margaritondo, "Heterojunction Band Discontinuities", North Holland, New York (1987).

12. T. P. Pearsall, "Gallium-Indium-Arsenide-Phosphide Alloy Semiconductors", Wiley, Ney York, (1982).

13. T.C.L.G. Sollner, W.D. Goodhue, P.E. Tannenwald, C.D. Parker, and D.D. Peck, Appl. Phys. Lett. 43, 588 (1983).

14. T. Mimura, S. Hiyamizu, T. Fujii, and K. Nanvu, Jpn. Appl. Phys. 19, L225-L227 (1980).

15. H. Kroemer, Proc. IRE 45, 1535 (1957).

16. H. C. Casey, Jr. and M. B. Panish, "Heterostructure Lasers", Academic, New York (1978).

17. S.Y. Chou and J.S. Harris, Appl. Phys. Lett. 53, (1988).

18. M.A. Reed, J. W. Lee, and H-L. Tsai, Appl. Phys. Lett.49, 158 (1986).

19. S.K. Diamond, E. Ozbay, M.J.W. Rodwell, D. M. Bloom, Y.C. Pao and J.S. Harris, Appl. Phys. Lett.54 (2), 153 (1989).

20. C.I. Huang, M.J. Paulus, C.A. Bozada, S.C. Dudley, K.R. Evans, C.E. Stutz, R.L. Jones, and M.E. Cheney, Appl. Phys. Lett. 51(2), 121 (1987).

21. Shunichi Muto, Tsuguo Inata, Yoshihiro Sugiyama, Yoshiaki Nakata, Toshio Fujii, H. Ohnishi and S. Hiyamizu, J J Appl Phys, Vol. 26, No. 3, March, 1987, pp. L220-L222.

22. E. Wolak, B.G. Park, Y.C. Pao, J.S. Harris, S.K. Diamond, E. Osbay, M.J.W. Rodwell, D.M. Bloom and E.R. Brown, unpublished.

23. K.L. Wand, R.P. Karunasiri, J. Park, S.S. Rhee, and C.H. Chern, Sprl. and Ms. 1989.

3. Tunneling Transport through a barrier system

In this chapter a method of modeling the current-voltage (I-V) characteristics of a resonant tunneling diode (RTD) is presented. Due to the presence of resonances in the current-voltage characteristics of these structures, it is possible to make comparisons between experiment and theory that are not possible for single tunnel barrier devices. In the first section, a general expression for tunneling through a barrier system is discussed. In the second section, the plane wave states of a finite superlattice system (a superset of RTDs) are solved within the effective mass approximation. The third section discusses the effects of non-parabolicity on tunneling. In section four, an expression for current flow through an arbitrary tunnel barrier is derived and current-voltage characteristics are modelled. Shortcomings of this approach are discussed at length in section five, and the sixth section contains a discussion of the comparison between the model and experimental results. Alternate approaches are compared with this model in section seven.

3.1 General expression for tunneling through a heterostructure potential barrier

The expression for tunneling through a heterostructure barrier system has been known for some time. The expression is derived within a time independent formalism. In principle it is possible to do this analysis within a time dependent formalism, however, the difficulty of formulating wave packets and propagating them through barriers greatly increases the computational difficulty and we do not pursue it.

The probability of tunneling from a given electron state through a barrier and into an empty state, is equal to the product of the probability of the initial state being occupied, the final state being unoccupied, and the transmission coefficient through the barrier[1]:

$$\text{State-state probability} = f_l(E)(1-f_r(E))\,|T(E,E_{\|},V)|^2 \ , \quad (3.1)$$

where $f_l(E)$ is the Fermi distribution function on the left side of the junction, $f_r(E)$ is the Fermi function on the right side of the junction, h is Plank's constant, and $|T(E,E_{||},V)|$, is the transmission amplitude as a function of the electron kinetic energy E, the energy parallel to the interface $E_{||}$, and the applied bias across the system V.

In order to obtain the total current from left to right due to tunneling, the contribution from all of the states on the l.h.s. of the barrier must be summed over. The || direction is defined as the direction parallel to the heterointerface, and the l or longitudinal direction is defined as the direction perpendicular to the heterointerface. Assuming the boundary condition that $k_{||}$ is the same in all components of the junction, the current transport from left to right is given by:

$$j_{lr} = \frac{e\,(2s+1)}{h} \int_0^{\infty} dE\, f_{(l)}(E)\,[1- f_{(r)}(E+eV)] \int_0^{\infty} \frac{d^2k_{||}}{(2\pi)^2} |T(E,E_{||},V)|^2 , \quad (3.2\ a)$$

where e is the electron charge, s is the spin and h is Planks constant. Similarly, transport from right to left is given by:

$$j_{rl} = \frac{e(2s+1)}{h} \int_0^{\infty} dE\ [1-f_{(l)}(E)]\, f_{(r)}(E+eV)] \int_0^{\infty} \frac{d^2k_{||}}{(2\pi)^2} |T(E,E_{||},V)|^2 , \quad (3.2\ b)$$

Quantitatively, the net current density through the barriers is given by the difference in current flow from left to right and that from right to left. The transmission coefficients,

$T(E,E_{||},V)$ are the same in equations (3.2a) and (3.2b) due to the use of the time independent, 1-d Schrodinger equation. Thus, we can write the net current through the barrier as:

$$j = \frac{e(2s+1)}{h} \int_0^{\infty} dE\, [f(E) - f(E+eV)] \int_0^{\infty} \frac{d^2k_{||}}{(2\pi)^2} |T(E,E_{||},V)|^2 , \qquad (3.3)$$

by taking the difference of (3.2a) and (3.2b). Differences in contact doping on each side of the device are accounted for by proper choice of the Fermi energy with respect to the conduction band minimum.

3.2 Wavefunction solution within the effective mass approximation

3.2.1 Use of the effective mass approximation

In order to model the current-voltage characteristics of the Resonant Tunneling Diode, we work within the effective mass approximation. Essentially, the dispersion relationship is assumed to be parabolic. This allows the use of the free space mechanics to calculate electron dynamics by assigning it an effective mass, m_n, for each epitaxial layer within which it travels. Bulk material values of m_n are used for the epitaxial structures.

The approximations inherent in the use of the effective mass approximation for solving a heterostructure transport problem must be considered. The effective mass approximation assumes a periodic potential due to the crystal lattice, this is an excellent approximation for a homogeneous pure crystal, or for a heterostructure where each material has the same periodic wave function; but it is possible that the periodic part of the wavefunction is

different in each of the materials of a heterointerface. In this calculation we assume that any differences in the periodic part of the wavefunction can be ignored and only the plane wave part of the electron wavefunction (or envelope function) is used. The effective mass approximation is also dependent on the bandstructure being parabolic near the band minimum. For GaAs this is a good approximation, however, for hot (or energetic) electrons or electrons tunneling through a high energy barrier it is important to consider the inclusion of non-parabolic effects.

3.2.2. The one dimensional wavefunction solution

The method used to calculate the transmission coefficient through a resonant tunneling diode is based on the assumption that the electron wavefunction through the device can be separated into the directions transverse to and along the direction of crystal growth (and/or current flow), which we define as the transverse and longitudinal directions, respectively. Under this assumption, the time independent envelope wavefunction along the longitudinal direction can be solved as a one dimensional problem. If we approximate the potential as a series of rectangular steps as shown in figure 3.1, the envelope function is locally given as:

$$\Psi_n = A_{1n}\exp(ik_n x_n) + A_{2n}\exp(-ik_n x_n)\,, \qquad (3.4)$$

Bastard's matching conditions[2] (matching electron flux) are used at each interface between segment n and segment n+1:

$$\Psi_n = \Psi_{n+1}\,, \qquad (3.5a)$$

$$(1/m_n)\, d\Psi_n/dz = (1/m_{n+1})\, d\Psi_{n+1}/dz\,, \qquad (3.5b)$$

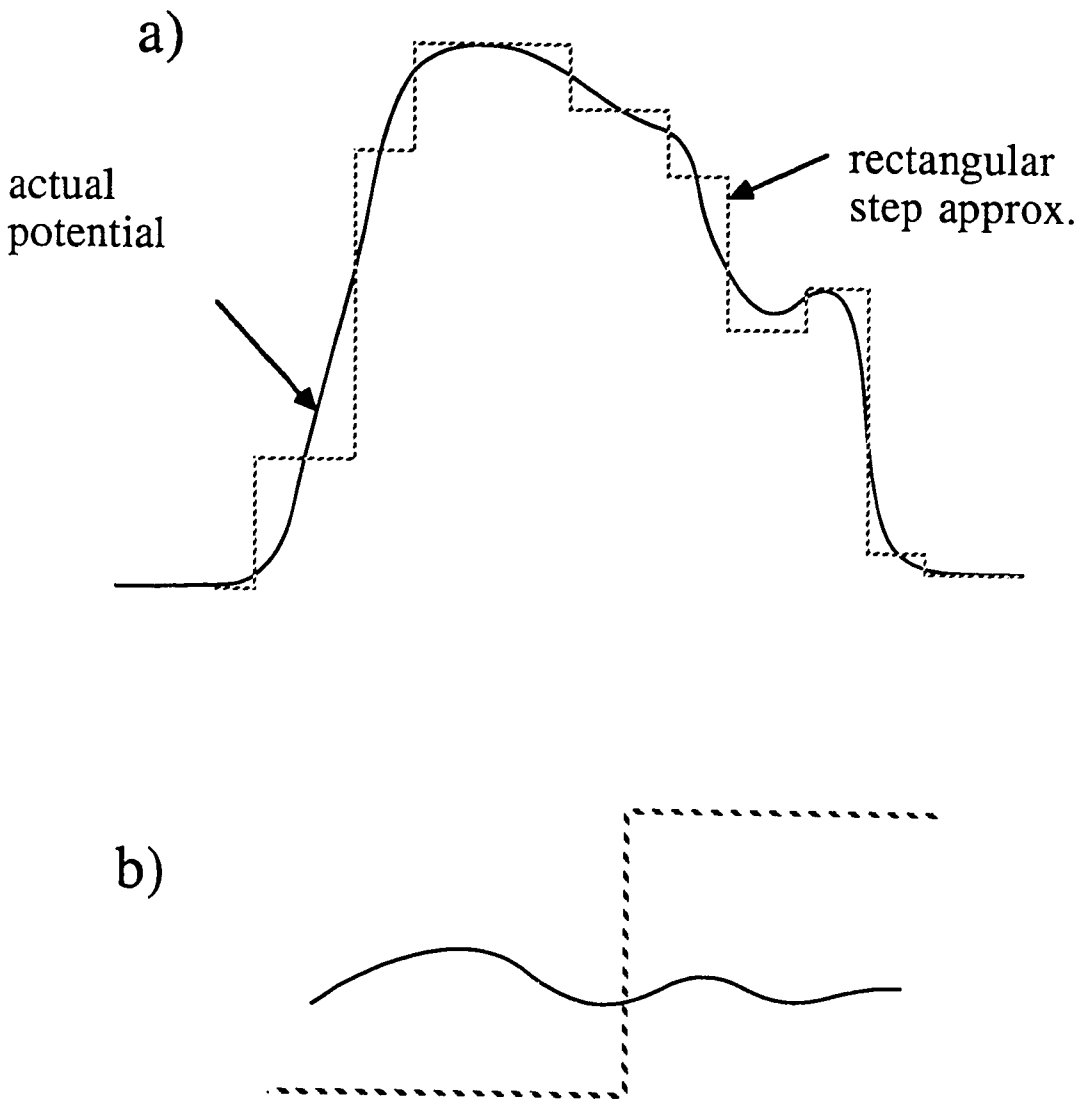

Figure 3.1 - It is shown how an arbitrary potential can be approximated as a series of rectangular steps in a), and the wavefunction A exp(kx)+B exp(-kx) can be matched at each interface in b), note that A, B and k can be complex and are generally different in each segment.

where m_n and m_{n+1} are the effective masses in each material. The envelope function for the entire structure can be found by using 2x2 matricies at each step to find the wave function amplitudes A_{1n} and A_{2n}:

$$\begin{bmatrix} A1_n \\ A2_n \end{bmatrix} = \frac{1}{2} \begin{vmatrix} (1+\frac{m_n k_{n+1}}{m_{n+1} k_n}) e^{i(k_{n+1}-k_n)x_n} & (1-\frac{m_n k_{n+1}}{m_{n+1} k_n}) e^{-i(k_{n+1}+k_n)x_n} \\ (1-\frac{m_n k_{n+1}}{m_{n+1} k_n}) e^{i(k_{n+1}+k_n)x_n} & (1+\frac{m_n k_{n+1}}{m_{n+1} k_n}) e^{i(-k_{n+1}+k_n)x_n} \end{vmatrix} \begin{bmatrix} A1_{n+1} \\ A2_{n+1} \end{bmatrix} \quad (3.6)$$

where x_n is the position at the nth interface, k_n and k_{n+1} are the values of the wavevector on each side of the interface, and m_n is the effective mass in each segment[3].

The 2x2 transfer matricies found in the above manner can be multiplied together for each interface so that the relationship between wavefunction amplitudes on each side of the superlattice are related by a 2x2 matrix. The transmission coefficient can be extracted by using the ratio of the wavefunction amplitudes on each side of the barrier structure:

$$T = \frac{A1_N m_N \sqrt{k_N}}{A1_1 m_1 \sqrt{k_1}} \quad , \quad (3.7)$$

where T is the transmission coefficient, k_N is the longitudinal component of the wavevector on the collector side of the barrier, k_1 is the wavevector on the emitter side, $A1_N$ is the wavefunction amplitude on the collector side and $A1_1$ is the amplitude on the emitter side[4].

3.2.3 The nature of the transmission coefficient

An understanding of the coherent tunneling current through a resonant tunneling device can only be achieved by analysis and implementation of all of the aspects of the expression for tunneling current, however, valuable insight can be gained by understanding some of the aspects of the transmission coefficient which lie at the core of the problem.

Depending on the bias across the RTD, the transmission coefficient can show distinct resonances as a function of incident electron energy. The transmission coefficient is shown for several applied biases in figure 3.2. As the bias across the device increases, the resonance is brought into alignment with the incident sea of electrons. Ultimately, additional bias will bring the lowest resonance below the incident electron sea resulting in a NDR condition.

As can be seen from inspection of equation 3.3, the transmission coefficient is essentially convolved with the incident electron flux to obtain the tunneling current. Thus the width and peak magnitude of the transmission resonances all effect the current-voltage characteristics of a RTD. These resonances have been shown to be Lorenzian in nature as a function of energy[5]. The width of the transmission probability is dependent on the relative transparencies of the tunneling barriers, and the peak of the transmission probability is based on equal transparency of the tunneling barriers at the resonant bias condition. For symmetric barriers it is possible for the maximum value of the transmission coefficient to be unity, however, in general the transparencies of the quantum barriers will only be equal under one bias condition (if at all). In fact, the barriers of most RTDs are symmetric under zero bias, and are assymetric under the resonance bias condition.

The width of the transmission resonance peak is important in considering the current-voltage characteristics of these structures. Relatively transparent barriers will tend to broaden the resonance, so that near the resonant bias condition more incident electrons will have a high transmission probability. Though thick barriers may increase the

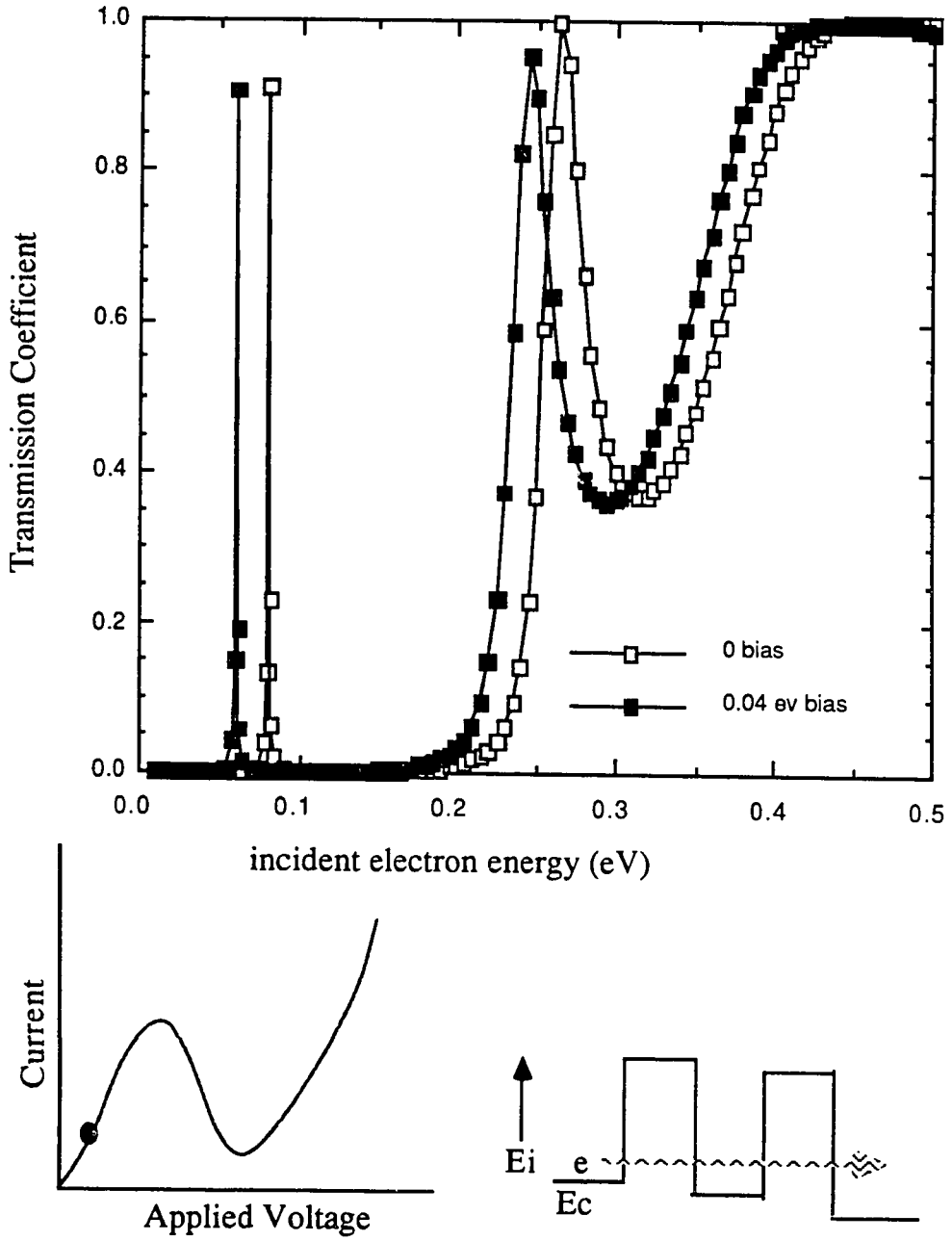

Figure 3a - The transmission coefficient for a resonant tunneling device is shown with 0 bias and 40 meV applied bias. Notice the shift in the incident electron energy needed for resonant transmission.

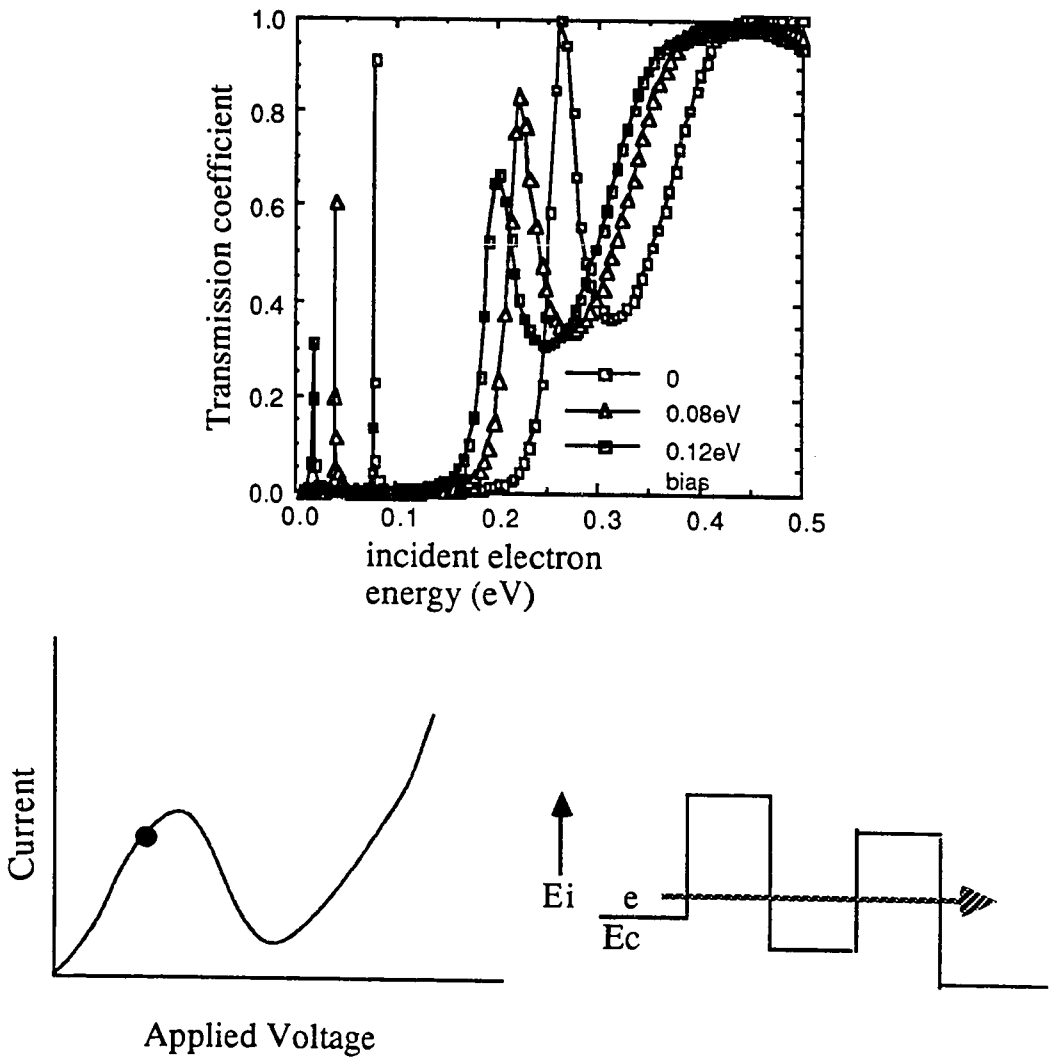

Figure 3.2 b - As bias is applied accross the resonant tunneling diode, the transmission resonance drops into the incident electron sea. Note that assymetry of the barriers under bias reduces the maximum of the transmission resonance.

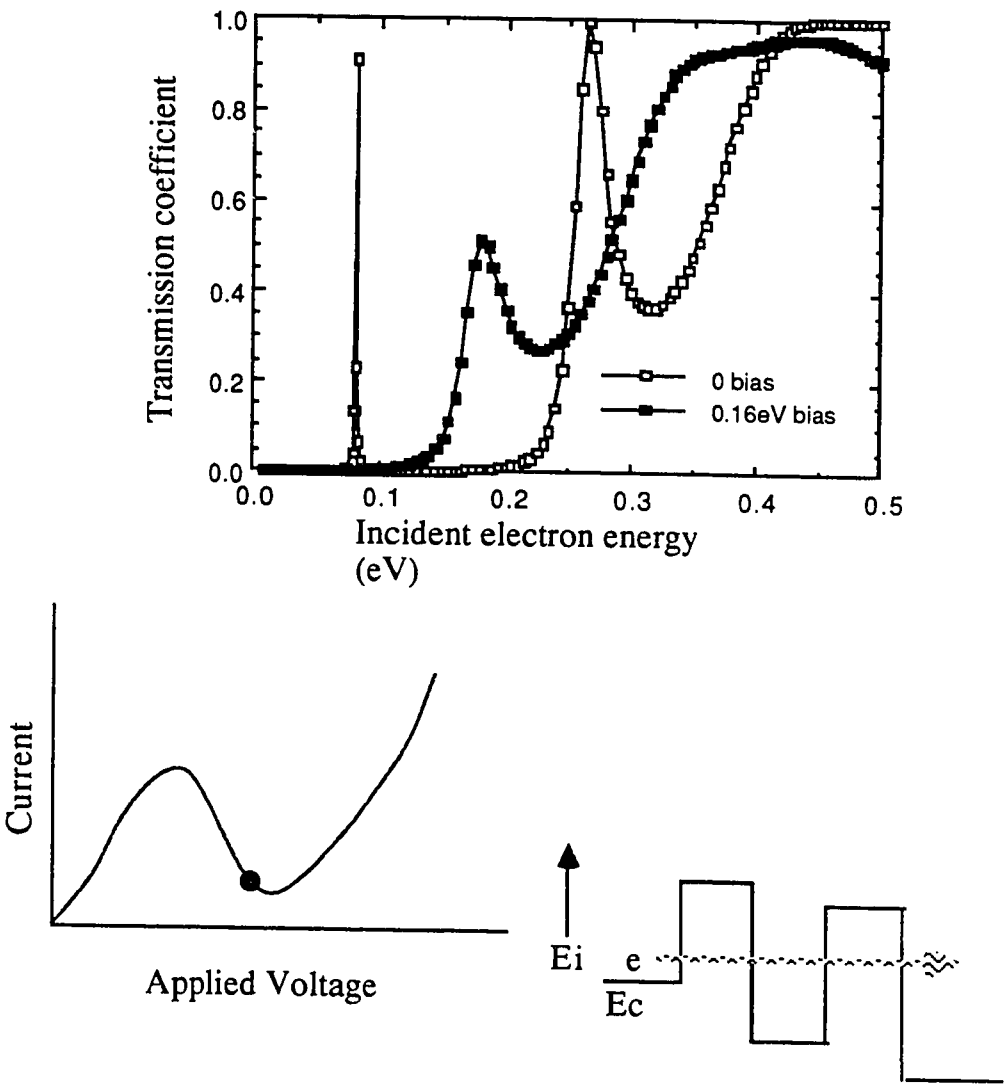

Figure 3.2 c - When enough bias is applied across the RTD, , it is no longer possible to coherently tunnel through the ground state resonance as evidenced by the low transmission coefficient. The result is negative differential resistance.

magnitude of the peak transmission resonance, the width of the resonance is decreased and the current will be diminished. This also holds true for the use of assymetric barriers; though the peak transmission probability may be increased by making one of the barriers thicker, the resonant current is decreased due to the resulting narrowing of the transmission resonance[6].

The proximity, width and strength of other transmission resonances must also be considered when analyzing the current-voltage relationships. If only a small additional bias is necessary to reach the next transmission resonance, it is possible for the peaks in the current-voltage characteristics to overlap, even to the point of becoming indistinguishable. A broad resonance can tend to add current over a broad range of applied bias, thus masking narrower resonances.

3.3 Complex Band Structure

3.3.1 Conduction band non-parabolicity

In the conduction band, the approximation $E=h^2k^2/2m^*$ is only an accurate approximation for low energy electrons as can be seen from the inspection of the band diagram in figure 3.3. The relationship between E and k can be found from LCAO, the k·p method or related methods. It is apparent that the parabolic approximation starts to break down when the electron energy is near 70 meV. The first corrective term may be found using a k·p method[7] to find the next term, however, this method is only useful to approximately 150 meV and it quickly becomes worse than not including the correction at all. It is possible to make a reasonably good approximation to the band structure by fitting a fourth order term to the E vs. k relationship. This type of approximation is good to about

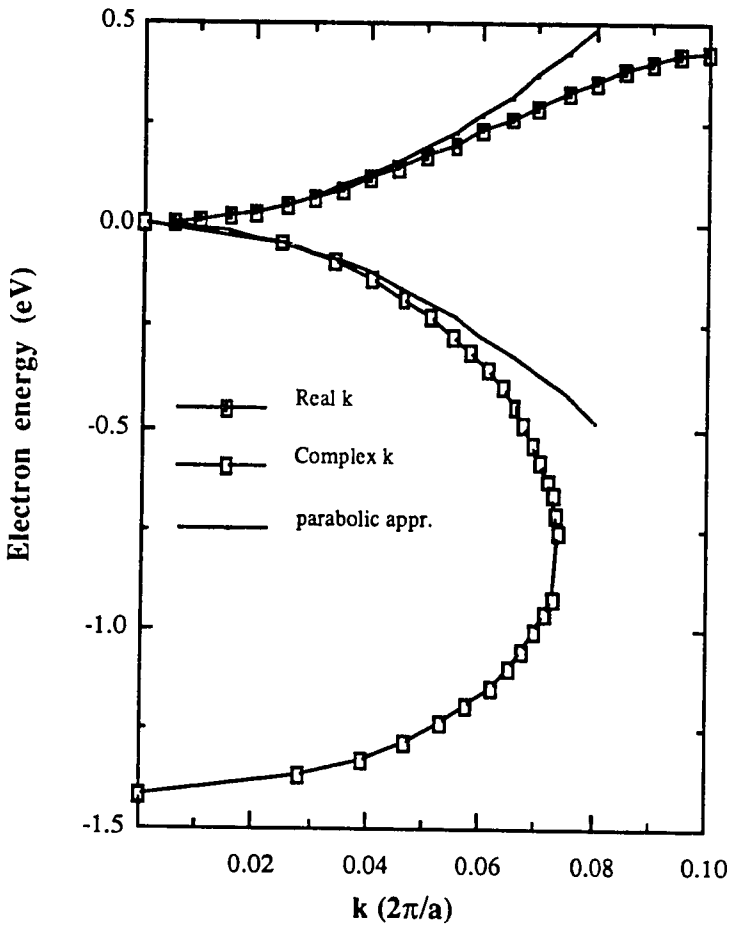

Figure 3.3 - The conduction band and imaginary band diagrams for GaAs, with parabolic dispersion relations drawn in for comparitive purposes.

500 meV and it can be extended by adding a higher order terms in the polynomial expansion or by using other numerical methods. In the implementation of this model, conduction band non-parabolicity is not addressed.

3.3.2 Imaginary band non-parabolicity

In an infinite unbounded crystal only solutions of the wavefunction with a real wave vector are allowed, or else the wavefunction amplitude would increase without limit. But at a heterojunction there can exist solutions with a complex wavevector (the imaginary part of the wave vector being perpendicular to the interface) for the part of the wavefunction which is within the energy gap. The dispersion relationship for such wavevectors can be found from k·p theory[8]. An analytical approximation for this dependence is plotted in figure 3.3:

$$E = E_o \pm h^2\gamma\,(k^2 + \gamma^2)^{1/2}/m_{\pm}^*, \qquad (3.9)$$

where k is the complex wave vector, m_+ is the effective mass at the conduction band minimum, m_- is the effective mass at the valence band maximum, E_o is the energy at which dk/dE=0 and γ is the absolute value of k at that point. The constants E_o and γ are given by:

$$E_o = E_c - E_{gap}/(1+ m_+/m_-)\,, \qquad (3.10a)$$

$$\gamma = \{\, E_{gap}/[h^2\,(1/m_+ + 1/m_-)]\}, \qquad (3.10b)$$

where E_{gap} is the energy gap of the material and E_c is the energy of the conduction band minimum. Equation (3.9) can be written such that k is a function of E:

$$k=[(E-E_o)^2 m_c^2 h^{-4}\,\gamma^{-2} - \gamma^2]^{1/2}, \qquad (3.11)$$

We include the complex band structure in the wavefunction solution by substituting (3.11) into the envelope function matching conditions (3.5) when the longitudinal energy of the electron is exceeded by the local potential.

3.3.3 Including the effects of non-parabolicity in the matching conditions

The non-parabolic dispersion relationship is included in the model by substituting the wavevector found from (3.11) into the wavefunction matching conditions and the transmission coefficient equations (3.5-3.7). This is essentially equivalent to approximating the dispersion relation as parabolic, except that the specific parabola is a function of the electron energy. A much more involved set of matching conditions would be required to treat the problem properly due to the fact that the matching conditions are themselves based on the effective mass approximation.

3.4. Modeling the current-voltage characteristics of RTDs

3.4.1 expression for tunneling through a finite superlattice

The above expressions establish the framework for modeling current transport through a RTD. Due to the nature of the RTD crystal structure, it is usually a good approximation to seperate the variables along the growth direction and perpendicular to it. The one dimensional wavefunction solution outlined above can be used to find the transmission coefficient strictly as a function of longitudinal energy of the incident electron. The integration of the expression for current density (3.3), over incident transverse wavefunctions becomes analytical, the result being an integral over the longitudinal energy[1,3]:

$$j = \frac{4\pi m^* kT}{h^3} \int_0^\infty dE_x \, |T(E_x,V)|^2 \ln\{\frac{1+\exp((E_f-E_x)/kT)}{1+\exp((E_f-E_x-eV)/kT)}\}, \quad (3.12)$$

where q is the magnitude of the electronic charge, E_l is the electron energy in the direction of tunneling, E is the total electron energy, f is the Fermi-Dirac distribution function, V is the applied voltage, h is the Planck constant, $E = E_l + E_t$, in which electronic energy transverse to the tunneling direction, E_t, is quantized, and $|T(E_l,V)|^2$ is the tunneling probability as a function of longitudinal energy and applied voltage.

3.4.2 Calculating the current-voltage characteristics of a RTD

Using the above expressions, the current-voltage characteristics of a RTD can be modelled. The local fluctuation in charge density is given by using a one dimensional Poisson equation solver along the direction of growth[9]. Up to 150 points are selected for each bias condition of interest, including points at each hetero-interface. The discontinuity of the quazi-Fermi level is taken to be at the first hetero-interface.

The potential is approximated by assuming an equal potential between each two adjacent points[10], with an abrupt step or interface at each point as shown in figure 3.1. The quantum region is taken to start within the heavily doped emitter layer so that any band bending before the heterointerface is accounted for in the transmission coefficient. The plane wave matching conditions are invoked at each interface to find the transmission coefficient as described in the previous section. Equation (3.12) is integrated using a Newton-Coates 8 panel quadrature method (Quanc8) to find the current-voltage characteristics of the device being simulated. The quantum region is taken to start within the heavily doped emitter layer so that any band bending before the heterointerface is

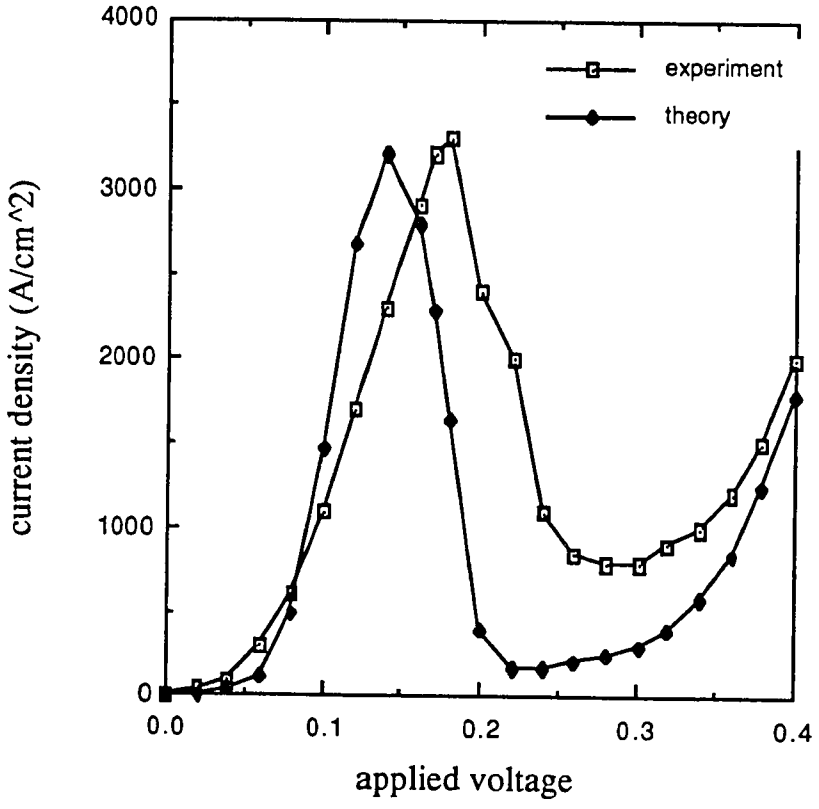

Figure 3.4 - A comparison of experiment with the coherent transport theory. The resonant bias position is in typically good agreement, the resonant current is typically predicted to within a factor of two. Notice that the valley currents are not accurately predicted by this model.

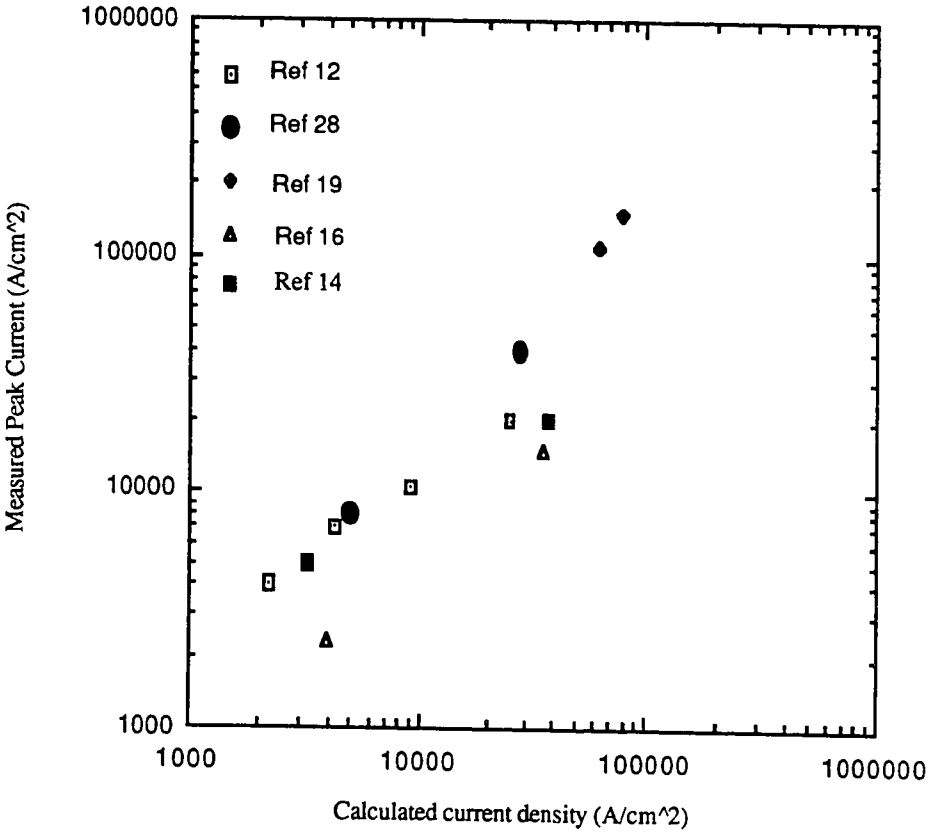

Figure 3.5 - The coherent model is compared against putblished data covering two orders of magnitude. The coherent model agrees with the published data to within a factor of 2, which is good agreement considering the strong dependence of the tunneling current on the well and barrier thicknesses.

accounted for in the transmission coefficient. The numerical integration is carried out for electron kinetic energies ranging from 0 to at least 500 meV, the upper limit depending on the specifics of the problem. If the upper limit is set correctly, than any contribution from the "thermionic" current component[11] is also included in the model.

3.4.3. Simulation results and discussion

The method described above is very effective in simulating the coherent part of the current voltage characteristics of resonant tunneling devices[12]. The main transmission resonance is accurately predicted, as are subsequent transmission resonances. The lowest energy resonance is typically much sharper than the higher energy (and less confined) resonances. In general, the simulation results will show much more extreme values of the peak to valley ratio than are observed in the actual device. This is largely due to the effects left out of the simulation.

The quantitative agreement of the model for peak current density is good as can be seen from the comparisons in figures 3.4 and 3.5. The peak position is usually estimated correctly within 50%, and much of the discrepancy is due to series resistance effects in the physical device. As a result, the measured peak voltage is almost invariably higher than the predictions of the coherent transport model. The peak current is usually correctly predicted to within a factor of 2, which is very good considering the fact that monolayer fluctuations can have a very strong effect on current densities in a tunneling device.

For a given barrier composition, thicker barriers tend to result in a strong decrease in the resonant current with only minor effects on the resonant voltage, as shown in figure 3.6. An increase in the potential offset at a heterointerface due to a changing barrier composition can have a similar effect. In the GaAs/AlAs materials system this is done by increasing the

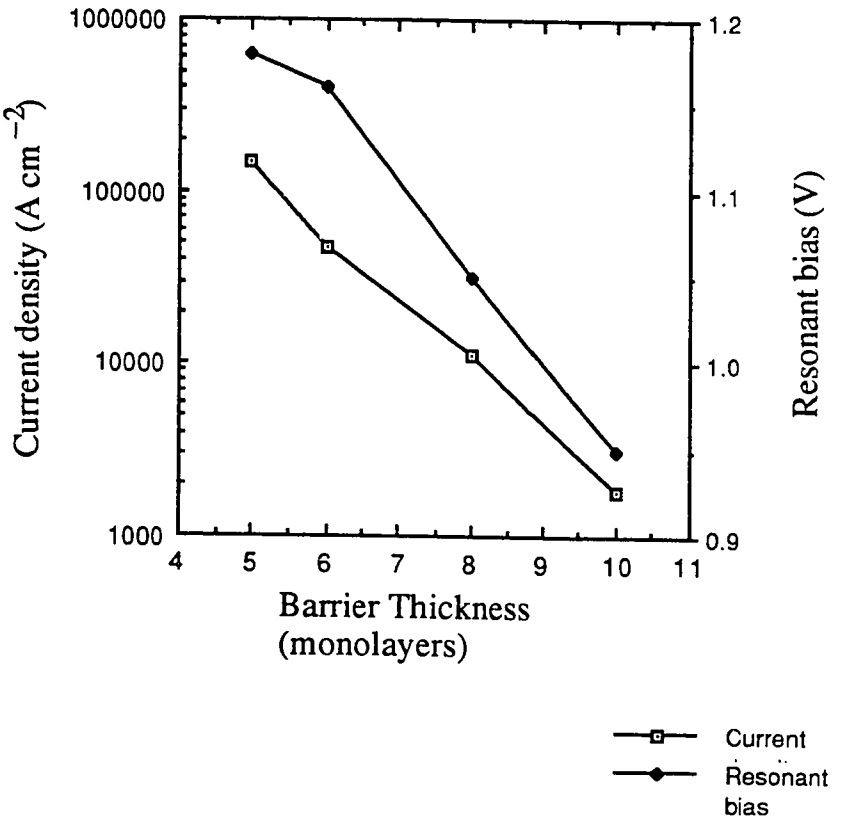

Figure 3.6 - The simulated dependence of the resonant current density and the resonant bias is plotted against barrier thickness for a device with 1E18 contact doping, a 100 Å first spacer layer, a 700 Å second spacer layer, and a 45 Å well operating at room temperature. Note that changing the barrier thickness by even a few monolayers has an exponential effect on the resonant current with only a minor impact on the resonant bias.

Al composition of the barrier alloy. As a result, it is possible to design different barriers of similar transparencies by choosing the correct combinations of barrier composition and thickness.

Usually, the best possible peak to valley ratio possible is sought for any given current density at resonance. With this in mind, it has been analytically demonstrated that the best choice in heterobarriers for any given transparency are high and thin instead of low and thick, as the higher barriers are more effective at reducing the thermionic component of the tunneling current[13]. This is numerically demonstrated in figure 3.7 for three $Al_xGa_{1-x}As$ barrier RTDs. The predicted peak to valley ratio and peak current density both increase with increasing Al mole fraction for the given choices of barrier thickness. Due to the X-Γ valley crossover, it is not clear whether this type of optimization can be extended beyond an Al mole fraction of x=0.4.

Most RTDs are designed with two equal barriers, however, such barriers are assymetric for an incident electron when the structure is biased into the resonant condition. The strongest resonance conditions are achieved when the reflectivities of the two barriers are roughly equal for the incident electrons at the resonant bias. A strong resonance condition can be created for a given bias by using barriers which are nominally dissimilar. As bias is put across the RTD, the transparency to incident electrons for the second barrier changes faster than that of the first, eventually resulting in roughly equal transparency. If the equal transparency is coincident with the resonant bias condition, the resonant current can be enhanced for any total barrier thickness by shifting material from the first barrier to the second as demonstrated in figure 3.8. This effect has been observed experimentally by applying bias in different directions across an RTD with assymetric barriers. If the thickness of the first barrier is fixed, however, an increase in the thickness of the second barrier results in a monotonic decrease in the resonant current as shown in figure 3.9.

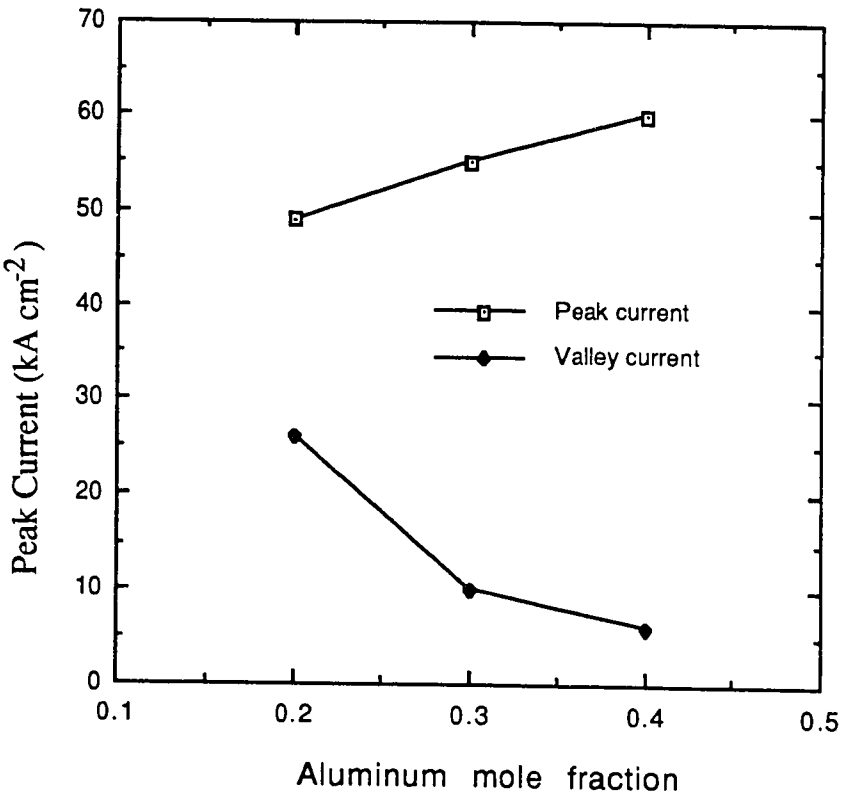

Figure 3.7 - The aluminum mole fraction of the barriers was raised from 0.2 to 0.4, the barrier thicknesses being 47 Å, 36 Å, and 30 Å respectively. At room temperature assuming 1E18 contact doping and a 90 Å undoped first spacer layer, the simulation shows an increase in the resonant current and a decrease in the valley current. This improvement in peak to valley current ratio is due to the reduction in thermionic processes with higher potential barriers.

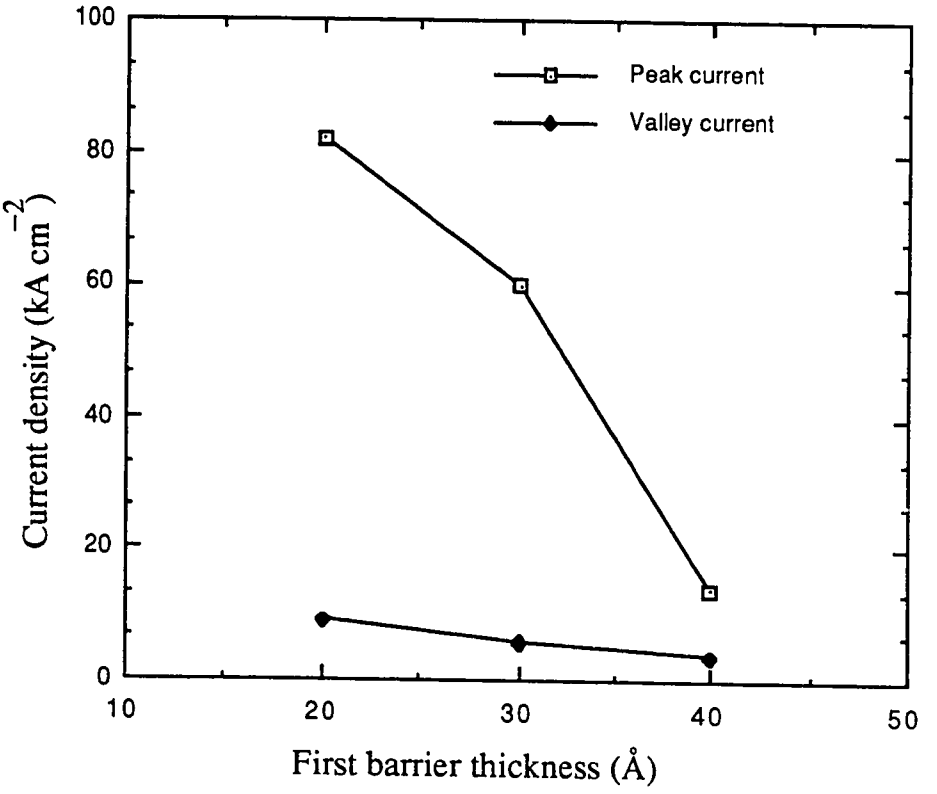

Figure 3.8 - For a fixed total barrier thickness, an increase in the peak current density is predicted when less of the barrier material is in the first barrier and less is in the second barrier. This is due to the barrriers becomming more symmetric at the resonant bias condition. This effect can be experimentally observed by using different bias conditions on a device with assymetric barriers. The total barrier thickness was fixed at 60 Å, a 50 Å well, 90 Å emitter spacer and 300 Å collector spacer were assumed.

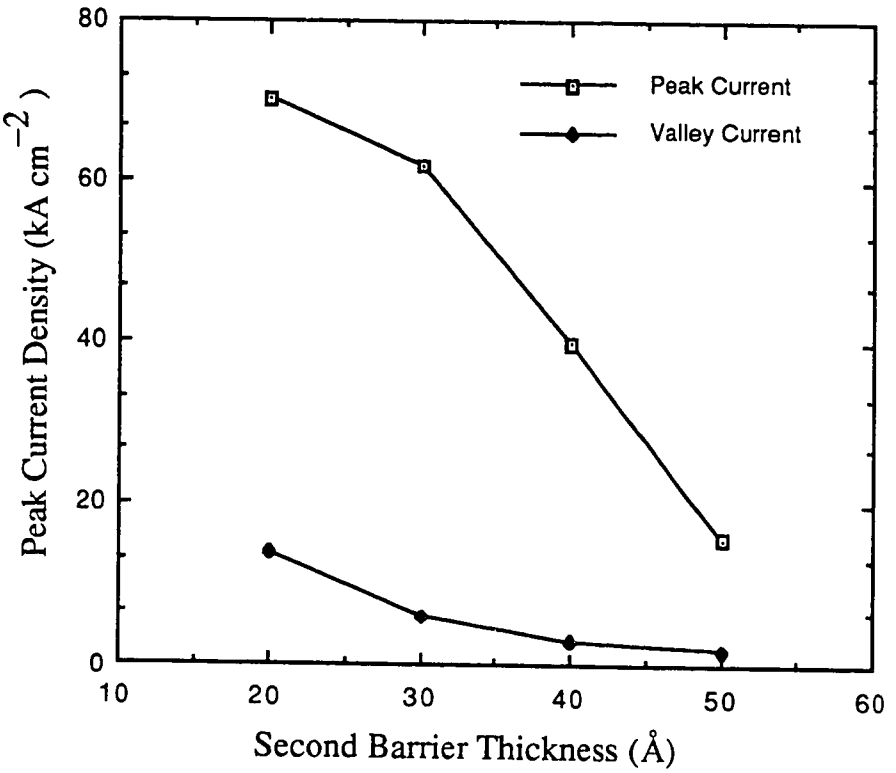

Figure 3.9 - The effects of assymetric barriers are examined by using a fixed first barrier and changing the thickness of the second barrier. The resonant and valley currents are plotted as a function of the thickness of the second barrier. An AlGaAs alloy with 40% Al mole fraction was used for the barriers, the first barrier thickness was 30 Å, the emitter spacer was 90 Å and the collector sapecr was 300 Å. Contact doping of $1x10^{18}$ cm^{-3} was assumed.

The width of the quantum well has a strong influence on both the bias needed to reach the resonant condition and the resonant current density as shown in figure 3.10. Similar to the case of the quantum barriers, increasing the width of the well decreases the resonant current in an exponential fashion. As a result of this similarity, even a slight miscalibration in crystal growth can have a huge impact on the resonant current as the change in resonant current, due to changes in both wells and barriers is complimentary instead of offsetting. For this reason, the factor of two agreement between the coherent model and the measured current density shown in figure 3.5 can be considered to be very good.

Wells containing In alloys can be made to drop the resonant level from what it would be otherwise. As a result, less bias is generally needed to achieve the resonant condition. In fact it is possible to lower the ground state resonant energy below the conduction band edge on the emitter side, thus making a ground state resonance impossible. This possibility has been explored in a preliminary fashion in RTDs made of both GaAs/AlAs and in InP lattice matched alloys.

The undoped collector spacer has it's principle influence on the amount of bias needed to achieve resonance and on the quality of the device itself. Larger undoped collector spacers require larger biases across the RTD to achieve resonance, due to the voltage drop across these spacer layers. There is little effect on the magnitude of the resonant current from changing the collector spacers, however, the valley current tends to decrease with increasing collector spacer due to improvements in crystalline quality and a reduction in scattering effects[12].

The width of undoped spacer layers on the emitter side of a RTD influences both the current density and the resonant bias as shown in figure 3.11. By increasing the amount of undoped spacer material on the emitter side of the device, a potential hill is formed which pinches off the resonant current as can be seen by comparing figures 3.11 and 3.12. The presence of the emitter spacer also influences the amount of bias needed to achieve

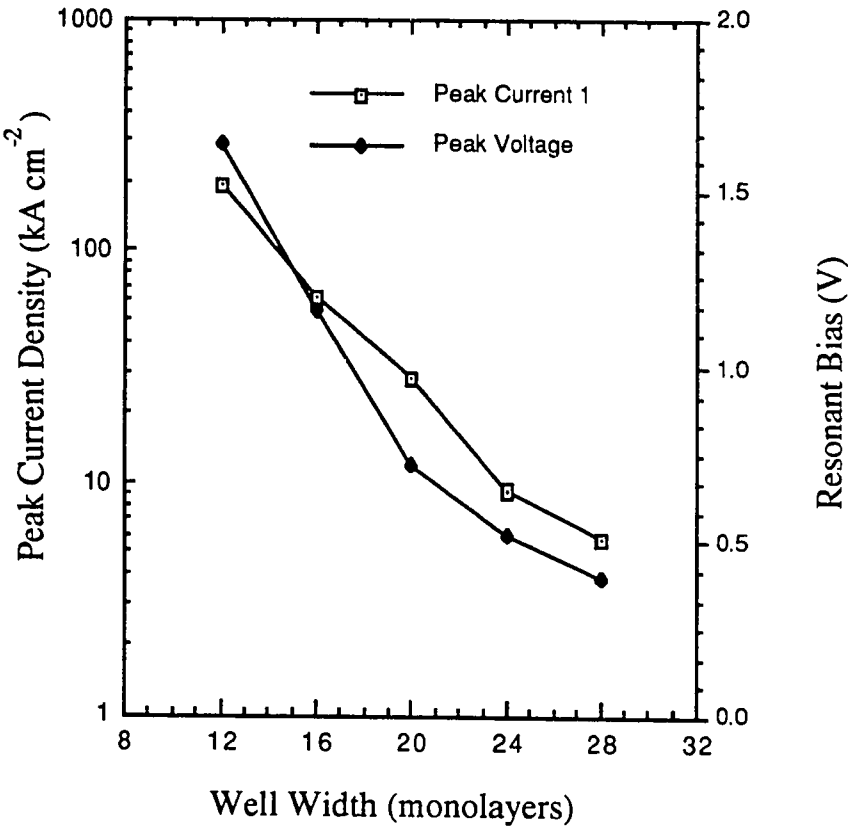

Figure 3.10 - The variation of the resonant bias and resonant current density with changing well width is shown. The devices simulated had 6 monolayer barriers, 100 Å emitter spacer layers, 700 Å collector spacer layers, and a contact doping of $1x10^{18}$ cm^{-3}. The variation in current density with well thickness is similar to, but not as strong as the variation with barrier thickness. The change in resonant bias is due to the shift in the energy of the resonant state with changing well width.

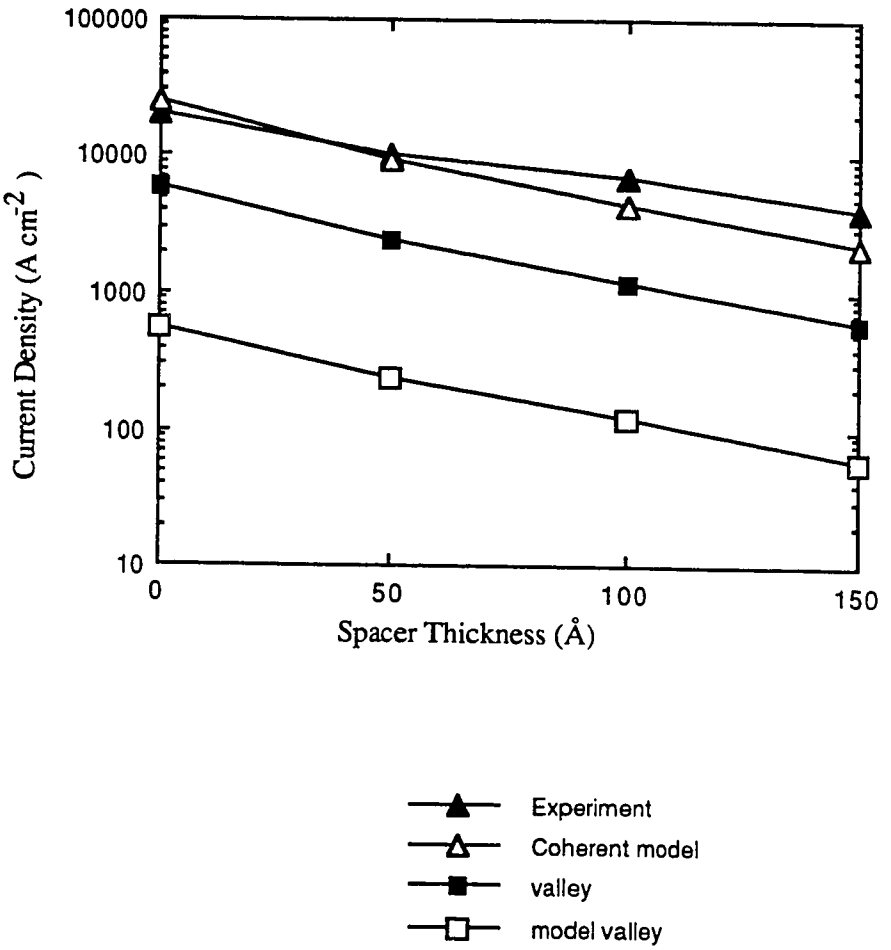

Figure 3.11 - A comparison of the data of Muto et. al. (please see reference 12, chapter 3) with the coherent model. The agreement between the predicted and measured resonant resonant current is good, though it starts breaking down for large emitter spacers. The valley current follows the predicted trend but is off quantitatively by an order of magnitude.

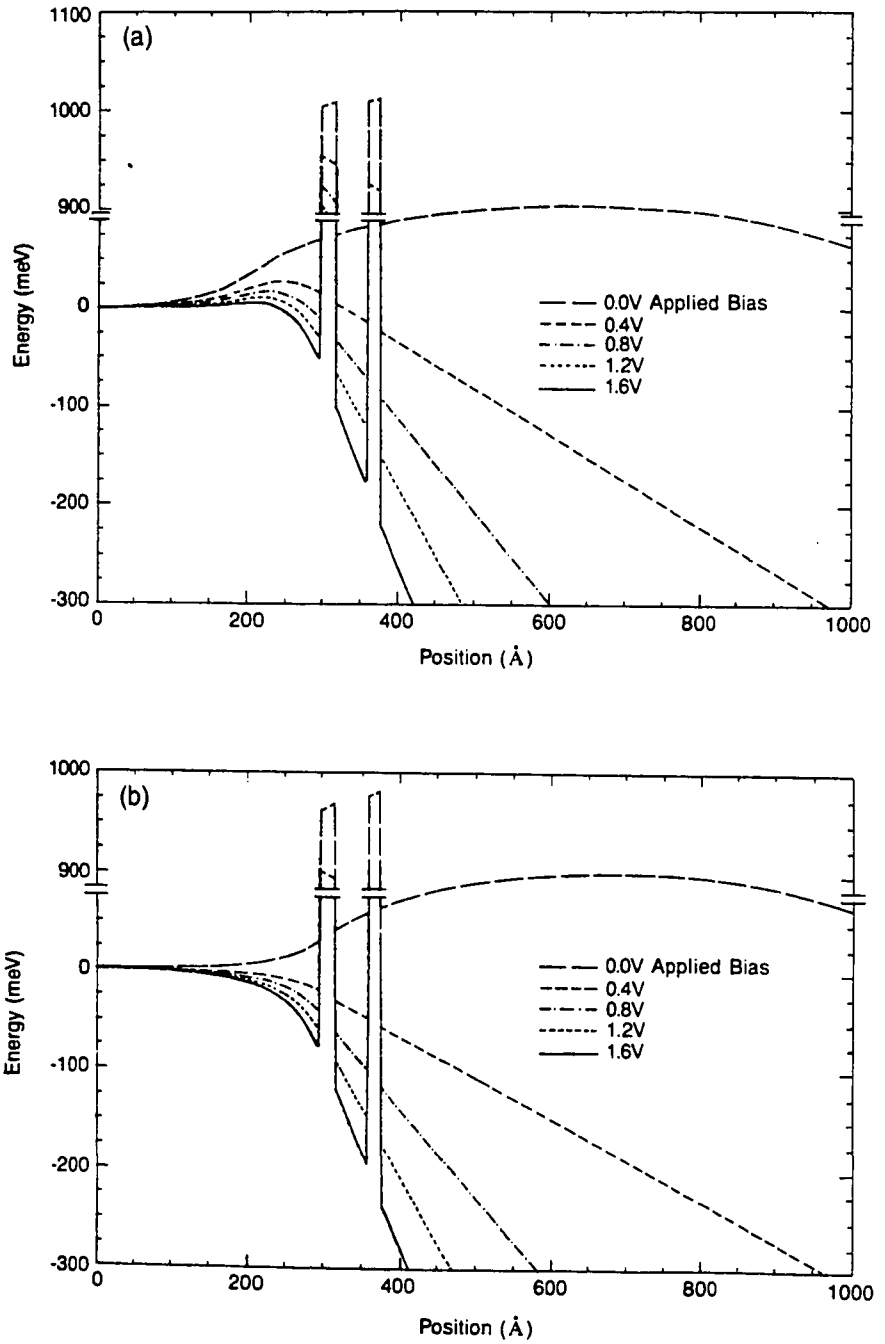

Figure 3.12 - The Poisson equation solution on the conduction band minimum is for resonant tunneling structures with a 700Å undoped second spacer and (a) no undoped emitter spacer and (b) a 100Å undoped emitter spacer. The 100Å emitter spacer helps reduce the effects of accumulation layer formation and impurity scattering.

resonance, as an increase in this layer generally leads to a decrease in the amount of bias needed to align the incident electrons with the resonant state.

The contact doping of a RTD influences the resonant bias condition and the resonant current as shown in figure 3.13. The Fermi energy was calculated assuming complete ionization of the dopants and using the Joyce Dixon approximation[14]. In general, increasing the contact doping will have a small effect on the resonant current once the incident spread of electrons is similar in width to the width of the transmission resonance. Changes in the contact doping also change the band structure in the emitter part of the RTD, thus complicating the predicted trends in the resonant current.

3.5. Limitations of this method

Knowledge of the effects which break down this analysis are crucial to making this model a useful tool for analysis and extrapolation of experimental results.

There are several factors which limit the applicability of the coherent transport model for double barrier resonant tunneling diodes, all of which are potential contributors to the deviations between the model and experiment. Any physical process which disturbs the condition of transverse momentum conservation will violate the separation of variables condition upon which this model is based[15]. Several such processes are possible, including; elastic scattering from ionized impurities[15], phonon scattering[16], scattering due to interface roughness[17], scattering due to alloy non-uniformity, and changes in the transverse effective mass.

As quantum transport is assumed through the undoped spacer layers, scattering or phonon emission in the emitter spacer may cause additional valley currents or even additional resonances. Thus undoped or lightly doped ($<10^{17}$ cm^{-3}) spacer layers of more than a few hundred Å on the emitter side can make this model ineffective. The effects of elastic impurity scattering and accumulation layer formation can contribute to the valley

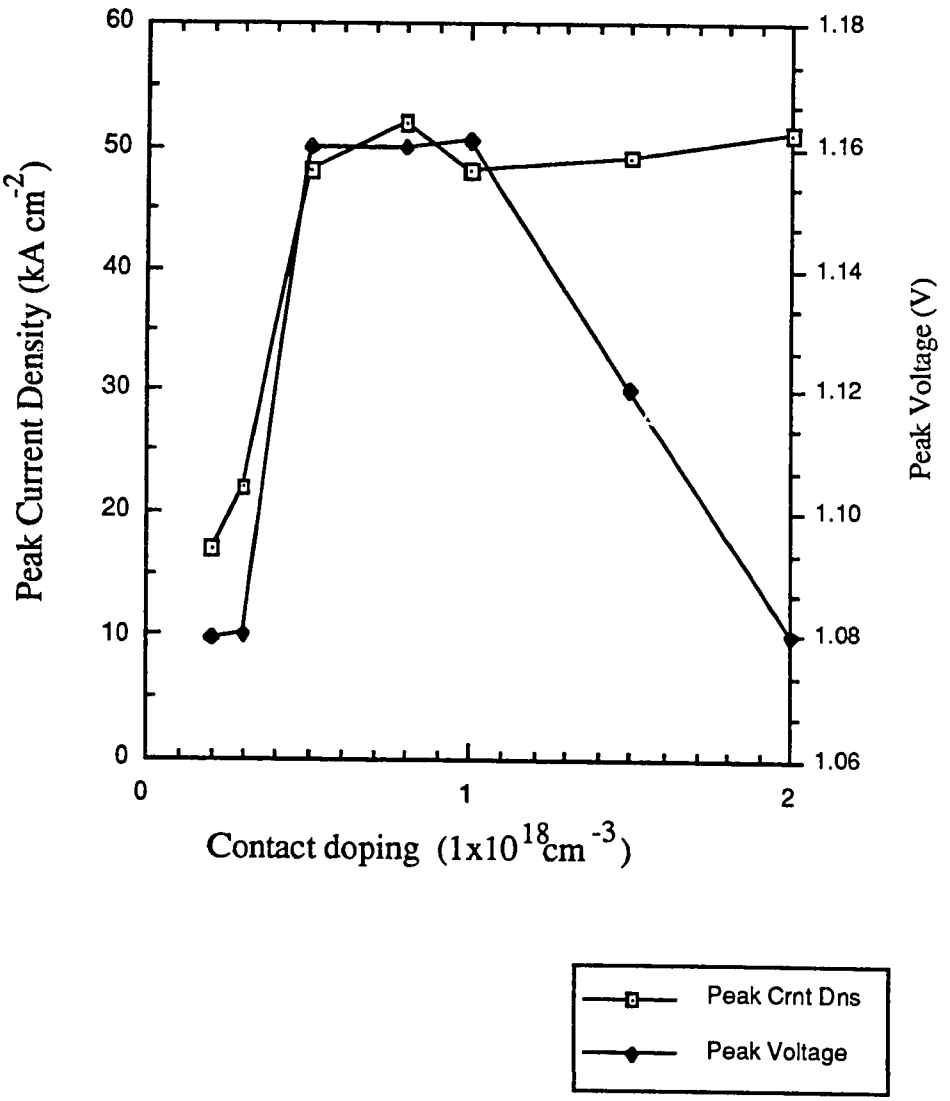

Figure 3.13 - The resonant current density and resonant bias for a device with varied contact doping. The barriers were chosen to be 6 monolayers, the well was 16 monolayers, and the undoped spacer layers were 100 Å on the emitter side and 700 Å on the collector side respectively.

current as shown in figure 3.14. Scattering due to impurities on the collector side may also contribute to increased valley current. Figure 3.12 shows how the use of a 100 Å spacer layer reduces the formation of the accumulation region . The resulting potential hill, however, can reduce the current flow. The use of multi-step or graded spacer layers may lead to better devices by reducing the bulge in the conduction band caused by the undoped spacer layer while suppressing accumulation layer formation under bias.

Inelastic scattering events should not change the resonant current of the device to first order if the incoming electrons have an energy distribution which is broader than the width of the resonance[16]. They may, however, alter the background non-resonant current of the device near room temperature. Phonon emission within the well of the DBRTD can add to the valley current by reducing the longitudinal energy of the incident electron such that it falls into an energy within the transmission resonance. A similar effect may result from phonon emission in the accumulation layer which is on the emitter side of the device.

Elastic scattering events can cause a degradation in the current-voltage characteristics of a RTD[12,15]. The most common sources of elastic scattering are ionized impurity centers and interface roughness. Ionized impurities are discussed at length in chapter 4 of this thesis. Interface roughness scattering is discussed by Sakaki et. al.[17] and it is shown to be a major source of the reduction of the peak to valley ratio of RTDs. In general, scattering events which change the longitudinal momentum component will effect the current-voltage characteristics, while scattering events which change the longitudinal momentum should not impact the I-V characteristics.

The possibility of electrons scattering into the X valley[18], specifically at a hetero-interface, must be considered in order to fully understand the behavior of these devices. This problem is very important in the case of AlAs tunnel barriers within a GaAs crystal due to the relatively small energy difference between the longitudinal X valley of AlAs and the Γ valley of GaAs. A substantial amount of work has been done on the

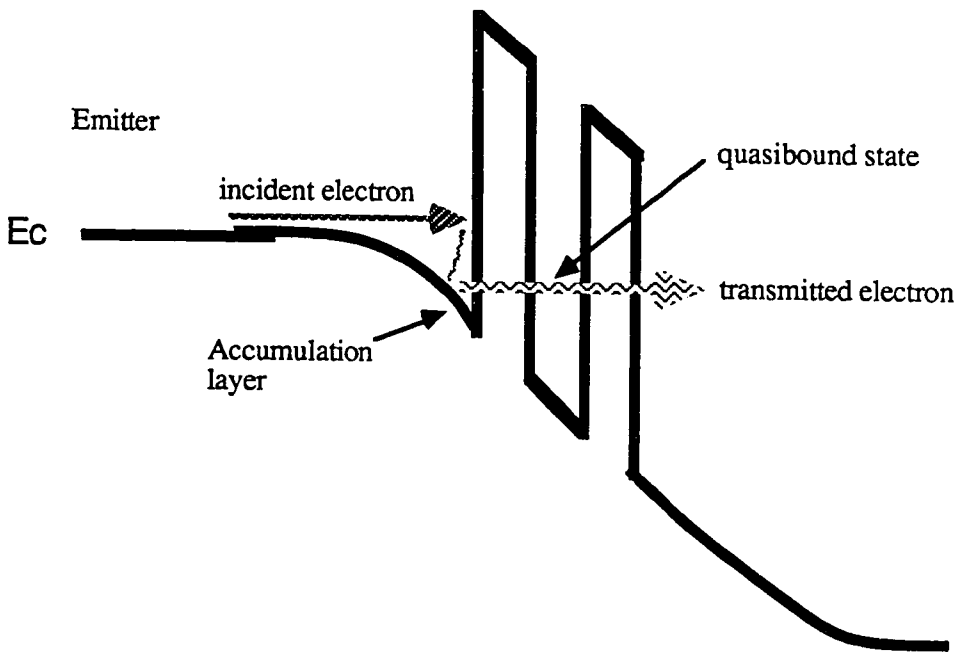

Figure 3.14 - Electrons filling the accumulation layer on the emitter side of the RTD add current in the valley bias condition. It is possible that quasibound states in the accumulation layer aligning with the resonant state in the well can cause peaks or additional structure in the current-voltage characteristics.

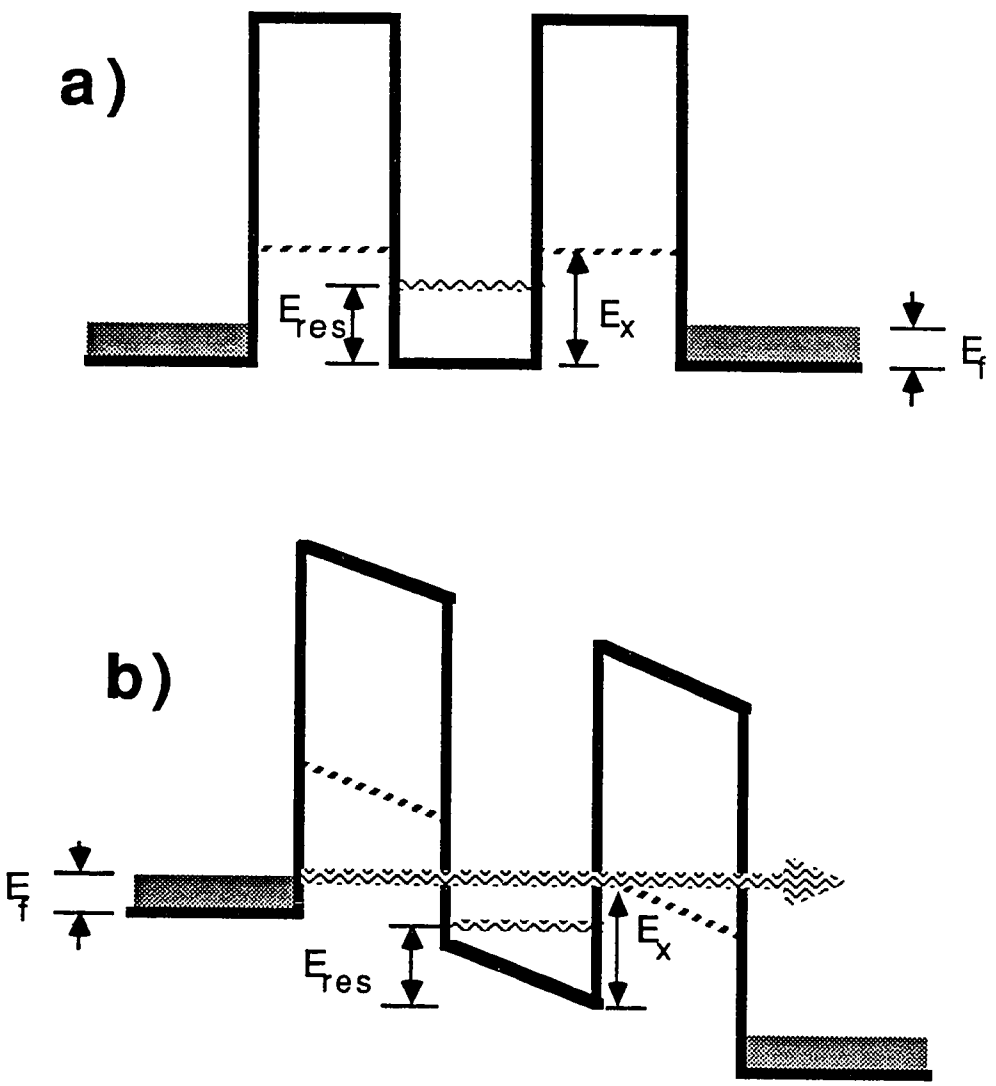

Figure 3.15 - At a heterointerface, it is possible for electrons to scatter into the longitudinal X valley, thus causing an additional current contribution not predicted by strict gamma valley transport. In figures a and b, it is shown how resonances above the X-valley minimum in AlAs cause severe degradation of the I-V curve.

problem of Γ - X band mixing, but a model of these effects which is both computationally accessible and physically reliable has yet to be developed.

Qualitatively, it is known that such effects can decrease the peak to valley ratio of a RTD. It is also known, that as the X barrier is lowered, tunneling through this pathway becomes more significant[19] as illustrated in figure 3.15. It is reasonable to conclude, therefore, that higher energy electrons incident on the tunneling barrier are more likely to be affected by Γ - X band mixing than the lower energy electrons. Thus, to avoid a low peak-to-valley ratio it is important to keep the resonant state below the X-point energy in the barrier. It is also important to keep the spread of incident electron energies, (and thus the emitter doping,) low enough so that when the bottom of the conduction band is at resonance, the electrons at the Fermi energy are below the X-point. From these considerations we arrive at a rough limitation on the applicability of the RTD model:

$$E_f + E_{res} < E_x$$

where E_f is the difference between the Fermi energy and the conduction band minimum, E_{res} is the resonant state energy at the resonant bias, and E_x is the energy of the X point of the collector barrier.

The use of the effective mass approximation and the envelope function to determine electron transport through the structure may also introduce deviations from experimental measurements for several reasons. The use of non-parabolic band structure only partially addresses this issue, notably in our implementation of the model. The possibility of dissimilar Bloch wavefunctions is not considered in the envelope function approximation, and this could lead to breakdown of this model if it were an important effect; apparently this is not the case in the GaAs/AlGaAs material system. For thin tunneling barriers, the effective mass approximation based on bulk parameters must fail, presently the limit for this breakdown is assumed to be 2-5 monolayers. In addition, the change of effective masses at the hetero interface violates the separation of variables condition; this effect is

thought to be small, but it becomes more important as the transverse momentum increases. At this time, however, the above assumptions are probably the best approach for making a model which is both computationally accessible and relatively accurate.

3.6 Using the model to Design RTDs

At present, our ability to compute all of the physical phenomena which occur in a RTD is incomplete, however, use of the available information at this time yields useful information about RTD design. The energy of the resonant state is very well understood and physical measurement of the resonant bias condition is well predicted by the model. The current density due to coherent transport through the double barriers is also accurately predicted. The processes which are not addressed in this model tend to cause degradation of RTD operation (as measured by the peak to valley ratio) and thus the RTD should be designed such that these effects are minimized.

The peak current of the RTD is largely determined by the width and magnitude of the transmission coefficient. By making devices with a larger peak transmission coefficient and a wider transmission resonance, it is possible to make devices with higher peak current densities[20]. The transmission coefficient is determined by both the energy difference and thickness of the quantum barriers. In general, it is best to achieve a desired transparency by using thin high barriers, as such barriers are more effective in blocking current flow due to more energetic electrons as shown in figure 3.7.

The choice of quantum well width is best determined by considering several physical phenomena. It is important to get good separation between the resonant states in order to achieve a high peak to valley ratio. In addition, the desired resonant state must be higher in energy than the Fermi level on the collector side if a large difference in electron distributions, and thus large current density, are to occur. Narrow quantum wells may be used to achieve this, however, the use of a narrow quantum well raises the lowest resonant

state and this increases the amount of bias needed to reach resonance. As a result, increased current flow through the X valley, and increased accumulation layer formation, may result in the degradation of the peak to valley ratio of the device. In addition, interface scattering effects become more important with narrower wells due to the increased resonant energy splitting from monolayer fluctuations in the barriers. As a result, wells of approximately 50 Å have been used for ground state resonance effects. Wider wells tend to have more resonances with a decreasing energy difference between them, and wells narrower than 30Å have not attained observable resonances for the reasons described in section 3.5.

Emitter doping is a parameter that can be used to directly trade off peak current density and peak to valley ratio for an RTD. As doping is increased, the energy distribution of electrons convolved with the transmission resonance is increased. This has two effects, first the peak current density is increased, however, as the spread of incident electron energies rises so does the possibility of tunneling through higher resonances, thus valley current is also increased.

In addition to determining the tunneling current by setting the Fermi level, doping concentrations change the tunneling current due to band banding effects. By the proper use of an undoped spacer layer on the collector side of the RTD, it is possible to reduce capacitance, and increase the peak to valley ratio by quenching the accumulation layer on the emitter side at little cost to the peak current density as shown in figure 3.11 and 3.12. Also, the degradation of the peak to valley ratio due to elastic scattering effects is reduced. The use of an undoped spacer also acts as a lever which changes the amount of bias needed across the device in order to achieve resonance. The effects of ionized impurities are discussed at length in chapter 4 of this thesis[15].

3.7. Comparison with other methods

There have been alternate methods proposed for modelling the current-voltage characteristics of RTDs, as well as some debate as to the interpretation of the underlying physical mechanism governing the negative differential resistance effect. These two subjects are very intimately related and are best covered together. The method outlined in this chapter assumes as it's basis a coherent wavefunction through the barrier system. The major shortcoming of the coherent method is that it is difficult to include the effects of scattering in the model. An alternative mechanism of achieving negative differential conductance through a double barrier structure has been proposed and labelled sequential tunneling[21]. Sequential tunneling does not assume coherence through the entire structure, and thus models which assume a scattering interaction within the device are often referred to as sequential tunnelling models.

3.7.1 Sequential vs. Coherent Tunnelling

There has been a substantial amount of controversy about the sequential and coherent mechanisms of tunneling[21,22,23]. In the original paper by Luryi[21], proposing the sequential tunneling mechanism, there was a calculation made of the fundamental time constant of coherent resonant tunneling which limited operation to a few GHz. This low estimate lead Luryi to conclude that an alternate mechanism for transport through the double barrier system should be explored, and this mechanism was dubbed sequential tunneling. It was stated that all that was needed for sequential tunneling to occur, was a reduction in the dimensionality of the conducting channel. In the case of the RTD, the reduction in dimensionality would arise from the double barriers themselves. This implied the possibility of resonant tunneling from bulk material to a 2 dimensional electron gas and subsequently draining this current by transverse electron transport. The apparent experimental realization of this was used to validate the sequential tunneling approach[20].

Many of the assertions made by Luryi in the original papers on sequential tunneling have been shown to be invalid[23,24,25]. Other workers recalculated the time constant for resonant tunneling assuming a coherent wavefunction through the structure, and obtained much higher frequencies of operation than Luryi did[24,25]. By using the coherent model presented in this chapter, it was shown that the "experimental realization" of resonant tunneling from a system with three degrees of freedom to a system with two degrees of freedom was ambiguous[23], (and that coherent tunneling was a plausible explaination). It has also been shown that if no scattering occurs, that a sequential model would yield the same current densities as a coherent model[16]; this is logical because a measurable quantity should not be dependent on the model used to describe it, assuming that both models are correct and that the same conditions exist in both cases .

If scattering does occur, however, the coherent model needs to be modified or reconsidered. Both the sequential and coherent approaches suggest that a change in the longitudinal momentum of the electron in a scattering event is required to change the I-V characteristics[15]. By using a modified transfer matrix model and examining the effects of level broadening due to scattering effects, the transition between a coherent and sequential tunneling mechanism has been examined[26]. Such an approach is useful, notably if sequential and coherent tunneling are viewed as approaches which are valid depending on the physical mechanisms which are occurring. Coherent tunneling is an accurate description with low scattering rates, and sequential tunneling could be used as a phrase to explain any scattering assisted tunneling phenomena. In subsequent chapters of this thesis, the effects of elastic scattering are approached analytically as a perturbation to the coherent model.

3.7.2 Alternative models of the current-voltage characteristics of resonant tunneling devices

Models which include the effect of scattering have been developed, and a variety of approaches have been used. These include a Wigner function method[24], a modified Boltzmann method[27], and the modification of the coherent model discussed above[26].

Using the Wigner function method fully can give information about both the D.C. and time dependent aspects of the resonant tunneling device. This approach also yields more realistic values of the peak to valley ratio at room temperature than coherent models though the agreement deviates for low temperatures. Implementation of the Wigner function method is computationally intensive, however, ultimately there is much promise to this approach.

A related approach has been to use a Boltzman transport approach, by treating the superlattice as a series of barriers and conductors. This may prove useful in the development of equivalent circuits for electronic applications and in the regime of heavy scattering effects where the coherent model breaks down. Such an approach must encompass quantum reflections if it is to be used to model RTDs with good peak to valley ratios.

References:

1. C.B. Duke, Tunneling in Solids, Solid State Suppliment 10.

2. G. Bastard: 'Superlattice band structure in the envelope-function approximation', Phys. Rev. B., 24, 5693 (1981).

3. R. Tsu and L. Esaki, Appl. Phys. Lett. 43, 588 (1983).

4. Alex Harwit, Thesis, Stanford University 1987.

5. E. R. Brown, W.D. Goodhue and T.C.L.G. Sollner, Journal of Applied Physics, 64 (3), 1519 (1988).

6. E.R. Brown, T.C.L.G. Sollner, W.D. Goodhue, and C.D. Parker, Appl. Phys. Lett., 50 (2), 83 (1987).

7. T. Hiroshima and R. Lang; Appl. Phys. Lett., **49**, 456 (1986)..

8. J.N. Schulman and T.C. McGill; Phys. Rev. B., 23, 4149 (1981).

9. M.S. Lundstrom and R. J. Schnelke, IEEE Trans. Electron Devices ED-30, 1151 (1983).

10. M.O. Vassel, J. Lee and H.F. Lockwood, Journal of Applied Physics 54, 5206 (1983).

11. Rhoderick and Williams, "Metal-Semiconductor Contacts", Mystery House Press, Atlantic City, New Jersey, (1988).

12. Shunichi Muto, Tsuguo Inata, Hiroaki Ohinishi, Naoki Yokoyama and Satoshi Hiyamizu, Japan Jour. Appl. Phys., 25 (7), L577 (1986).

13. Masahiro Tsuchiay and Hiroyuki Sakaki, Appl. Phys. Lett. 50 (21), 1503 (1987).

14. Herbert Kroemer, Journal of Applied Physics, 52, 873 (1981).

15. E. Wolak, K.L. Lear, P.M. Pitner, E.S. Hellman, B.G. Park, T. Weil, and J.S. Harris Jr., Appl. Phys. Lett. 53 (3), 201 (1988).

16. T. Weil and B. Vinter, Appl. Phys. Lett. 50, 1281 (1987).

17. M. Tsuchiya and H. Sakaki, Appl. Phys. Lett. 49, 88 (1986).

18. David Yuk Kei Ko and J C Inkson, Semicond. Sci. Technol. 3, 791 (1988).

19. E.E. Mendez, E. Calleja, and W.I. Wang, Appl. Phys. Lett. 53, 977 (1988).

20. S.K. Diamond, E. Ozbay, M.J.W. Rodwell, D.M. Bloom, Y.C. Pao, E. Wolak and J.S. Harris, Electron Device Letters, 10, 104 (1989).

21. S. Luryi: Appl. Phys. Lett. 47, 490 (1985) .

22. H. Morkoç, J. Chen, U.K. Reddy, T. Henderson, and S. Luryi, Appl. Phys. Lett. 49, 70 (1986).

23. E. Wolak, Alex Harwit, J.S. Harris, Jr., Appl. Phys. Lett. 50, 1610 (1987).

24. W. R. Frensley, Phys. Rev. Lett. 57, 2853 (1983).

25. D.D. Coon and H.C. Liu, 49 (2), 94-6 (1986).

26. Rita Gupta and B.K. Ridley, Journal of Applied Physics, 64, 817 (1988).

27. J. Sikkoken, Superlattices and Microstructures 4, (3), 1988.

4. Ionized impurities in RTDs

4.1 Motivation for studying elastic scattering centers

4.1.1 Ionized impurities as a design parameter

Ionized impurities are a crucial element of RTD operation, yet they can be detrimental to the device because any ionized donor is in fact an elastic scattering center. As the location and quantity of ionized impurities can be controlled by MBE, it is important to their understand their effect on the tunneling current of the device. Large undoped spacer layers surrounding the double barrier structure shift the resonant bias of the RTD through band bending effects. This shift can be controlled and is thus a design parameter for adjusting the resonant bias. The presence of dopants near the RTD, however, have been shown to reduce the peak to valley ratio of resonant tunneling devices. Therefore, it is important to study the effect of elastic scattering within and near the well of a resonant tunneling diode. The ballistic model outlined in the previous chapter does not include this effect, as the major impact of elastic scattering is to break the separation of variables condition upon which the ballistic model is based.

Several workers have investigated the role of elastic scattering events in resonant tunneling devices, including the effect of ionized impurities in the layers immediately outside of the device[1,2,3,4] as well as scattering due to interface roughness. The use of doping impurities within the RTD itself has been intentionally implemented[5] and also occurs unintentionally due to background impurities and diffusion; in addition, related structures are being proposed and implemented which include ionized impurities in the wells and barriers of the device[6,7]. In this chapter, we demonstrate experimentally that ionized impurities in a RTD shift the resonant voltage and reduce the peak to valley ratio of the device. The shift in resonance voltage is predicted by the coherent transport model

from chapter 3, the reduction in peak to valley ratio is not. A scattering assisted tunneling mechanism which raises the valley current of these devices, and is consistent with the change in peak to valley ratio observed in this experiment, is proposed and analyzed.

4.1.2 Elastic scattering in momentum space and scattering assisted transport

In order to understand the role of elastic scattering centers placed in a barrier system with a one dimensional potential profile V(1), we separate the problem into a longitudinal part, (motion perpendicular to the quantum barriers) and a transverse part (motion parallel to the barriers). In the absence of scattering, transverse momentum is conserved, thus we can define the quantities $E_t \equiv h^2 k_t^2/(2m^*)$ and $E_l \equiv E - E_t - V(1)$ which can be thought of as energies parallel and perpendicular to the wells, respectively; where h is Plank's constant, m* is the effective mass of the electron in GaAs, and E is the sum of the kinetic and potential energies of the electron. Total kinetic energy is conserved in an elastic scattering event, however, the quantum barrier structure removes three dimensional symmetry resulting in the possibility of momentum transfer between the longitudinal and transverse directions. Elastic scattering events which conserve transverse energy, as depicted in figure 4.1a, will not change the I-V characteristics of the device[8]. On the other hand, elastic scattering events which transfer momentum from the longitudinal to the tranverse direction, or vice versa, break the condition of transverse energy conservation upon which ballistic transport models are based.

Scattering allows transitions though the DBRTD which would otherwise be improbable. A specific example of this is the scattering of an electron by impurities in the well of a DBRTD; such scattering could allow an electron which has an incident longitudinal momentum higher than the transmission resonance, to scatter into a longitudinal momentum within the resonant band as shown in figure 4.1b, thus resulting in the transmission of the

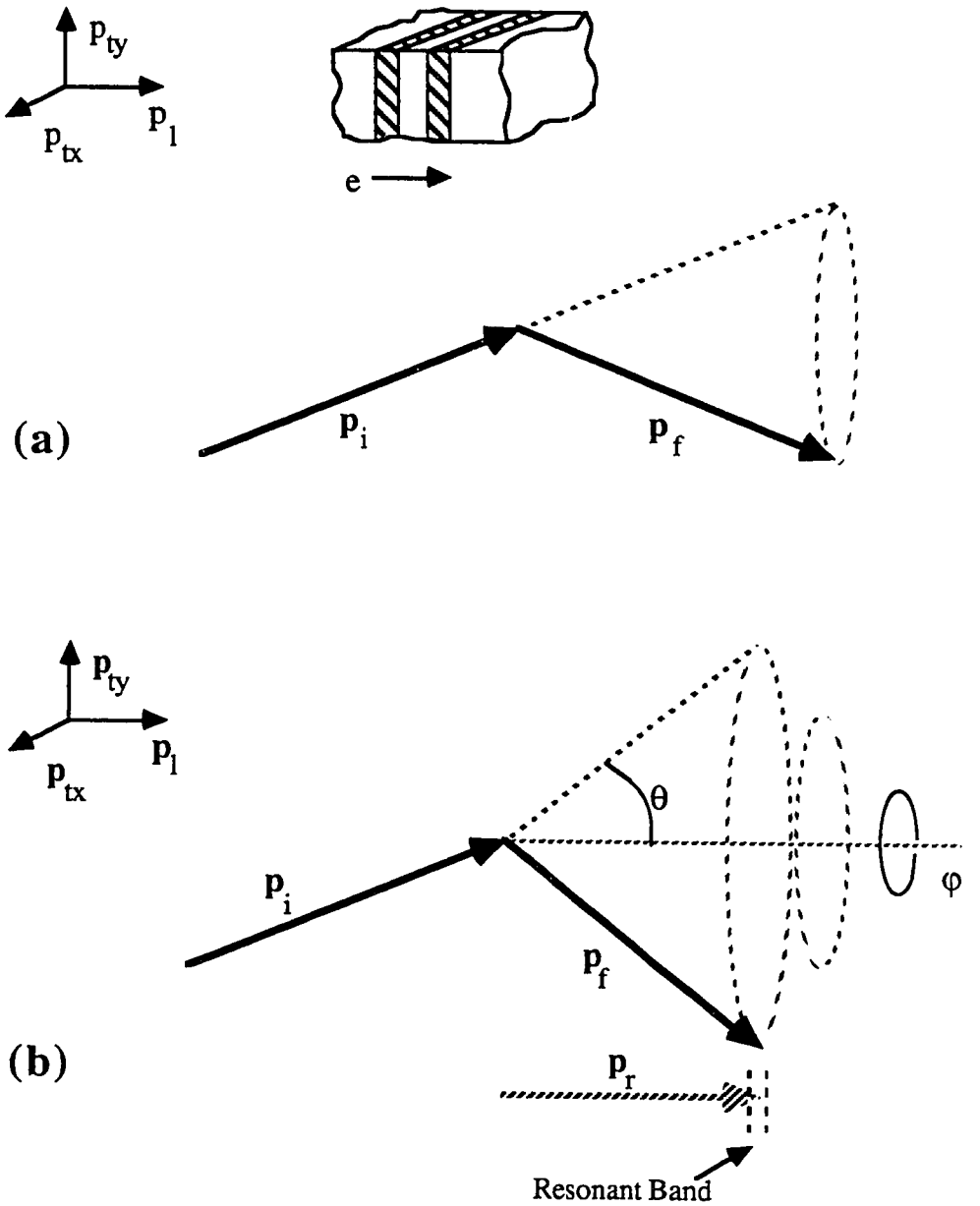

Figure 4.1 - Elastic scattering events which conserve longitudinal energy (a), and do not conserve longitudinal energy (b) are shown in momentum space.

electron through the double barrier structure. We define the resonant band as the electron states within the full width at half maximum of the resonant state (in longitudinal energy). The net effect of such scattering events is to add current in the valley part of the I-V characteristic, as most incident electrons would have a small transmission probability with no scattering under this bias condition. It is not clear what the effect on the current is near resonance, but it is probably small as the most likely result is to scatter from one resonantly transmitted state to another, resulting in little change to the resonant current.

An experimental study is made of the effects of ionized impurity scattering by growing MBE samples with several types of doping in the well of a RTD, which is described in sections 2 and 3 of this chapter. In section 3, it is shown that a shift in the resonant bias of the RTD which is dependant on the dopant charge in the well is explained by the coherent transport model, however, a measured decrease in the peak to valley ratio for the doped devices is not explained by the coherent model. In section 4, a rough calculation of scattering into the resonant band is made which indicates the magnitude of the additional contribution to the valley current made by these impurities. The experiment and theory is discussed in section 5.

4.2. Experiment with varied well dopings

4.2.1 MBE Growth

In order to measure the effect of scattering centers in the well on the I-V characteristics of DBRTDs, four double barrier structures were grown with different dopant profiles using molecular beam epitaxy (MBE) in a modified Varian Gen II. The control sample had an undoped well region, the second sample had 16.7Å of 1.0^{18} cm^{-3} Si n-type doping centered in the well, the third was similarly doped with Be and the fourth sample had 16.7 Å of alternating Si and Be doping to create a highly compensated doping effect in the well's center. As the doped wells have n-type, p-type and compensation doping, the effects

of band bending on the I-V characteristics should be separable from the effects of elastic scattering events in the well.

The growths consisted of a 2500 Å GaAs buffer layer with 10^{18} cm^{-3} Si doping, an 80 Å undoped GaAs spacer layer, an undoped 60 Å $Al_xGa_{1-x}As$ (x=0.3) barrier, a 50 Å GaAs well with the aforementioned doping profiles, a 40 Å undoped $Al_xGa_{1-x}As$ (x=0.3) barrier layer, a 40 Å undoped GaAs spacer layer, a 1500 Å GaAs capping layer with 10^{18} cm^{-3} Si doping, and a GaAs/InGaAs superlattice non-alloyed ohmic contact[9,10]. The barriers were intentionally grown to be asymmetric at zero bias so that at the resonance bias condition, the reflections from the two barriers would be nearly equal, thus enhancing the peak resonance current. A 20 second growth interruption was performed 20 Å before the quantum barrier system, in order to smooth the first interface, while minimizing the accumulation of any impurities at the interface itself.

4.2.2 Device Fabrication

All of the structures were processed by wet etching mesas to isolate the devices as shown in figure 4.2. The mesas were designed to be squares ranging from 2-20 μm on a side with outward slopes along the direction of the interconnect metallization. Large area mesas of 100 μm and 500 μm on a side were also fabricated. A nickel-gold-germanium alloy was deposited to provide ohmic contact to the region surrounding the mesas. SiO_2 was deposited by plasma enhanced chemical vapor deposition to passivate the structure. The alloyed ohmic contacts were subsequently annealed at 450° C for 30 seconds in forming gas. Buffered HF was used to etch openings for the interconnect metallization to connect the ohmic contacts and the bonding pads. Dice from each wafer were mounted and bonded on to 24 pin carriers which were submerged in liquid nitrogen for low temperature measurements.

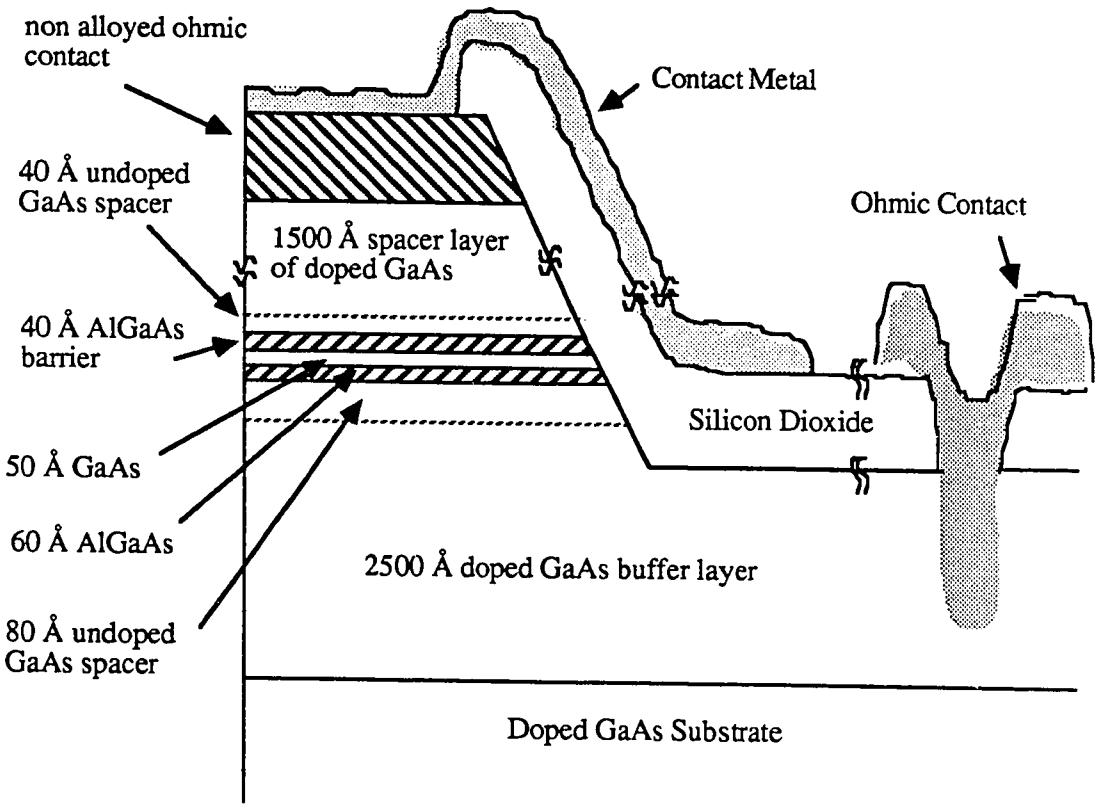

Figure 4.2 - Schematic of processed RTD's for the elastic scattering experiment. The process sequence includes mesa isolation, ohmic metalization, rapid thermal anneal, oxide deposition, etching of contact holes and interconnect metal deposition. The 50 Å GaAs well contains varied dopant types for the purpose of a systematic comparison.

4.3 Measurements at 77 K

4.3.1 Effects of asymmetry

The asymetry in the tunneling barriers and spacer layers lead to asymetry in the D.C. I-V characteristics. With negative bias on the top contact the barriers have a similar transparency near resonance and thus the maximum transmission coefficient is very large and a high resonant current density results. With positive bias on the top contact, the reverse is true and a substantially lower peak current density results. The very high peak current densities realized with negative bias on the top contact resulted in large voltage drops across series resistances in the diodes. As a result of this, the measurements under negative bias had a large statistical scatter. Therefore, in this work, we have only shown results with a positive bias on the top contact.

It can be seen from simulation of the band diagram[11], that the negative bias condition results in a large accumulation region near the 40 Å barrier when the device is biased past resonance. Scattering in the accumulation layer may result in additional valley current due to a scattering assisted tunneling mechanism similar to the one we describe for scattering in the well. With positive bias on the top contact, the bottom of the device is now the emitter; simulation of the band diagram shows that the 80 Å buffer undoped buffer layer minimizes the accumulation region.

4.3.2 Summary of measurments

Measurements at 77 K revealed a systematic shift in the voltage of the peak current, as shown in figure 4.4. This systematic shift can be explained by band bending effects due to the ionized impurities placed in the well of the device. Ionized p-type dopants in the well bend the conduction band such that the resonant state is raised, thus increasing the amount of bias necessary to achieve resonance. On the other hand, ionized n-type dopants cause an accumulation outside the barriers and bend the bands lower inside the well, thus lowering

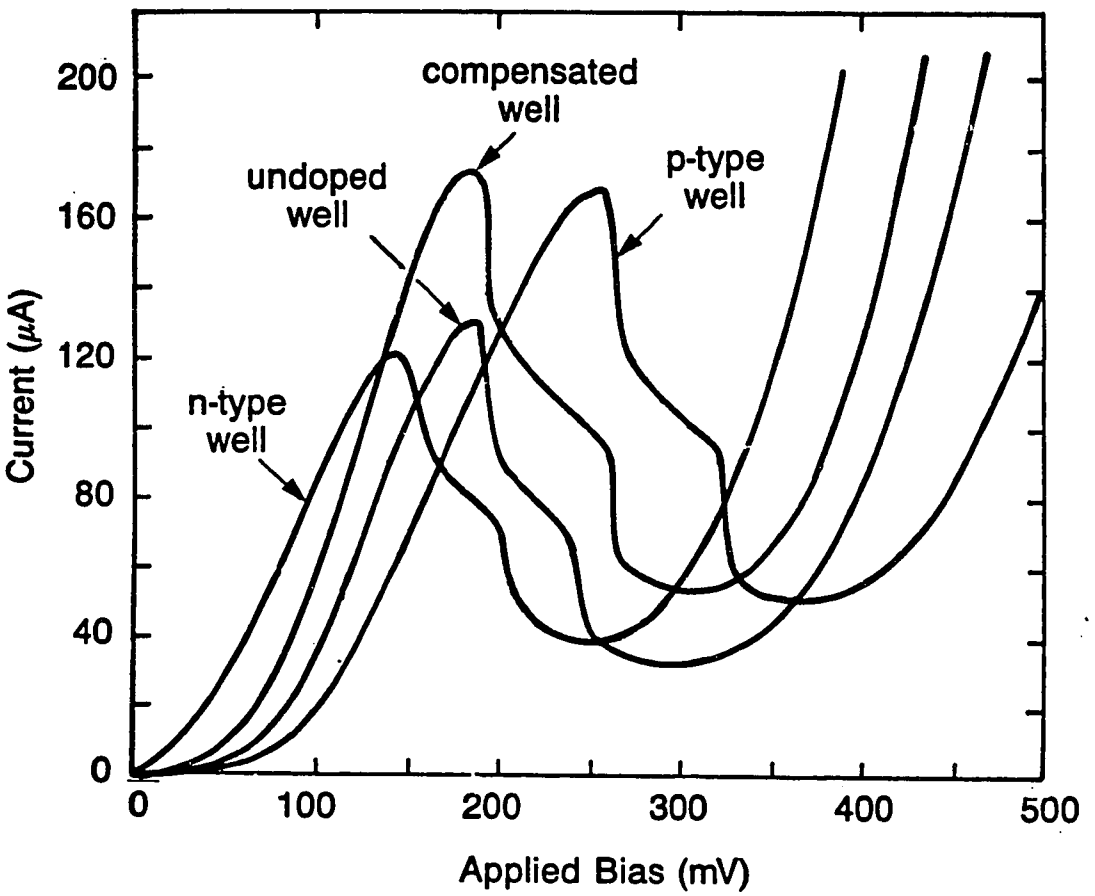

Figure 4.3 - The current - voltage characteristics at 77K for devices 2 microns on a side are shown above for devices with n-type, p-type, compensated and undoped wells. Note the systematic shift in resonant bias with dopant type, and the reduction in the peak to valley ratio for the doped well devices.

the resonant state.

Lowering of the peak to valley ratios occurred in all of the devices with doped wells, as can be seen from figures 4.3 and 4.5. It is not clear from the experimental results if the peak to valley ratio decreased due to an increase in the valley current or a decrease in the peak current. The latter explanation, however, seems to be more plausible.

4.3.3. Comparison to coherent transport model

The above results are compared with predictions from a coherent model (see chapter 3). A Fermi energy of 0.056 eV above the conduction band and a temperature of 77 K were assumed. The results of this calculation are shown in figures 4.4, 4.5 and 4.6. We can see that the predicted peak and valley voltages show good agreement with the data in figure 4.6 The model predicts a higher peak to valley ratio for doped devices due to band bending effects, in contradiction with the experimental results. Thus, the experimentally observed reduction in peak to valley ratios in the doped devices cannot be attributed band bending, and must be explained by scattering from the impurities which were intentionally placed in the well, or some other effect. It is not clear from the experimental results whether this reduction in peak to valley ratio is due to a decrease in the peak current or an increase in the valley current due to the large standard deviation of the current densities in the samples (the peak to valley ratios were more consistent).

4.4 Estimate of additional valley current

The calculation of the change in current due to elastic scattering in the well of a resonant tunneling diode is a complex one. As shown in the previous chapter, it is necessary to integrate over the incident electron states to find a current density. For any given incident electron, there is a spherical surface in k-space which includes all of the energetically allowed final states. The probability of scattering into any such state depends not only on

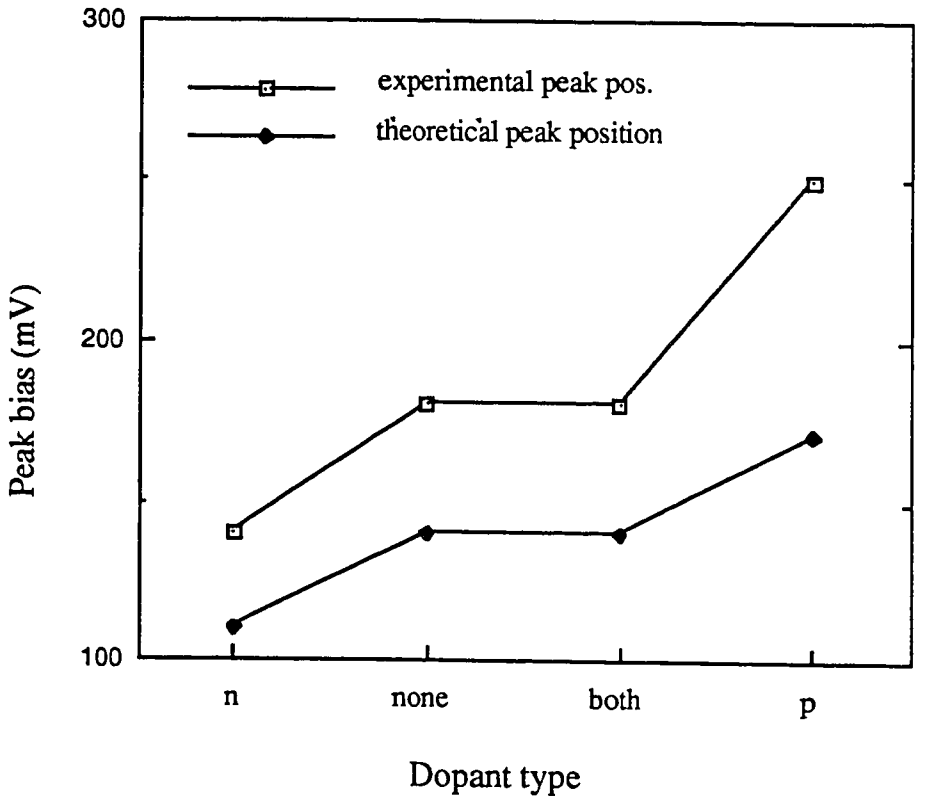

Figure 4.4 - The bias needed to achieve resonance with different types of well doping is compared with the predictions of the coherent transport theory. The model correctly predicts the shift in resonant bias with impurity type. Notice that the predicted resonance occurs at a lower applied voltage than in the experiment, this is a typical result.

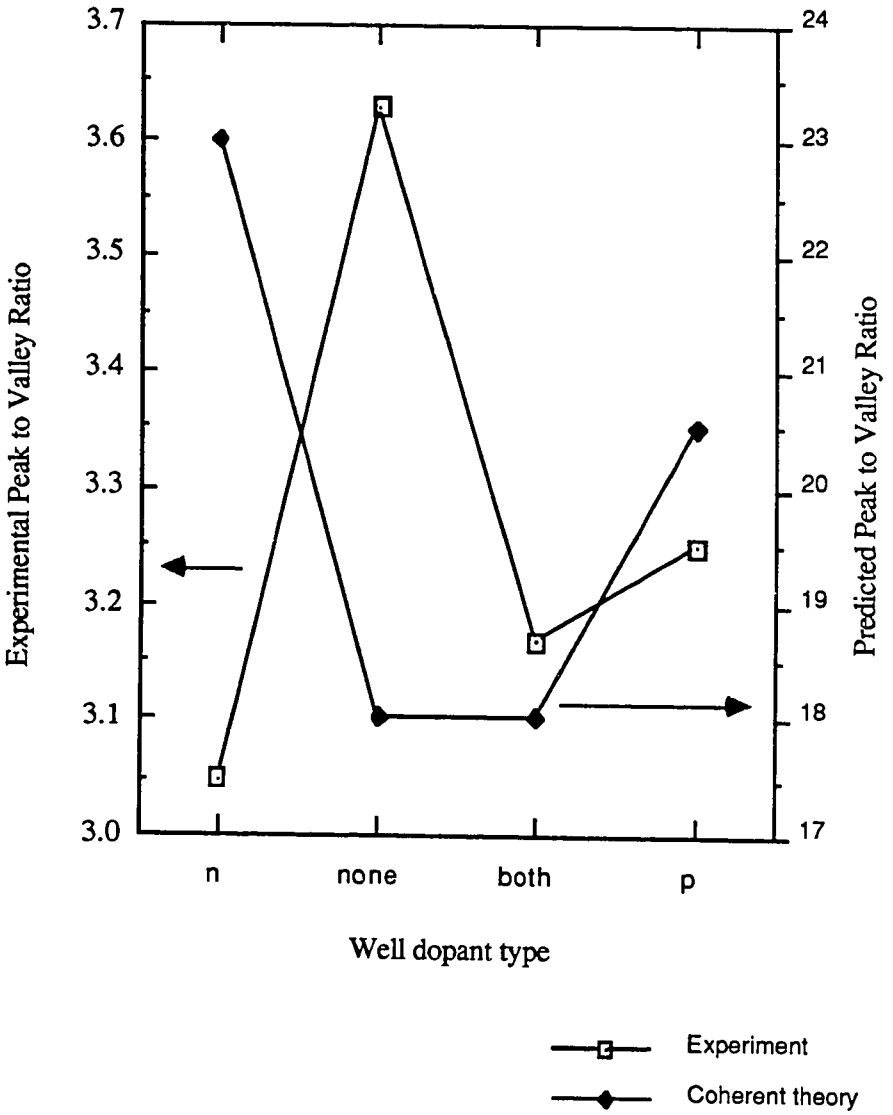

Figure 4.5 - The peak to valley ratios for devices with several different types of well doping are compared with the coherent transport theory. The theory is incorrect by an order of magnitude and does not explain the higher peak to valley ratio of the undoped samples.

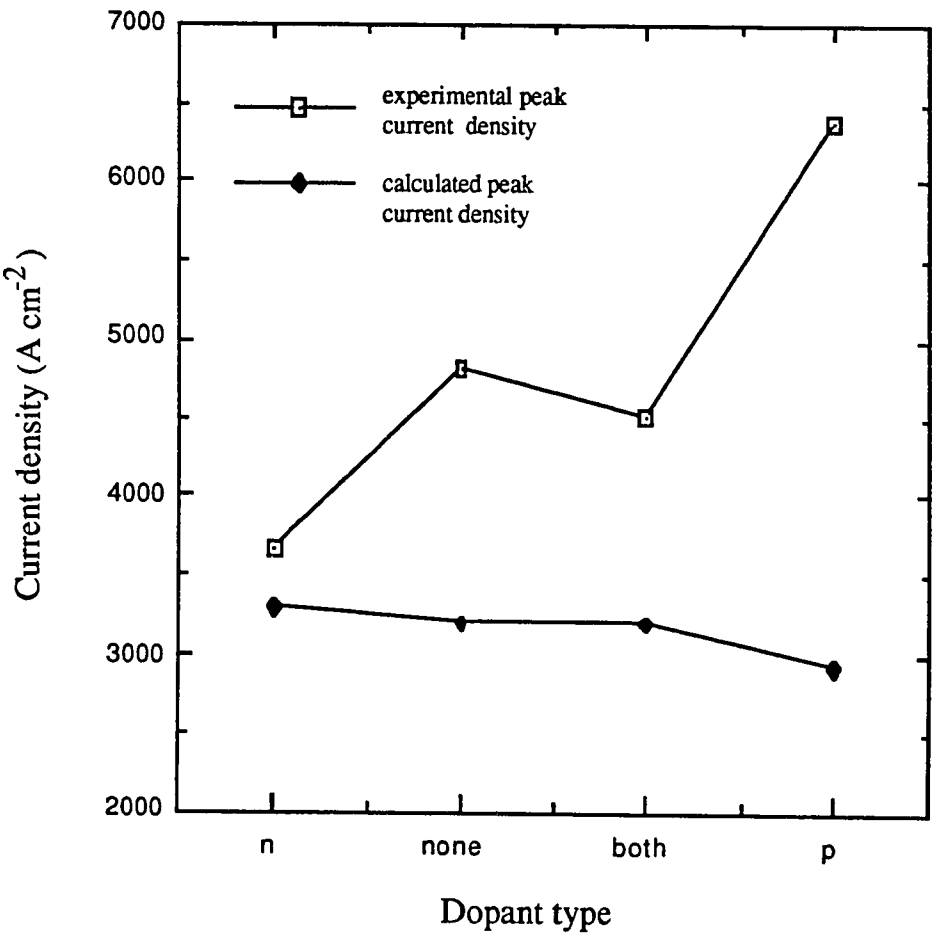

Figure 4.6 - The change in peak current density with well doping is also not correctly predicted by the coherent transport model. It is not clear if this is due to fluctuations in the thickness of the RTD's or a more sophisticated effect.

the scattering potential and the scattering angle, but also upon the shape of the unperturbed potential. This is because the longitudinal density of states within the well of the device is a strong function of the spacing between the barriers and their respective transparencies.

To make a crude estimate of the effect of ionized impurities on the valley current in the devices with doped wells, we consider electrons which scatter from states with non-resonant longitudinal momentum into resonantly transmitted states. We assume that such electrons would not have contributed to the valley current had they been unperturbed. The probability of these electrons passing through the structure is taken to be equal to the product of the transmission coefficient into the well, and the probability that once inside the well, the electron will scatter into the resonant band. We assume that the rate of electrons scattering into the bound state in the well is lower than the rate of electrons tunneling out of the well through the second barrier, so that we can neglect the occupation of the well. In order to calculate the probability of an electron scattering into the resonant band, the unscreened Born approximation is used to find the differential cross section per unit solid angle:

$$\delta\sigma/\delta\Omega = e^4\, m^{*2}/\{\varepsilon_s^2\, (\, \mathbf{p}_f - \mathbf{p}_i\,)^4\}\ , \qquad (4.1)$$

where ε_s is the susceptibility of GaAs, e is the charge of an electron, $\delta\sigma/\delta\Omega$ is the differential scattering cross section per unit solid angle, and $\mathbf{p}_i$ and $\mathbf{p}_f$ are the initial and final electron momentum vectors respectively. To apply equation (4.1), we take the initial and final momentum components in the l direction to be $p_{li} = (2m^*E_{li})^{1/2}$ and $p_{lf} = (2m^*E_T)^{1/2}$, with E_{li} taken to be in the well and E_r taken to be the resonant energy, thus

ignoring the effect of the barriers and the backscattering case (the transverse components, $p_{ti}= (2m^*E_{ti})^{1/2}$, and p_{tf} are found from energy conservation).

The use of the Born approximation is based on the variation of the potential being small compared to the electron energy. Clearly, this condition is violated by the tunneling barriers, however, due to the nature of the Coulomb interaction much of the interaction between the initial and final states occurs in the well. In addition, we used the unscreened Born approximation, which is reasonable for the relatively large scattering angles we are considering. The use of a resonant band is a way of approximating the summation over all possible final states by using a summation over the narrow band of final states which have a high probability of being in the well; and thus have a high probability of a scattering event occurring. The width of the resonant band, and the magnitude of it's wavefunction in the well, is based on a wavefunction matching formalism similar to that used to find the transmission coefficients in the calculation of the current-voltage characteristics[12]. Though such approximations may not be completely justifiable in a DBRTD, it does give a tractable solution and an indication of the magnitude of this interaction; this method may produce very accurate results by using it for devices with somewhat wider wells.

The additional current is calculated for the device biased past resonance, so we only consider electron transmission from the emitter side to the collector side; thus the additional valley current is written as[13,14]:

$$j_{add} = 4\pi e m^*/h^3 \int dE_l\, T(E_l) \int dE_{t\,i}\, f(E_k)\, S(E_{ti},E_{li}) \ , \qquad (4.2)$$

where $T(E_l)$ is the transmission coefficient into the well as a function of E_l (in the emitter),

$f(E_k)$ is the Fermi distribution function, $E_k \equiv E_{ti}+E_l$ is the kinetic energy of electrons in the emitter, and $S(E_{ti},E_{li})$ is the probability of an electron of incident transverse energy E_{ti}, and incident longitudinal energy E_{li} (in the well) to scatter into the resonant band. $S(E_{ti},E_{li})$ is computed by integrating the scattering cross section per unit solid angle over the forward propagating states within the resonant band. The set of final states which are within the resonant longitudinal energy band and also satisfy energy conservation lie within a ring in momentum space at angle θ around the l axis, as shown in figure 4.1b, where $\sin\theta=(E_i-E_r)^{1/2}E_i^{-1/2}$, and $E_i = E_{ti}+E_{li}$ and E_r is the resonant energy. Integrating the differential cross section from equation (4.1) around this ring, we obtain:

$$\delta\sigma/\{\delta\theta \sin\theta\} = \int_0^{2\pi} \delta\phi \, (\delta\sigma/\delta\Omega) = \frac{\pi e^4 (E_i - \sqrt{E_{li}E_r})}{8E_l^{3/2}\epsilon_s^2 (\sqrt{E_{li}}-\sqrt{E_r})^3} , \qquad (4.3)$$

We define ΔE_r as the width of the resonant state, and M as the relative strength of the final state wavefunction in the well at resonance; thus to first order we can write:

$$S(E_{ti},E_{li}) = (\delta\sigma/\delta\theta)\cdot(\delta\theta/\delta E_r)\cdot\Delta E_r\cdot n = (\delta\sigma/\delta E_r)\cdot\Delta E_r\cdot n\cdot M , \qquad (4.4)$$

where n is the number of scattering centers per unit area and $\delta\theta/\delta E_r$ can be derived from geometric considerations. Equations (4.3) and (4.4) are substituted into (4.2) to get the

additional current through the device due to scattering assisted tunneling in a more explicit form:

$$j_{add} = 4\pi em^*/h^3 \int dE_l T(E_x) \int dE_{t\,i} f(E_k) \pi e^4 n \Delta E_r M (E_i - \sqrt{E_{li}} E_r) / \{16 \epsilon_s^2 (\sqrt{E_{li}} - \sqrt{E_r})^3 E_i^2 \sqrt{E_r}\} \quad (4.5)$$

In order to evaluate the integral over E_t analytically, the temperature was taken to be zero. The integral over E_l was done numerically for parameters corresponding to our devices: a Fermi level of 54 meV above the conduction band minimum, with $1.7 \times 10^{11}/cm^2$ scattering centers in the well. There is an additional current on the order of 300 A/cm^2 at 320 meV applied bias if we find M by backpropagating the wavefunction in a simplified rectangular approximation to the potential. If we can interpret the decrease in peak to valley ratios in the doped devices to be due to an increase in the valley current, then this mechanism is consistent with our experimental results. The large number of assumptions made to do this calculation, and the fact that for M>1 first order estimates will break down due to multiple scattering events, mean that this calculation is only useful for order of magnitude estimates.

4.5 Discussion

Elastic scattering centers in the well of a DBRTD can change the voltage and magnitude of features in the I-V characteristics of resonant tunneling devices. The effects of band bending due to impurities in the well on the I-V characteristics of the devices have been calculated using the model from chapter 3, and a shift in resonant voltage is predicted which shows good agreement with experiment. The band bending model predicts an increase in the peak to valley ratio of the devices with doped wells, whereas the

experimental results show a decrease in the peak-to-valley ratio for these devices. Additional valley current is evident in the samples with p-type and compensated doping in the well, but not in the n-type sample; due to the large uncertainty in measured current densities, it is unclear whether it is proper to interpret the decline in peak to valley ratios of the devices with doped wells in this manner. Elastic scattering centers in the barriers of a DBRTD show similar effects, with the devices with additional doping in the barriers showing a shift in the resonant voltage and a degradation of the peak to valley ratio[15]. These experiments show that elastic scattering can reduce the peak to valley ratio of a DBRTD, however, it is also apparent that a measured quantity of these centers will not destroy the negative differential resistance of these devices.

These results are also applicable to ionized impurities in the barriers and immediately adjacent contact layers. The ionized impurities in this experiment (which were intentionally placed in the well of the device) occupy an area of roughly 250 Å on a side. For an electron experiencing quantum barriers and a well on the order of 50 Å in the longitudinal direction, the displacement of the scattering center by this amount should not matter much if the electron can be thought of as 100 Å to the side of the impurity. The relative insensitivity to longitudinal placement of the the impurity is exaggerated by the non-localized nature of an unscreened Coulomb potential and the electron wave packets themselves (the weaknesses of the method of calculating additional valley current in section 4.4 contribute to the insensitivity in impurity placement). Thus, ionized impurities will weakly degrade the peak to valley ratio of an RTD if placed in the barriers or within a few nanometers of the quantum structure. The number of impurities typically used in the contact layer thus warrents the use of undoped or lightly doped spacers surrounding the device to reduce scattering degradation.

In the cases we consider, roughly 20% of the valley current experimentally observed can be accounted for by coherent tunnelling through the structure. As the intentional doping in

the wells is orders of magnitude above typical background doping levels, it is unlikely that the deviation between calculated and measured current densities is due to scattering from background impurities (though scattering due to impurities in the contact layers may be an important component of the valley current). Other possible sources of additional valley current include scattering due to interface roughness, inelastic scattering events, scattering into other valleys[16] and scattering due to Coulomb potentials originating in the doped contact layers.

4.5.1 Implications for device design

These results have important implications for RTD design. Combined with the studies on scattering centers immediately outside the device, these results emphasize the importance of using undoped spacer layers around a resonant tunneling device. Clearly, ionized impurities serve to degrade the current voltage characteristics from what the ballistic model predicts and their use in the well and barriers of the device is only advisable as a last resort in RTD design, changing the resonant bias can be accomplished by changing the well composition or thickness, as well as changing the surrounding undoped spacer layers. The thickness of spacer layer to use surrounding the double barrier structure is a more difficult question. This is due to the fact that larger spacer layers are beneficial for the purpose of reducing elastic scattering, however, the peak to valley ratio and peak current density predicted by the ballistic model degrade with larger emitter spacer layers. Thus in choosing the correct spacer layers, the tradeoff between ideal transport characteristics and the effects of elastic scattering must be considered. The relatively large number of donors used in the wells of these devices show that the use of lightly doped regions surrounding the spacer layers, may be a reasonable approach to achieving good band structures yet minimizing impurity scattering effects.

4.5.2 Possibilities for future studies

Further studies of the effects of elastic scattering centers depends on the goals of the researcher. If the goal is device optimization, existing models of elastic scattering only indicate qualitative trends with only rough quantitative agreement, however, they provide a reasonable guide for experimental work. Device designers who are optimizing RTDs would probably be served by empirical optimization of the doping profile instead of further attempts at modelling the effects of scattering centers. For the physicist who wishes to understand the role of elastic scattering in semiconductor transport phenomena, interesting experiments and calculations remain to be undertaken. Experimentally, the related questions of elastic scattering in RTDs with transverse confinement and with magnetic fields applied remain to be addressed. A basis for computing these effects is given in chapter 5 of this thesis.

Better calculations of the additional current due to elastic scattering centers in a quantum well are certainly possible, but empirical models require more data while fundamental models require considerable computational power. The semi-empirical approach of Lebens, Silsbee, and Wright[3] has merit in this respect, as it is not computationally overwhelming, however, it has a correctable flaw in it's analysis and presentation. This is due to the nature of the wavefunctions that they assume for their scattering calculation, and as a result they conclude that scattering centers adjacent to the device are not as serious as scattering centers slightly further away.

References

1. Hiroaki Ohnishi, Tsuguo Inata, Shunichi Muto, Naoki Yokoyama, and Akihiko Shibatomi, Appl. Phys. Lett. **49** (19), 1248, 1986.

2. Tadashi Nakagawa, Takahiro Fujita, Yutaka Matsumoto, Takeshi Kojima and Kimihiro Ohta, Japanese Journal of Applied Physics Vol. 26, no. 6, June 1987, pp. L980-L982.

3. John A. Lebens, Robert H. Silsbee and Steven L. Wright, Applied Physics Letters **51**(11), 840, 1987.

4. N.M. Cho, S.B. Ogale, and A Madhukar, Appl. Phys. Lett. **51** (13), 1016, 1987.

5. This was done by T.C.L.G. Sollner et. al, see reference 2, chapter 2.

6 C. J. Summers, K.F. Brennan, A. Torabi, and H.M. Harris, Appl. Phys. Lett. **52** (2), 132, 1988.

7. This is typically done in THETA devices, see for example M. Heiblum, I. M. Anderson, and C. M. Knoedler; Appl. Phys. Lett. **49** (4), 207, 1986.

8. T. Weil, Ph.D. thesis, L'Universite Paris 6, 1987.

9. W.S. Lee, D.G. Schlom and J.S. Harris Jr., unpublished

10. Takumi Nittono, Hiroshi Ito, Osaake Nakjima, Tudao Ishibashi, Extended abstracts of the 19th conference on Solid State Devices and Materials, Tokyo 1987.

11. Mark S. Lundstrom and Robert John Schnelke, IEEE Transactions on Electron Devices, Vol. ED-30-No. 9, Sept 1983.

12. Alex Harwit, Ph.D. thesis, Stanford University, 1987.

13. C.B. Duke, Tunneling in Solids, Solid State Suppliment 10.

14. R. Tsu and L. Esaki, Appl. Phys. Lett. **22**, 562 (1973).

15. E. Wolak, K.L. Lear, P.M. Pitner, B.G. Park, E.S. Hellman, T.Weil, J.S. Harris Jr., and D. Thomas, SPIE no 943, 36, 1988.

16. F.W. Wise, I.A. Walmski, and C.L. Tang, Appl. Phys. Lett. **51** (8), 605, 1987.

5. Transport in a system with reduced dimensionality

5.1 Introduction

Resonant tunneling of electrons with three degrees of freedom (DOF) through a one dimensional quantum barrier system has been studied extensively both experimentally[1] and theoretically[2]. Recent advances in semiconductor processing technology have lead to the possibility of fabricating double barrier tunneling diodes with transverse cross sections of 1000 Å or less as shown in figure 5.1. In these confined small structures, additional quantum confinement perpendicular to the direction of charge transport is introduced. Due to this transverse quantum confinement, the electrons incident upon the tunneling barriers no longer have the nature of a 3-DOF Fermi sea, but instead have 2-DOF or 1-DOF with the possibility of several transverse states being occupied as shown in figure 5.2.

In this chapter, analytical methods are used to predict the effects of reduced dimensionality under various conditions. The explicit expressions for tunneling transport in a system with reduced dimensionality are derived in section 5.2 under the assumption of a separable Hamiltonian. In section 5.3 we show that if the variables of the Hamiltonian can be separated transverse and parallel to the direction of transport, that no increase in the sharpness of the resonance occurs from the reduced dimensionality[2]. Additional structure in the I-V characteristics, such as shoulders and feet near the major resonances, are predicted for electrons with 1-DOF due to the shift in relative Fermi energy for each transverse state. Additional sharp peaks, however, are not expected under the above conditions for double barrier structures (though it may be possible to create a special case where this does occur). Experiments have shown additional peaks in the I-V characteristics of such reduced dimensional structures[1] which are not predicted by the simple model[2], and thus there is a need to consider a transversely confined RTD within a formalism which does not assume a separation of variables condition and allows coupling between different

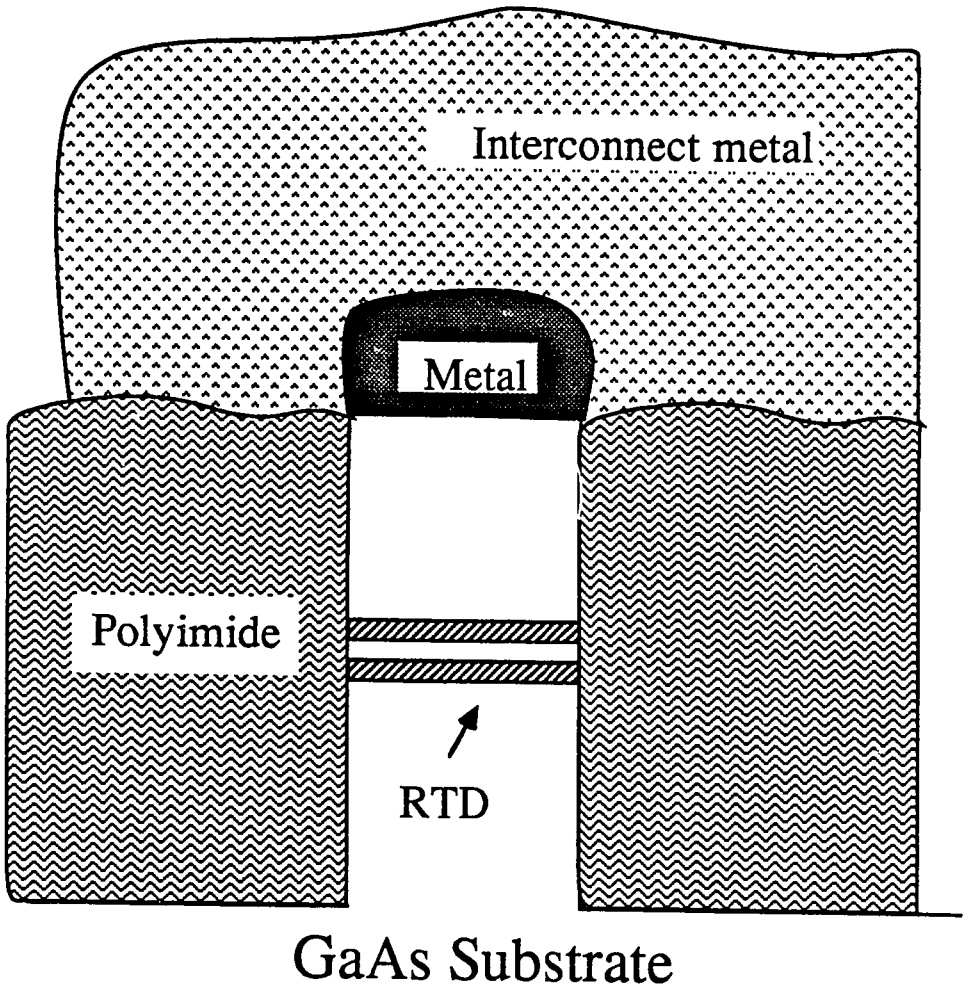

Figure 5.1 - The first RTD with tranverse confinement down to quantum dimensions is schematically illustrated above (Reed, Randall, Aggarwal, Matyi, Moore, and Wetsel Physical Review Letters, 1988). The physical transverse dimension is approximately 1000 Å, however, surface depletion further confines the electrons transversely so that discrete transverse states are formed.

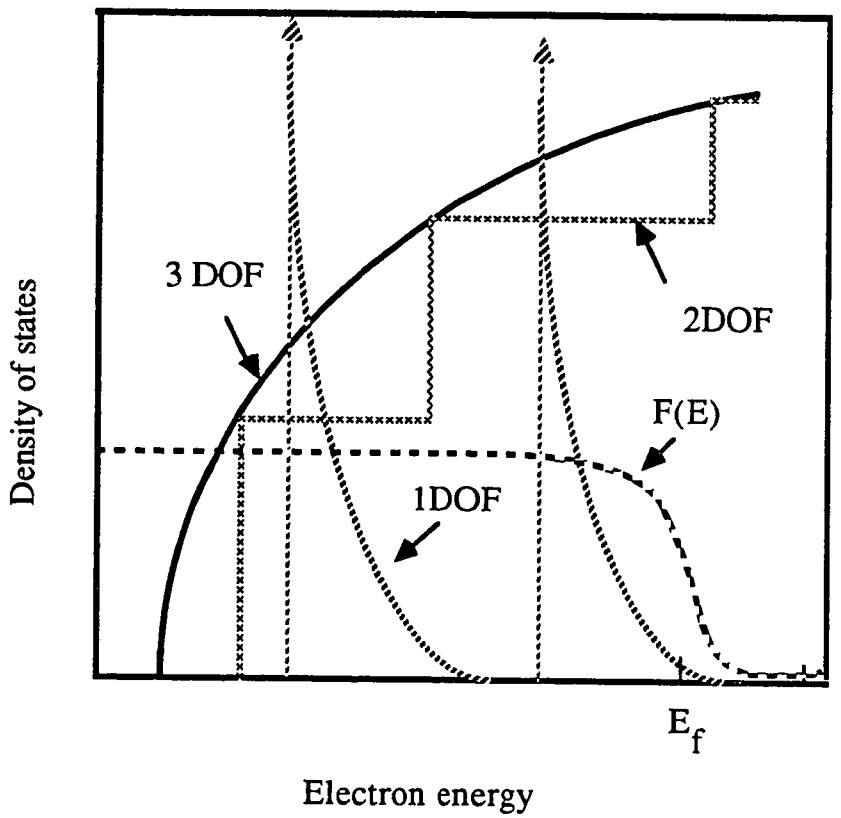

Figure 5.2 - The density of states is schematically illustrated for electrons with 1, 2 and 3 degrees of freedom as a function of total electron energy. The Fermi function is also drawn in to show how multiple transverse energy levels may be occupied as the Fermi energy is increased.

transverse states. In section 5.4 a formalism for tunneling transport is presented which allows perturbation of the separation of variables condition. The case of elastic scattering in the well of a RTD is studied in detail in section 5.5, and we show that additional structure in the current-voltage curve can result from breaking the separation of variables condition under transverse confinement. The validity of this method and the extent of it's usefulness are discussed in section 5.6.

5.2 Expression for the tunneling current in reduced DOF with separation of variables

The analysis of RTDs with 3-DOF typically starts with the assumption of a separable Hamiltonian in order to reduce the difficulty of the problem, as was shown in chapter 3. More complex phenomena are typically accounted for by the use of perturbation theory, or by the use of Greens function techniques or Monte Carlo calculations. We approach the problem of reduced DOF tunneling transport within the spirit of initially assuming a separable Hamiltonian, in order to understand the changes to the current-voltage characteristics which arise from such transverse confinement.

A comparison of the magnitude of experimental and calculated results is complicated by the fact that the specific energy levels of the confined transverse states and their relative occupation are not measurable with sufficient accuracy at this time. The confined energy levels are difficult to measure directly because of the small size of these devices, for photoluminesense several such devices may be required to acheive enough signal strength and the confined levels are blurred out. Estimating the confined levels is also difficult, as surface depletion plays a large role in the confinement adding to the uncertainty inherent in the transverse dimensions of the confining structure. The transverse confinement also changes the nature of the electron density of states, resulting in differences in the ionization of electrons and of the Fermi level for a given electron density. If good estimates are made

of the confined levels and the quasi-Fermi levels, it is possible to estimate the tunneling currents to within an order of magnitude, and to discover the qualitative aspects of their nature.

We work within the independent electron approximation and assume a Hamiltonian of the form:

$$H_s(t,l) = H_t(t) + H_l(l) \qquad (5.1)$$

where l is the direction of electron transport and t is the transverse direction(s). The wavefunction Ψ may then be written as:

$$\Psi(t,l) = \Psi_t(t)\,\Psi_l(l)$$

and the longitudinal and transverse components of the wavefunctions, $\Psi_l(l)$ and $\Psi_t(t)$ respectively, may be solved separately. We take $\Psi_l(l)$ to be a series of plane and exponential waves matched at each longitudinal heterojunction, and $\Psi_t(t)$ to be dependent upon the exact nature of the transverse confinement. For transverse confinement in one direction, $\Psi_t(t)$ has discrete eigenstates in the direction of confinement and a continuum of states in the unconfined transverse and longitudinal directions, such electrons can be thought of having 2 DOF. For complete transverse confinement, the transverse wavefunction is completely quantized and the incident electrons in any transverse state have only 1 DOF in the longitudinal (or tunneling) direction.

With a separable Hamiltonian, a general expression for electrons tunneling through a double barrier can be written as[3]:

$$J = 2q \int_0^{\infty} \mathbf{dk}\; g(\mathbf{k})\, v_l\, [f(E)-f(E+qV)]\, |T(E_l,V)|^2 \,, \qquad (5.2a)$$

where q is the magnitude of the electronic charge, E is the total electron energy, f is the Fermi-Dirac distribution function, V is the applied voltage, E_l is the electron energy in the direction of tunneling, and $|T(E_l,V)|^2$ is the tunneling probability and independent of electron transverse energy. The detailed expressions for **dk** and **g(k)**, the density of states as a function of momentum, depend on the degree of freedom of the electrons. Using the relation $v_l\, dk_l = dE_l/h$ we have for 1-DOF:

$$J = \sum_i^N \frac{2q}{h} \int_0^{\infty} dE_l\, [f(E)-f(E+qV)]\, |T(E_l,V)|^2 , \qquad (5.2b)$$

where E_l is the electron energy in the direction of tunneling, h is the Planck constant, $E = E_l + E_t$, in which electronic energy transverse to the tunneling direction, E_t, is quantized. The summation is over the transversely quantized energy levels E_t. Due to the separation of variables condition, transverse energy and momentum are conserved; therefore, only tunneling transitions between states with the same transverse momenta contribute to the current. For 2-DOF:

$$J = \sum_i^N \frac{q}{\pi h} \int_0^{\infty} dE_l\, |T(E_l,V)|^2 \int dk_y\, [f(E)-f(E+qV)] , \quad (5.2c)$$

where $E = E_l + E_x + E_y$ in which E_x is quantized. The indicated summation is over the transversely quantized states E_x. For 3-DOF we get equation 3.12:

$$j = \frac{4\pi m^* kT}{h^3} \int_0^{\infty} dE_l |T(E_l,V)|^2 \ln\{\frac{1+\exp((E_f-E_l)/kT)}{1+\exp((E_f-E_l-eV)/kT)}\} , \qquad (5.2d)$$

where m* is the electron effective mass, k is Boltzmann's constant, T is the temperature, and the integration over the available transverse wave states has been carried out analytically.

Electrons in any transverse state in a 1 or 2 DOF system experience the same double barrier in the transport direction as that in a 3 DOF system. The difference in computing the current lies in the summation or integration over the transverse states, as these states are either discrete or quasi-continuous. The calculation of tunneling current for the different transverse quantum states in a 1 or 2 DOF system is the same as that for their ground state except for the increase in the transverse energy relative to the Fermi energy. This can be treated by using an effective Fermi level, $E_F = E_f - E_i$, where E_i is the energy of a transverse state relative to that of the ground state.

5.3 Numerical results

To see the difference between the I-V characteristics in resonant tunneling electrons with different DOF, we first discuss the case in which only tunneling through the lowest confined state is considered. Figure 5.3 shows the computer simulation for the tunneling current for electrons with 1, 2 and 3-DOF tunneling through a GaAs/AlGaAs double-barrier quantum well with 50 Å barriers and well, a 238 meV barrier height, and a Fermi level 35 meV above the conduction band minimum at room temperature (300K). A uniform effective mass and a simple five step approximation to the potential was used (as in figure 3.2) for the sake of simplicity. For comparison, the values of the current peaks were normalized and only one transverse state was considered (for the transversely quantized cases). It can be seen that as the number of DOF is reduced, the peak to valley ratio decreases. This is in apparent contradiction to the density of states becoming sharper with

a lower DOF, however, the density of states shown in 5.2 are for total kinetic electron energy, and we are concerned with the density of states as a function of electron kinetic energy in the longitudinal or transport direction.

By closer examination of the expressions for current density with different dimensionalities, the cause of the decline in peak to valley ratio can be uncovered. The expressions (5.2) can be written for the condition of zero temperature in the case of the applied bias being larger than the Fermi energy; for 1-DOF:

$$I = \frac{2q}{h} \int_0^{E_f - E_t} dE_l \, |T(E_l,V)|^2 \qquad (5.3\ a)$$

for 2-DOF:

$$I = \frac{q(2m^*)^{0.5}}{h^2} \int_0^{E_f - E_t} dE_l \, (E_F - E_x - E_l)^{0.5} \, |T(E_l,V)|^2 \qquad (5.3\ b)$$

for 3-DOF:

$$I = \frac{4\pi q m^*}{h^3} \int_0^{E_f - E_t} dE_l \, (E_F - E_l) \, |T(E_l,V)|^2 \qquad (5.3\ c)$$

Where I is the zero temperature current, and E_{tx} is the transverse energy in the confined direction for a structure with 2-DOF. The electron supply function is defined as the density of states times the difference in Fermi functions. From equations (5.3 a-c) we can write the electron supply functions for 1-DOF:

$$S_1 \ \alpha \ \begin{matrix} 1, E_l < E_f \\ 0, E_l \geq E_f \end{matrix}$$

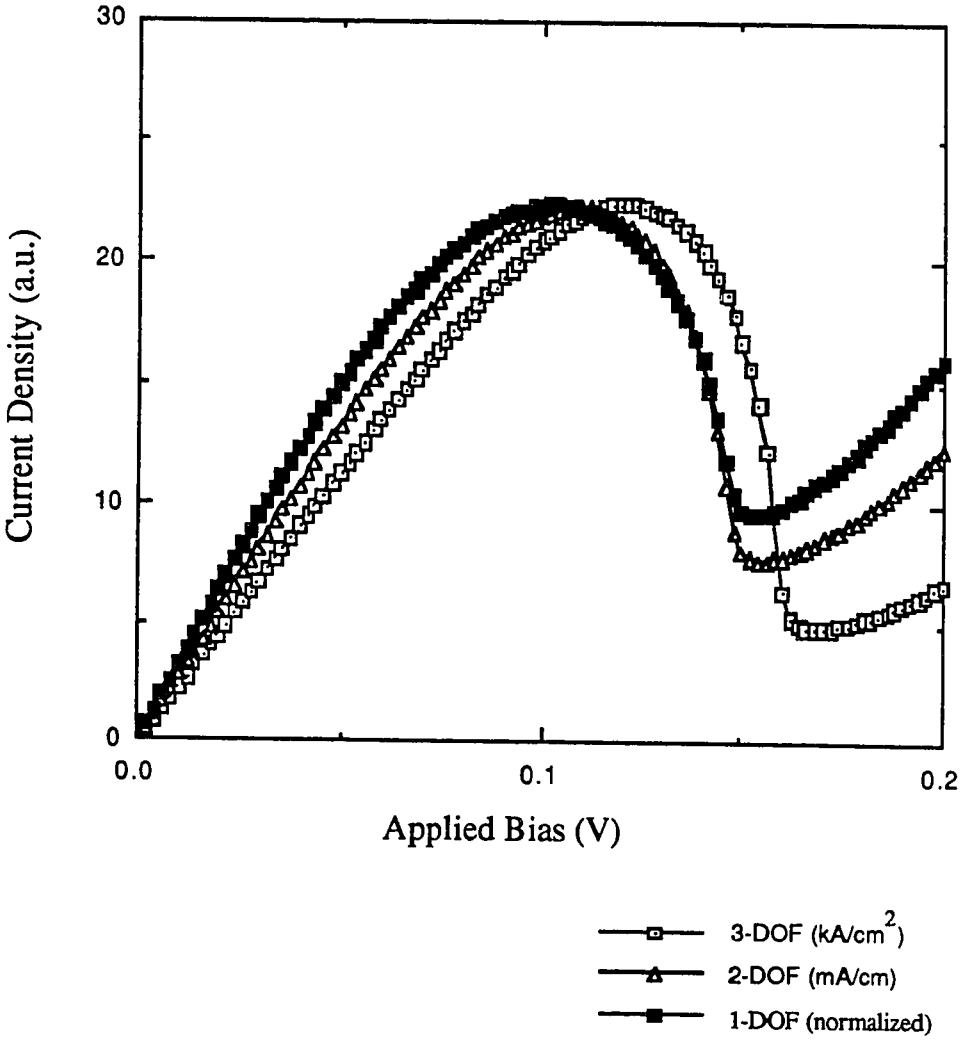

Figure 5.3 - The tunneling current with 1, 2 and 3 DOF is plotted for a single transverse state (where applicable) 35 meV below the Fermi energy at 300K. A five step model was used (see fig. 3.2) using 50 Å barriers with a 30% Al mole fraction and a 50Å GaAs well.

for 2-DOF:

$$S_2 \alpha \begin{cases} (1 - (E_l + E_{tx})/E_F)^{0.5}, & E_l < E_f \\ 0, & E_l \geq E_f \end{cases}$$

and for 3-DOF:

$$S_3 \alpha \begin{cases} (1 - E_l/E_F), & E_l < E_f \\ 0, & E_l \geq E_f \end{cases}$$

under the conditions of zero temperature and $qV>E_f$. As the number of DOF is increased, so is the sharpness of the supply function which peaks near the conduction band minimum for 2 and 3-DOF. The supply function is flat for 1 DOF, thus resulting in more high energy electrons incident on the barriers for the reduced dimensional case. It is the combination of the sharpness of the supply functions for higher DOF, and the number of high energy electrons impinging on the barriers in the valley bias condition for lower DOF, which causes the observed decline in peak to valley ratio with a decline in DOF. Raising the temperature will smear out the supply functions, but it does not change the result of this comparison.

It must be pointed out that, for a given degree of freedom, reduction in the Fermi level can increase the PTV ratio and reduce the width of the current peak. This implies that if the contact doping concentration of a tunneling diode is fixed, the reduction in the DOF of the incident electrons may lower the Fermi level required to ionize all of the impurities due to the sharpness of the density of states. This drop in the Fermi level may overcome the degradation in PTV ratio from the supply function shape effects.

We examine the possibility of additional resonant peaks under the separation of variables condition. Due to the separation of variables, the tunneling probability in the

direction of electron transport is independent of the transverse energy, thus the only possible reason for additional peaks is the relative change between the Fermi level and the minimum total incident energy for each transverse bound state. In order to achieve separate resolvable peaks, a significant separation in peak position must occur concurrently with similar peak current densities. Inspection of Equations 5.1, 5.2 and 5.4 reveals that the effect of different transverse energy levels is to change the width of the supply function, thus changing both the magnitude and position of the resonant peak. Numerical analysis of these shifts must be used to determine if additional structure will result from the transverse confinement.

For electrons with 1-DOF, there is a strong shift in resonance with a change in the effective Fermi level, as shown in figure 5.4. This shift arises from the transmission resonance becoming weaker as the bias across the device is increased, thus the peak current occurs soon after the effective Fermi level crosses the transmission resonance. As a result, it is possible that additional structure such as shoulders and feet on the major resonances will occur in the current-voltage characteristics. Due to the nature of the supply function for 1 DOF, these features are not sharp and thus additional regions of NDR would not be predicted under the assumption of a separable Hamilitonian and barriers that are symmetric under zero bias. It may be possible to create additional regions of NDR by using barriers which are asymmetric under zero bias, thus exaggerating the tendency towards dispersing the resonant peaks with energy. By using higher, less transparent barriers, the sharpness of the peaks would be enhanced somewhat, also contributing to additional NDR regions.

For electrons with 2 DOF, there is less of a shift in the resonant bias with change in effective Fermi energy, as shown in figure 5.5. This is because the decline in the transmission resonance at higher bias is partially offset by the peak in the supply function at low longitudinal electron energies. As this peak is coincident with the bottom of the conduction band, the resonant bias tends to occur near the alignment of the bottom of the conduction band and the resonant state.

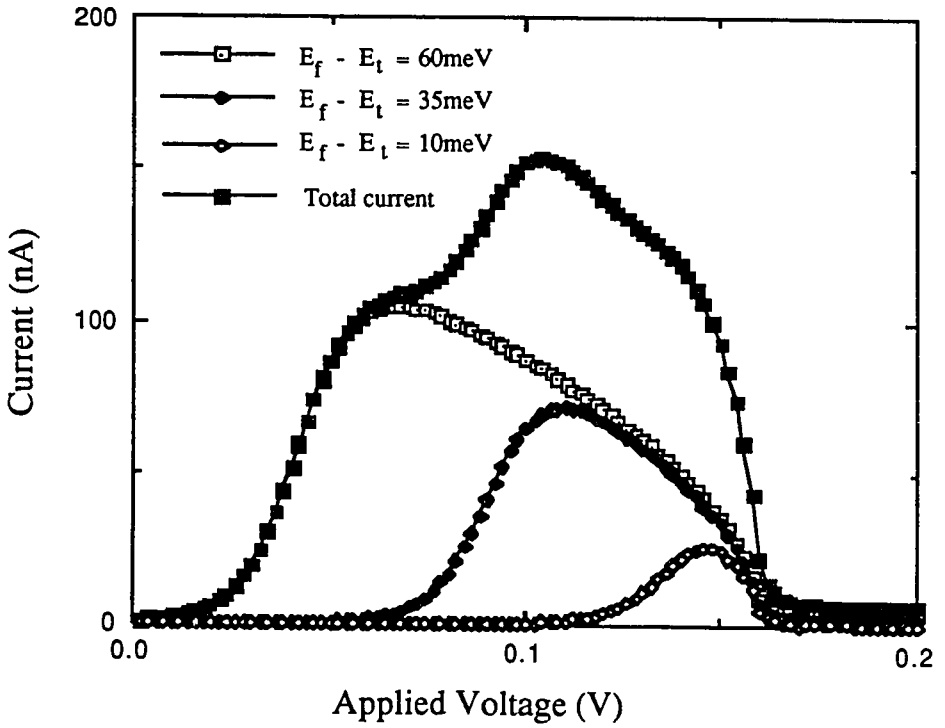

Figure 5.4 - The individual contributions to the tunneling current for transverse states 10, 35, and 60 meV below the Fermi level are shown at 4K, along with the total current for a system with 1 DOF. A simple 5 step model was used (see fig. 3.2) and 50 Å barriers with 30% mole fraction Al, and a 50 Å GaAs well were assumed.

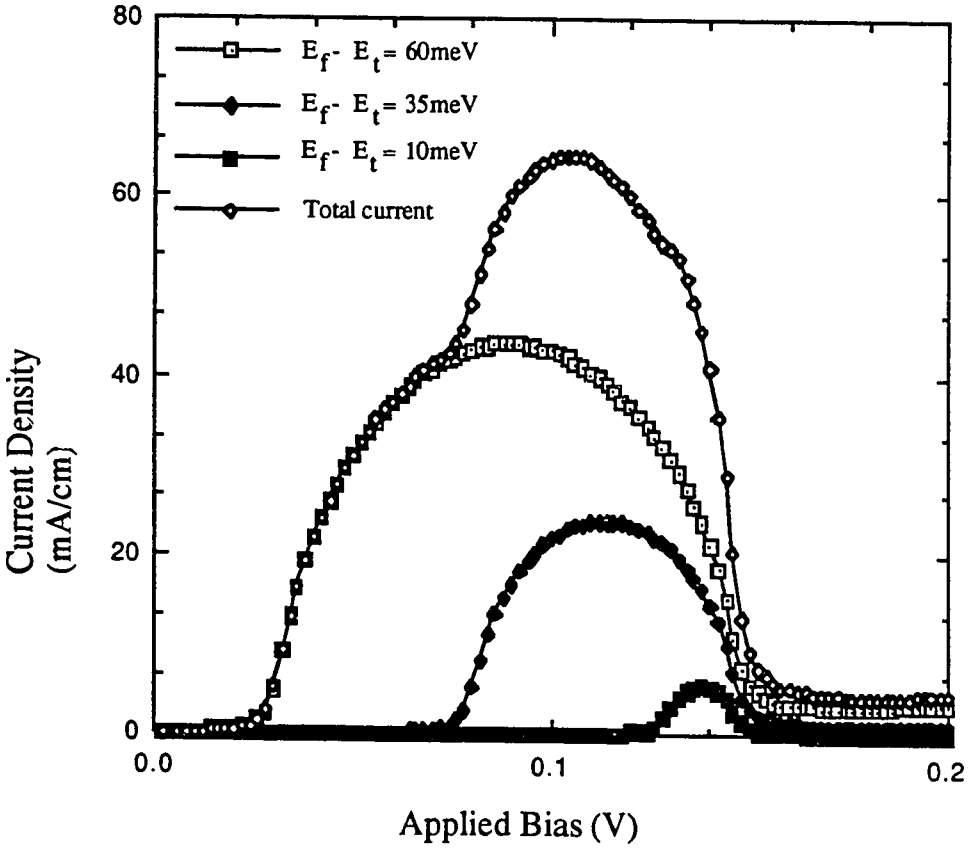

Figure 5.5 - The individual contributions to the tunneling current for transverse states 10, 35, and 60 meV below the Fermi level are shown at 4K, along with the total current for a system with 2 DOF. A simple 5 step model was used (see fig. 3.2) and 50 Å barriers with 30% mole fraction Al, and a 50 Å GaAs well were assumed.

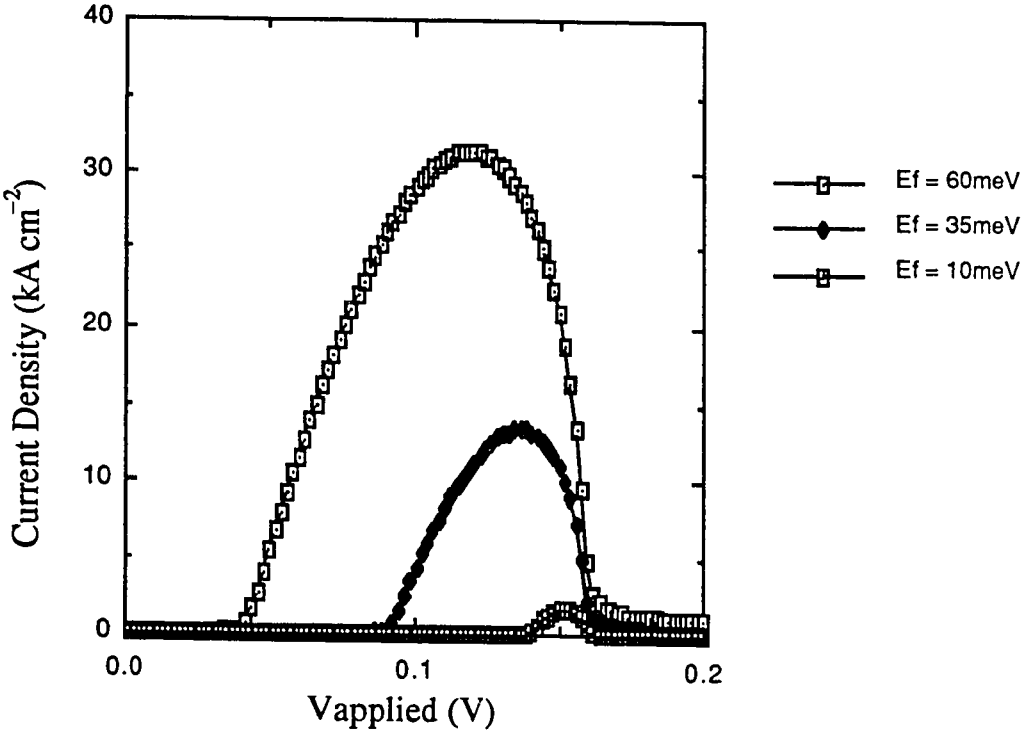

Figure 5.6 - The effect of different Fermi levels on the current-voltage characteristics of a RTD with 3DOF is simulated at 4K with the 5 step model (shown in figure 3.2). The device simulated has 50 Å barriers of 30% Al mole fraction AlGaAs, and a 50 Å well. Band bending and non-parabolic effects were neglected for the sake of simplicity.

For electrons with 3-DOF, the supply function has an even stronger peak near the conduction band minimum, and therefore the peak shifts even less than the 2-DOF case as a function of Fermi energy as shown in figure 5.6.

5.4 A Formalism for perturbation of the separation of variables condition

The separation of variables condition limits us to Hamiltonians of the form of (5.1) where l is the direction of electron transport and t is the transverse direction(s). By using eigenstates which solve (5.1) as the basis for a perturbation expansion, a larger group of Hamiltonians may be treated. In general we can write:

$$H(t,l) = H_s(t,l) + H_p(t,l), \qquad (5.4)$$

where $H_p(t,l)$ is the perturbation to the separation of variables condition. For perturbation methodology to work well, we must have $H_p << H_s$; however, valuable qualitative insight may be gained even when this condition is strained. Several methods of doing a perturbation calculation are possible, the best approach being dictated by the nature of the unperturbed Hamiltonian, the perturbation itself, the information to be extracted, and the computational complexity one wishes to indulge in.

We choose to study the effect of a highly localized potential in a transverse state with an otherwise separable Hamiltonian. As described in the previous chapter, the transverse confinement in the unperturbed Hamiltonian quantizes the transverse states. The longitudinal part of the unperturbed potential is broken into rectangular steps, plane wave matching conditions are used at each step to find the time-independent wavefunction within the independent electron approximation. The perturbation may allow the transfer of

longitudinal momentum to the transverse direction, or vice versa, allowing coupling of different transversely quantized states shown in figure 5.7.

In order to analyze the effect of the interaction between different transverse states on the I-V characteristics of a transversely confined RTD, the longitudinal wavefunction matching formalism is extended to include multiple transverse states simultaneously instead of considering each state in isolation. Interactions between transverse states will result in changes to the transmission coefficients, and thus to changes in the I-V characteristics. If a system of N transverse states is considered, each interface in the longitudinal direction yields a 2Nx2N matrix which has N 2x2 matrices along the diagonal:

$$\begin{vmatrix} B_1 \\ B_2 \\ \cdots \end{vmatrix} = \begin{vmatrix} G_{11} & 0 & \cdots \\ 0 & G_{22} & \cdots \\ \cdots & \cdots & \cdots \end{vmatrix} \begin{vmatrix} A_1 \\ A_2 \\ \cdots \end{vmatrix} , \qquad (5.5a)$$

where the G_{ii}'s are 2x2 matrices which determine the wavefunction amplitudes on either side of the interface. The other elements vanish indicating the lack of interaction between states of different transverse confinement under the separation of variables condition. The vector **A** has 2N elements, with each of the N transverse states having a set of two elements A_i:

$$A_i = \begin{bmatrix} a_{ri} \\ a_{li} \end{bmatrix} , \qquad (5.5b)$$

which represent the amplitude of the plane waves on one side of the interface as described in equations (3.4-3.6); the vector B represents the amplitudes the other side.

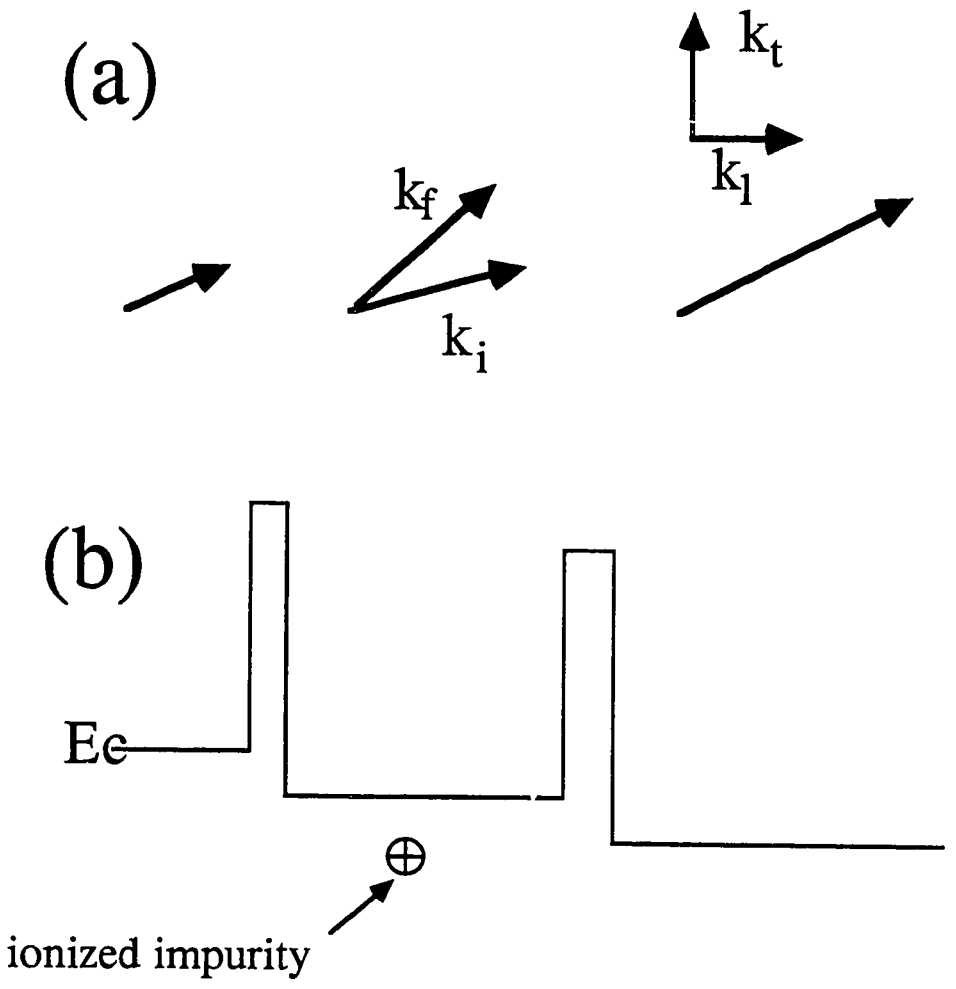

Figure 5.7 - In (a), the electron wavevector is shown for different stages of the potential shown in (b), with a scattering event occuring in the middle region or well. Elastic scattering events transfer momentum between the longitudinal and transverse directions, thus, resonances coupling different transverse quantum states are allowed. The transverse energy states are quantized, thus only certain transisitions determined by the quantization and the conservation of energy will occur.

The scattering matrix for the elastic scattering center has off diagonal two by two matricies with non-zero elements which mix the transverse states:

$$\begin{vmatrix} C_1 \\ C_2 \\ \cdots \end{vmatrix} = \begin{vmatrix} S_{11}S_{21}\cdots \\ S_{12}S_{22}\cdots \\ \cdots \ \cdots \ \cdots \end{vmatrix} \begin{vmatrix} B_1 \\ B_2 \\ \cdots \end{vmatrix} , \quad (5.5c)$$

where each B_i and C_i are two element vectors, and each S_{ij} is the scattering matrix from transverse states i to j. The scattering matricies serve to transfer probability amplitudes from one transverse state to another. By assuming a highly localized elastic scattering potential, transmission through a structure with a localized scattering center can now be written as:

$$\begin{vmatrix} D_1 \\ D_2 \\ \cdots \end{vmatrix} = \begin{vmatrix} F_{11}\ 0\ \cdots \\ 0\ F_{22}\cdots \\ \cdots \ \cdots \ \cdots \end{vmatrix} \begin{vmatrix} S_{11}\ S_{21}\ \cdots \\ S_{12}\ S_{22}\ \cdots \\ \cdots \ \cdots \ \cdots \end{vmatrix} \begin{vmatrix} E_{11}\ 0\ \cdots \\ 0\ E_{22}\cdots \\ \cdots \ \cdots \ \cdots \end{vmatrix} \begin{vmatrix} A_1 \\ A_2 \\ \cdots \end{vmatrix} , \quad (5.5d)$$

where the $E_{i\text{-}i}$ matrix elements give the propagation and matching conditions of the wavefunction from the emitter to the scattering center, and the $F_{i\text{-}i}$ matrix elements give the propagation of the wavefunction from the scattering center to the collector.

If an electron is incident upon the structure from the emitter in the transverse state i, and it is energetically possible for the electron to scatter into one of n transverse states (including i), then a total of n transmission and reflection coefficients must be calculated for this event as shown in Figure 5.8. The n elements of **D** in equation (5.5d) which represent flux away from the barriers will be non-zero, the same is true for **A** with the exception of state i. By solving n linear equations, it thus becomes possible to obtain the n transmission coefficients, T_{ij}, for the incident state i, which are defined as the ratio of the transmitted flux in state j over the incident flux in state i.

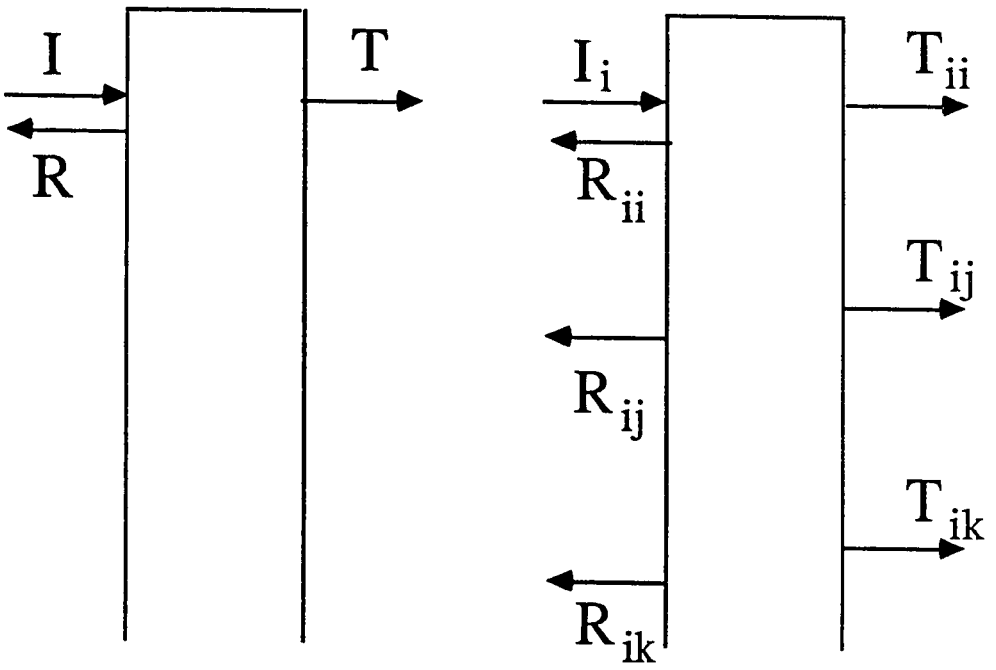

Figure 5.8 - An incident electron can only propagate or reflect in one transverse state if transverse momentum is conserved as shown above left. If scattering is allowed between different transverse states, however, several transmission and reflection coefficients must be considered for each incident electron as shown above right.

The current through the device based on the transition i-j for incident electrons with 1-DOF can now be written:

$$J_{i\text{-}j} = \frac{2q}{h}\int_0^{\infty} |T(E_l,V)_{ij}|^2 [f(E)\text{-}f(E+qV)]\, dE_l \quad , \quad (5.6)$$

where $|T(E_l,V)_{ij}|^2$ is derived in the manner outlined above. Several transverse states are available for incident electrons, and each transverse state may be coupled to several other transverse states via the scattering matrix. Thus we can write the total tunneling current, J, as:

$$J = \sum_{i}^{N} \sum_{j}^{n(i)} J_{ij} \ , \quad (5.7)$$

where the outer summation is over initial transverse states i, and the inner summation is over the final states f, which are allowed by conservation of energy. In the absence of scattering between transverse states, the above expression reduces to the equation (5.2 b).

Since equation (5.5) is derived within the independent electron approximation, it is possible to have $\Sigma_i T_{ij} > 1$ for some final states j. This may be treated by noting that for a given transition T_{ij}, the probabilities of j being an available state to tunnel into is reduced by a factor of $(1\text{-}T_{ij})$. This implies that in summing the transition probabilities into a final state j, that a modified sum rule should be used:

$$\widetilde{\sum_{i=1,n}} T_{ij} = \widetilde{\sum_{i=1,n-1}} T_{ij} + T_{nj}\left(1 - \widetilde{\sum_{i=1,n-1}} T_{ij}\right), \quad (5.8)$$

where the summation sign with the tilde represents the modified sum rule. The resulting

probability of tunneling into the final state will be less than unity and independent of the order of the modified summation so long as the individual T_{ij}'s are less than 1. For very small T_{ij}'s the above expression reduces to a normal summation. In order to treat this problem properly, higher order perturbation theory must be used.

5.5 Application to ionized impurity scattering in reduced dimensionality

Ionized impurities, acting as elastic scattering centers, break the conservation of transverse energy condition[4,5]. Kinetic energy is conserved in elastic collisions, however, it becomes possible to scatter elastically between states with different transverse momenta by interchanging longitudinal and transverse energy. As a result, the initial and final longitudinal momenta may be different at the point of scattering, as shown in figure 5.7. Only certain transitions are allowed, due to the discrete nature of the transverse states and the conservation of kinetic energy condition. Unintentional elastic scattering centers within a device can result from impurity diffusion or silicon surface riding during the MBE growth of the epitaxial layers.

Due to the highly localized nature of the screened Coulomb potential, the method outlined above is suitable to treating the coupling between the transverse states. To first order in the scattering potential, the scattering matrix elements are given by:

$$S_{i\text{-}f} = 2m_{eff} < \Psi_i \mid V \mid \Psi_j > (2\pi)^2 \, h^{-2} \, k^{-1/2} \, k'^{-1/2} \ , \qquad (5.9)$$

where the wavefunctions Ψ_i and Ψ_j consist of normalized transverse wavefunctions, multiplied by longitudinal plane wave states, V, is the scattering potential, and k is the longitudinal wavevector of the incident state at the point of scattering. The longitudinal final state wavevector, k', is chosen on the side of the device where the final density of

states is determined. This expression can be derived through a time independent formulation.

For the sake of tractability, we approximate the potential of the elastic scattering center by a Dirac delta function[5]. As a result, the transmission coefficient is weighted by a factor $|\Psi_{ti}(\mathbf{r_o})|^2\ |\Psi_{tj}(\mathbf{r_o})|^2$, where $\Psi_{ti}(\mathbf{r_o})$ and $\Psi_{tj}(\mathbf{r_o})$ are the transverse wavefunctions for states i and j evaluated at the position of the scattering center $\mathbf{r_o}$. Within this approximation, it is possible that a given transition would be very weak by the coincident location of a transverse wave node and the scattering center. Thus, the location of the scattering center and the transverse wave function will make some transitions allowed, or highly probable and others much less likely.

Consider the case of only two transverse states, denoted i and j. For $|X|=|E||S||F|$, the ratio of the transmitted flux in the transverse channel j to the incident flux in the transverse channel i is:

$$T_{ij} = \frac{x_{31}^{-1}\sqrt{k_f}}{[x_{11}^{-1}x_{33}^{-1}-x_{31}^{-1}x_{13}^{-1}]\sqrt{k_i}} \quad , \qquad (5.10)$$

where k_i and k_f are the initial and final longitudinal wavevectors of state i and j respectively, and T_{ij} is the ratio of the transmitted flux in state j over the incident flux in state i. We use the notation x^{-1} to signify elements of the inverted matrix $|X|^{-1}$. The transmission coefficients T_{ii}, T_{ji}, and T_{jj} can be similarly found, the summation over the final states being done by the modified sum rule. The treatment of more states simultaneously is a straightforward extension of this.

The transmission coefficients calculated in the above manner are plotted in figure 5.9 as a function of applied bias. A structure with 50 Å $Al_xGa_{1-x}As$ (x=0.3) barriers, and a 50 Å $In_yGa_{1-y}As$ (y=0.1) well was assumed and resonant tunneling through the excited state

was used. Transverse energy levels spaced 20 meV apart and an incident electron energy of 25 meV were assumed for this calculation. Three different values of energy transitions were used to calculate the transmission coefficient as a function of applied bias for a fixed incident electron energy, each showing distinct peak positions. A constant weighting of the scattering was assumed for the three transitions. In order to simplify the calculation of the inverted matrix elements, (which may become divergent), the Hermitian properties of the matrix for an unbiased RTD were used to get the relation $x^{-1}_{ij} = x^*_{ji}$. Though this is not strictly correct in the case of non-zero bias, it should not change the priciple result which is to create independent resonant peaks.

Less bias is needed to achieve a resonance condition for electrons which gain longitudinal energy in the well, and more bias is needed to obtain resonance for electrons which lose longitudinal energy in the well. The magnitude of the transmission coefficient decreases with larger changes in longitudinal energy. Due to the shift in the transmission coefficient, there will be a different resonant peak in the current-voltage characteristics of the device for each different transverse energy transition, S_{i-j}. The resulting additional currents which occur due to electrons scattering to different transverse energy states in the well may account for the additional peaks that have been observed in the current voltage characteristics of these structures[1]. The peaks in the transmission coefficent shown in 5.9 would not result in sharp peaks in the I-V characteristics, however, by increasing the barrier thickness or height, sharper resonances at the same bias points would result for a given scattering assisted transition. This would result in additional structure in the I-V characteristics.

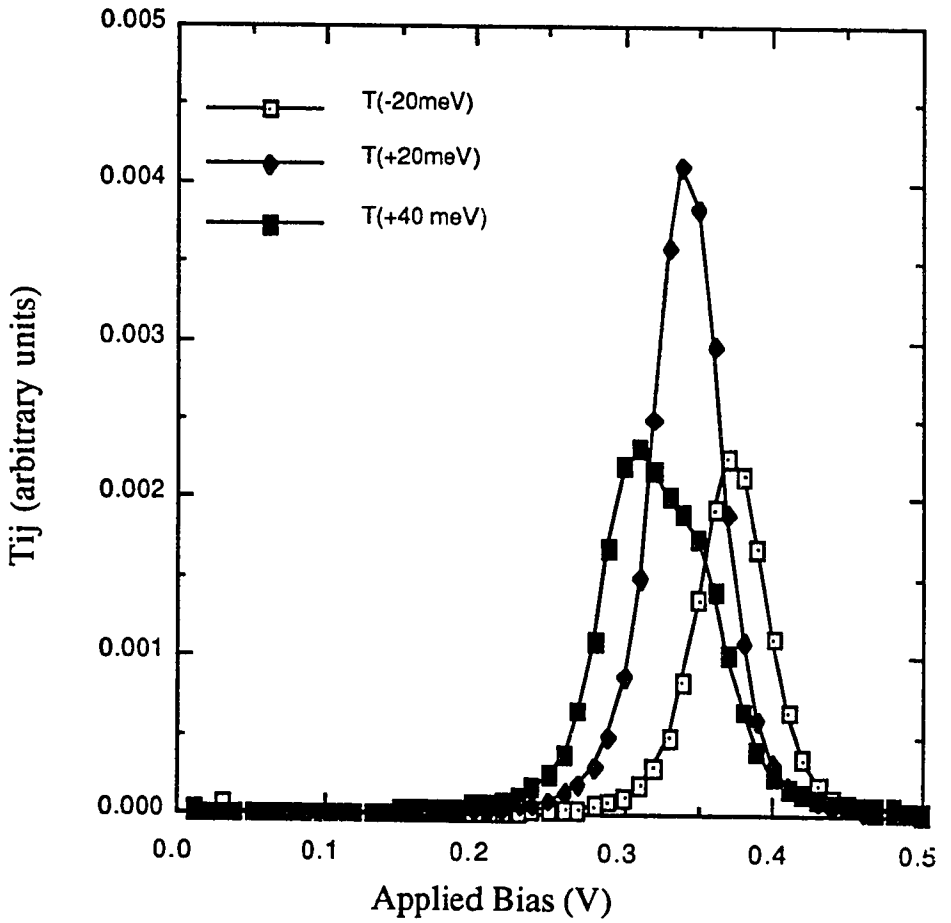

Figure 5.9 - The transmission coefficient is plotted for several different changes in longitudinal energy for a fixed incident ele ctron energy as a function of applied bias. The shift in the relative peak position indicates that additional strucutre in the current-voltage characteristics could arise from such scatttering events.

5.6 Discussion

It is possible to elastically scatter between states with different transverse momenta in a RTD with transverse confinement. The effect on the transmission coefficient through the device was derived using a perturbation approach. By computing the transmission coefficients for several different energy transitions, we showed that additional structure in the current-voltage characteristics of such devices could result from the reduced dimensionality.

While this method shows shifts in the resonances, it has several limitations, 1) it is only valid for small perturbations, 2) The single electron approximation can lead to a greater than unity tunneling probability into a single finite state, 3) it is not a including self-consistend calculation, 4) it ignores phonon effects, and 5) the Coulomb potential is approximated by a delta function.

More exact results could be found by using a higher order expansion for the scattering matrix, other perturbation expansions, the use of wave packets, Wigner functions, Green's functions and the use of a density matrix. Other perturbation expansions may be appropriate for other types of problems, such as the problem of changing well width in the confined conducting channel. The other methods, such as wave packet and Wigner function formulations, essentially entail self-consistent solutions and are vastly more taxing computationally. Such advanced methods would only be warrented once more knowledge about the confined states, the perturbing potentials, and Fermi energies can be determined.

References

1. M. Reed, J.N. Randall, R.J. Aggarwal, R.J. Matyi, T.M. Moore, and A. E. Wetsel, Physical Review Letters, **60**, 535 (1988).

2. S.Y. Chou, E. Wolak, and J.S. Harris Jr., Applied Physics Letters **52**, 657 (1988). 3. M.O. Vassell, Johnson Lee, and H.F. Lockwood, Journal of Applied Physics, **54**, 5206 (1983).

3. M.O. Vassell, Johnson Lee, and H.F. Lockwood, Jorunal of Applied Physics, 54, 5206 (1983).

4. E. Wolak, K.L. Lear, P.M. Pitner, E.S. Hellman, B.G. Park, T. Weil, J.S. Harris Jr, and D. Thomas, Applied Physics Letters, **53**, 18 July 1988.

5. J.A. Lebens, R. H. Silsbee, and S. L. Wright, Applied Physics Letters **51**, 840 (1987).

6. Conclusions:

6.1. Summary of contributions

This work represents several contributions towards advancing the physical understanding and functionality of RTDs.

A model based on coherent electron transport through the RTD was developed and compared with experiments. Predictions of the model for variations of each of the major device parameters was summarized. It was found that the model is useful in many circumstances, but that physical effects not included in the model could lead to significant deviations between predicted and measured results. The causes of these deviations were discussed as well as proposals for using the model for device optimization.

The role of elastic scattering due to ionized impurities was explored both experimentally and analytically. This consisted of designing and executing the first experiment with systematic variation of the well doping in a RTD. It was found that ionized impurities could shift the resonance in a fashion which is predicted by the ballistic model. Ionized impurities were also shown to act as elastic scattering centers, and to add additional valley current which is not predicted by the coherent transport model. This is explained by a transport mechanism, proposed in chapter 4, which results from scattering from a low transmission probability longitudinal energy to a high transmission probability longitudinal energy in the valley bias condition. Little change the current is expected due to scattering in the resonant bias condition, as the most likely incident electron states, those in resonance, are most likely to scatter in to similar states.

Transport through RTDs with additional transverse confinement was explored theoretically as part of a collaboration with Steve Chou. It was found that despite the increased sharpness of the one dimensional density of states, that there is no predicted

increase in the sharpness of the resonant tunneling current, assuming a fixed distance between the conduction subband minimum and the Fermi energy. It was also found that no additional structure is predicted (for symmetric RTDs) due to the transverse confinement assuming a separation of variables condition.

A multichannel transport formalism for RTDs was developed and applied to the problem of elastic scattering in a system of reduced dimensionality. It was found that by breaking the separation of variables condition, that elastic scattering could manifest additional structure in the current voltage characteristics of a RTD.

6.2. Fundamental questions to be resolved

Much work remains to be done in the fundamental aspects of tunneling transport. Understanding the true physical relationship between the physical tunneling phenomena and the device design parameters fully, will allow for the rapid optimization of RTDs.

A practical model of the band mixing problem needs to be developed and tested against experiments. Systematic studies of different AlAs barrier configurations may help shed new light on this problem. Specifically, an experiment involving asymmetric AlAs barriers, where one barrier is varied in thickness and the other is not, could prove most revealing. This is because the leverage effect from changing the barrier thickness can be eliminated if the changing barrier is on the collector side and the collector spacer is suitably varied. More work with triple AlAs barriers would also be helpful.

The role of the accumulation layer in adding to the valley current needs to be more fully understood, this is a complex question to approach due to the multitude of physical phenomena involved in the process. It is possible to model resonance effects due to quantum reflections in the accumulation layer with the model developed in chapter 3, and this effect has been observed for devices with large undoped spacer layers. Resonance effects which involve a change in the longitudinal energy of the tunneling electron cannot

be predicted by such models. Specifically, it is possible for an electron to scatter or emit a phonon such that it has a longitudinal energy within one of the resonant bands of the accumulation layer. Under certain bias conditions, it is possible that there will be a resonance between the states in the accumulation layer and the quantum well. The occupation of the accumulation layer, the band structure of the accumulation layer, the scattering rate into the accumulation layer and the tunneling rate out, are all interdependent, making such effects very difficult to approach analytically.

For lightly doped emitters, or for large spacer layers, the existing coherent transport model outlined in chapter 3 is inadequate due to the neglect of self-consistent quantum charge effects. More experimental effort and analysis are needed to understand these effects.

6.3. Future high performance RTDs

From the discussion of the previous section, it is apparent that some work remains to be done in order to empirically find an optimal set of parametric values for a high performance RTD in GaAlAs/GaAs. Once devices with the desired current density, resonant peak voltage, and peak to valley ratio are achieved, there will be additional effort required to make these devices reproducibly, due to the strong dependence of their characteristics on very precise dimensional device parameters. Much of this additional work will lie in the area of MBE growth, as opposed to device fabrication or design. At the time of this writing, room temperature peak current densities as high as 1.4×10^5 A cm^{-2} with a peak to valley ratio of 2.5 had been achieved on a GaAs substrate[1], this figure will probably be improved upon.

The greatest commercial promise of RTDs and related structures lies in the InP lattice matched materials system. The best peak to valley ratios for RTDs have been obtained with these materials. Devices with high peak current densities are expected from this

material system in the very near future. Studies have already been done on optimizing barrier composition, but systematic work on barrier thickness, well width, and the use of doping and spacer layers have yet to be done. In addition, the use of a sunken well RTD and asymmetric barrier RTDs in these materials should be investigated.

Reference:

1. S.K. Diamond, E. Ozbay, M.J.W. Rodwell, D.M. Bloom, Y.C. Pao, E. Wolak, and J.S. Harris, EDL 10, 104 (1989).